

**Identification and functional analysis of novel sporozoite surface proteins in the rodent malaria parasite *Plasmodium yoelii***

**Inaugural-Dissertation**

to obtain the academic degree

Doctor rerum naturalium (Dr. rer. nat.)

submitted to the Department of Biology, Chemistry and Pharmacy  
of Freie Universität Berlin

by

**Anke Harupa**

from Hennigsdorf

2015

All experiments for this thesis were conducted from April 2010 to February 2014 in the group of Dr. Stefan H.I. Kappe at Seattle Biomedical Research Institute (Seattle, USA).

1<sup>st</sup> Reviewer: Prof. Dr. Stefan H.I. Kappe  
Seattle Biomedical Research Institute  
307 Westlake Ave N, Suite 500  
Seattle, WA 98109  
USA

2<sup>nd</sup> Reviewer: Prof. Dr. Rupert Mutzel  
Freie Universität Berlin  
Institute for Biology - Microbiology  
Königin-Luise-Straße 12-16  
Room 133  
14195 Berlin

Date of defense: March 20<sup>th</sup>, 2015

## Summary

*Plasmodium* sporozoites are the infectious forms of the malaria parasite transmitted by mosquitoes. Upon transmission to the mammalian host, sporozoites embark on a complex journey to the liver where they infect hepatocytes to generate pathogenic merozoites which infect red blood cells. It is largely unknown how sporozoites achieve this journey. The aim of this thesis was to expand our knowledge of sporozoite surface and secreted proteins, since they are likely involved in host-parasite interactions in this initial phase of malaria infection. The *Plasmodium* 6-Cys protein P38 is a member of a small, conserved family of parasite surface and secreted proteins. Several 6-Cys proteins have been implicated in cell-cell interactions and represent targets for malaria vaccine development. Here, it is shown by epitope-tagging and immunofluorescence microscopy that P38 localizes to secretory organelles in salivary gland sporozoites in the rodent malaria parasite *P. yoelii*. Targeted deletion of *P38* does not reveal a function during the entire parasite life cycle. Cell surface biotinylation and mass spectrometry were used to identify novel putative sporozoite surface proteins in *P. yoelii* and in the human parasite *P. falciparum*. Four proteins identified in both *Plasmodium* species were selected for functional analysis in *P. yoelii*. Three of them are encoded by genes that were previously found to be upregulated in infectious sporozoites (UIS): a putative sugar transporter and two proteins that lack any functional annotation. Several UIS proteins are essential for liver infection. However, using a reverse genetics approach, it is shown that none of the here analyzed UIS proteins is required for establishing infection in mice. The fourth protein is a type I transmembrane protein encoded by the sporozoite-specific gene *S23*. Epitope-tagging and specific antibodies to *S23* in conjunction with immunoelectron microscopy confirm surface localization of *S23* in salivary gland sporozoites. Interestingly, the ectodomain of *S23* appeared to be inaccessible to antibodies in non-permeabilized sporozoites. Antibody-induced shedding of the major surface protein circumsporozoite protein exposed the *S23* ectodomain to antibodies in some sporozoites. Targeted deletion of *S23* adversely affected sporozoite locomotion *in vitro*, which surprisingly did not impact sporozoite infectivity.

## Zusammenfassung

*Plasmodium*-Sporozoiten sind die infektiösen Stadien des Malaria-Erregers und werden von Mücken übertragen. Nach der Übertragung auf den Säugetier-Wirt begeben sich die Sporozoiten auf eine komplexe Reise zur Leber, wo sie in Leberzellen eindringen, um dort die pathogenen Merozoiten zu bilden, die wiederum rote Blutzellen befallen. Wie Sporozoiten diese komplexe Reise zur Leber bewältigen, ist weitestgehend unbekannt. Ziel dieser Arbeit war es, das Wissen über Oberflächen- und sezernierte Sporozoitenproteine zu erweitern, da sie wahrscheinlich an Parasit-Wirt-Interaktionen in dieser ersten Phase der Malaria-Infektion beteiligt sind. Das 6-Cys-Protein P38 gehört zu einer kleinen, konservierten Familie von Oberflächen- und sezernierten Parasitenproteinen. Einige 6-Cys-Proteine sind nachweislich an Zell-Zell-Interaktionen beteiligt und stellen Zielmoleküle für die Malaria-Impfstoffentwicklung dar. Durch die Herstellung von Parasiten, die P38 als Fusionsprotein mit einem Hämagglutinin (HA)-Epitop exprimieren, wird mittels Immunfluoreszenzmikroskopie festgestellt, dass P38 in sekretorischen Organellen von Sporozoiten lokalisiert ist. Durch gezielte Deletion von P38 wird gezeigt, dass das Protein keine bedeutende Rolle im Lebenszyklus von *P. yoelii*, einem Erreger der Nagetier-Malaria, spielt. Durch Biotinylierung der Zelloberfläche von Sporozoiten und Massenspektrometrie konnten mehrere mutmassliche Oberflächenproteine in *P. yoelii* und in *P. falciparum*, dem gefährlichsten Malaria-Erreger in Menschen, identifiziert werden. Es wurden vier Proteine, die in beiden *Plasmodium*-Arten detektiert wurden, für eine funktionelle Analyse in *P. yoelii* ausgewählt. Drei dieser Proteine werden von Genen kodiert, die bereits zuvor in infektiösen Sporozoiten als erhöht exprimiert nachgewiesen wurden, den sogenannten UIS-Genen (UIS, upregulated in infectious sporozoites): ein mutmaßlicher Zuckertransporter und zwei Proteine ohne Homologien zu bekannten Proteinen. Einige UIS-Gene sind essentiell für die Infektion der Leber. Mit Hilfe reverser Genetik wird gezeigt, dass keines der hier analysierten UIS-kodierten Proteine für die Infektion des Säugetier-Wirts nötig ist. Das vierte Protein ist ein Typ-1-Transmembranprotein, das von einem Sporozoiten-spezifischen Gen kodiert wird, bekannt als S23. Mittels Epitop-tagging, spezifischer Antikörper gegen S23 und Immunelektronen-Mikroskopie wird bestätigt, dass sich S23 hauptsächlich auf der Oberfläche von Speicheldrüsen-Sporozoiten befindet. Die S23 Ektodomäne scheint allerdings für Antikörper in unpermeabilisierten Sporozoiten nicht zugänglich zu sein. Antikörper-induziertes

Ablösen des Haupt-Oberflächenproteins CSP (circumsporozoite protein) führte zur Freilegung der S23 Ektodomäne in einigen Sporozoiten. Gezielte Deletion von *S23* schränkte die *in vitro* Gleitbewegung der Sporozoiten drastisch ein, was sich überraschenderweise nicht auf die Infektivität der Sporozoiten auswirkte.

## Table of contents

Summary .....	I
Zusammenfassung .....	II
List of figures .....	VII
List of tables .....	VIII
List of abbreviations .....	IX
1 Introduction .....	1
1.1 Malaria .....	1
1.2 The <i>Plasmodium</i> life cycle .....	1
1.3 Pathology and immunity .....	3
1.4 Approaches to control malaria .....	5
1.6 Malaria research .....	7
1.5 The <i>Plasmodium</i> sporozoite .....	8
1.5.1 Morphology and organelles .....	8
1.5.2 Gliding motility .....	9
1.5.3 Host cell invasion .....	11
1.5.4 Cell traversal .....	12
1.6 Parasite proteins involved in the sporozoite's journey through its hosts .....	12
1.6.1 Into the salivary gland .....	12
1.6.2 From the skin to the liver .....	14
1.6.3 Into the hepatocyte .....	16
1.7 The 6-Cys protein family .....	17
1.8 Aims and outline of the thesis .....	19
2 Materials and methods .....	20
2.1 Materials .....	20
2.1.1 Chemical and biological reagents .....	20
2.1.2 Equipment .....	21
2.1.3 Commercial kits .....	22
2.1.4 Antibodies .....	22
2.1.5 Cells and organisms .....	23
2.1.6 Solutions .....	23
2.2 Molecular biology techniques .....	23
2.2.1 Polymerase chain reaction .....	23
2.2.2 Sequence overlap extension PCR .....	24
2.2.3 Colony PCR .....	24

2.2.4 Agarose gel electrophoresis .....	24
2.2.5 Agarose gel DNA extraction.....	24
2.2.6 Restriction digest of DNA .....	24
2.2.7 DNA ligation .....	25
2.2.8 Bacterial transformation .....	25
2.2.9 Plasmid isolation.....	25
2.3 Animal work.....	25
2.4 <i>P. yoelii</i> methods .....	26
2.4.1 Giemsa staining.....	26
2.4.2 Cryopreservation of <i>P. yoelii</i> -infected blood .....	26
2.4.3 Maintenance of the <i>P. yoelii</i> life cycle .....	26
2.4.4 Evaluation of sporozoite loads in mosquitoes .....	27
2.4.5 Generation of transgenic <i>P. yoelii</i> parasites.....	27
2.4.6 Extraction of genomic DNA from <i>P. yoelii</i> blood stages .....	34
2.4.7 Southern blot of genomic DNA from <i>P. yoelii</i> blood stages.....	35
2.5 Cell biological assays.....	36
2.5.1 Blood stage parasite growth curve.....	36
2.5.2 Sporozoite gliding motility assay .....	36
2.5.3 Sporozoite cell traversal and invasion assay.....	36
2.5.4 <i>In vivo</i> sporozoite infection assays .....	37
2.5.5 Liver stage burden by quantitative real-time PCR.....	37
2.5.6 Immunofluorescence assays .....	38
2.5.7 Immunoelectron microscopy.....	39
2.6 Biochemical techniques.....	39
2.6.1 Western blot.....	39
2.6.2 Surface biotinylation of sporozoites .....	40
2.6.3 Recombinant S23 expression and antiserum production.....	41
3 Results .....	43
3.1 Functional analysis of the 6-Cys protein P38 in <i>P. yoelii</i> .....	43
3.1.1 <i>P. yoelii</i> P38.....	43
3.1.2 Generation of parasites expressing epitope-tagged P38.....	43
3.1.3 P38 localizes to micronemes in sporozoites .....	45
3.1.4 Generation of P38-deficient parasites.....	47
3.1.5 The lack of P38 does not affect blood stage growth or mosquito stage development.	48
3.1.7 P38-deficient sporozoites glide and traverse cells normally <i>in vitro</i> .....	50

3.1.8 P38 is not required for sporozoite infectivity to the rodent host.....	51
3.2 Identification of putative sporozoite surface proteins .....	53
3.2.1 Surface biotinylation of live sporozoites.....	53
3.2.2 Analysis of surface protein-enriched fractions .....	54
3.3 Functional analysis of UIS surface proteins .....	57
3.3.1 PY02432 – a small tyrosine-rich protein .....	57
3.3.2 PY06766 – a conserved apicomplexan protein with four transmembrane domains...	57
3.3.3 PY05332 – a putative sugar transporter.....	58
3.3.4 PY06766 and PY05332 localize to the periphery of sporozoites .....	59
3.3.5 Generation of <i>UIS</i> knockout parasites .....	62
3.3.6 UIS knockout sporozoites are infectious to mice .....	62
3.4 Characterization of the sporozoite surface protein S23 .....	65
3.4.1 S23 is a type I transmembrane protein with conserved cysteine residues.....	65
3.4.2 S23 localizes to the periphery in salivary gland sporozoites .....	66
3.4.3 The ectodomain of S23 is not readily accessible to antibodies .....	68
3.4.4 Immuno-EM determines surface localization of S23 .....	71
3.4.5 S23 is not shed following sporozoite activation .....	74
3.4.6 Accessibility to S23 on the sporozoite surface might be masked by CSP .....	75
3.4.7 S23-deficient parasites are viable but are defective in gliding motility.....	76
3.4.8 S23 is not required for cell traversal and invasion.....	78
4 Discussion .....	81
4.1 The 6-Cys protein P38 is dispensable throughout the entire parasite life cycle .....	81
4.2 The sporozoite surface proteome .....	83
4.3 Novel sporozoite surface proteins encoded by UIS genes are dispensable for infection of the mammalian host.....	85
4.4 S23 is a novel type I transmembrane protein with a role in gliding motility.....	87
References .....	90
List of publications.....	106
Appendix A .....	107
Appendix B .....	108
Appendix C .....	112
Acknowledgements .....	115

## List of figures

Figure 1.1 The life cycle of mammalian <i>Plasmodium</i> spp. ....	3
Figure 1.2 <i>Plasmodium</i> sporozoite morphology .....	9
Figure 1.3 Schematic representation of the <i>Plasmodium</i> glideosome.....	10
Figure 1.4 Progression of sporozoite invasion of the salivary gland .....	13
Figure 1.5 The <i>Plasmodium</i> sporozoites' journey from the skin to the liver .....	16
Figure 2.1 Schematic procedure for the generation of transgenic <i>P. yoelii</i> parasites .....	28
Figure 3.1 Generation of <i>Py P38HA</i> parasites .....	45
Figure 3.2 Localization of P38HA in schizonts and salivary gland sporozoites .....	46
Figure 3.3 Generation of P38-deficient <i>P. yoelii</i> parasites .....	48
Figure 3.4 Blood stage growth of <i>p38</i> <sup>-</sup> is similar to wild type <i>in vivo</i> .....	49
Figure 3.5 <i>p38</i> <sup>-</sup> salivary gland sporozoites show normal gliding motility <i>in vitro</i> .....	50
Figure 3.6 <i>p38</i> <sup>-</sup> salivary gland sporozoites show normal cell traversal activity <i>in vitro</i> .....	51
Figure 3.7 Western blot analysis of biotinylated proteins .....	54
Figure 3.8 HA-tagging of putative sporozoite surface proteins .....	60
Figure 3.9 Localization of PY05332 and PY06766 in sporozoites .....	61
Figure 3.10 Generation of gene knockout parasites .....	62
Figure 3.11 Schematic of the predicted protein structure of S23 and sequence alignments .....	66
Figure 3.12 Generation of <i>Py S23cMyc</i> parasites.....	67
Figure 3.13 Expression of S23 increases during sporozoite maturation .....	68
Figure 3.14 Expression and localization of double-tagged S23 in sporozoites .....	70
Figure 3.15 IFA on sporozoites with polyclonal antibodies specific to PyS23.....	71
Figure 3.16 Localization of PyS23 by immuno-electron microscopy .....	73
Figure 3.17 S23 is not shed during sporozoite gliding motility .....	74
Figure 3.18 Accessibility to S23 might be masked by CSP .....	75
Figure 3.19 Generation of <i>Py s23</i> <sup>-</sup> parasites.....	76
Figure 3.20 <i>Py s23</i> <sup>-</sup> sporozoites show a gliding defect <i>in vitro</i> .....	78
Figure 3.21 <i>Py s23</i> <sup>-</sup> sporozoites show normal cell traversal and invasion <i>in vitro</i> .....	79
Figure 3.22 Lack of S23 has no effect on the liver stage burden <i>in vivo</i> .....	80

## List of tables

Table 2.1 Primers used for cloning the targeting constructs .....	29
Table 2.2 Primers used for genotyping of transgenic parasites.....	31
Table 3.1 <i>Py p38</i> parasites show normal development in the mosquito vector.....	49
Table 3.2 <i>Py p38</i> sporozoites are able to establish blood stage infection in mice .....	52
Table 3.3 A selected group of putative surface-exposed sporozoite proteins .....	56
Table 3.4 Sporozoite numbers isolated from salivary glands are similar between wild type and knockout parasites .....	63
Table 3.5 Knockout sporozoites are able to infect the rodent host.....	64
Table 3.6 <i>Py s23</i> show normal development in the mosquito vector .....	77
Table 3.7 <i>Py s23</i> sporozoites successfully establish liver infection and transition to blood stage infection in mice .....	80

## List of abbreviations

6-Cys	6-Cysteine
BiP	binding immunoglobulin protein
CSP	circumsporozoite protein
DAPI	4',6-diamidino-2-phenylindole
DHFR/TS	dihydrofolate reductase-thymidylate synthase
ER	endoplasmic reticulum
GAP	genetically attenuated parasite
GPI	glycosylphosphatidylinositol
HA	hemagglutinin
HSPG	heparan sulfate proteoglycan
IFA	immunofluorescence assay
IMC	inner membrane complex
LS	liver stage
MG	midgut
MJ	moving junction
MSP-1	merozoite surface protein 1
MTIP	myosin A tail-interacting protein
Pb	<i>Plasmodium berghei</i>
Pf	<i>Plasmodium falciparum</i>
Pv	<i>Plasmodium vivax</i>
PV	parasitophorous vacuole
PVM	parasitophorous vacuole membrane
Py	<i>Plasmodium yoelii</i>
RBC	red blood cell
RON	rhoptry neck protein
S23	sporozoite-expressed gene 23
SG	salivary gland
SPZ	sporozoite
Tg	<i>Toxoplasma gondii</i>
TRAP	thrombospondin-related anonymous protein
TSR	thrombospondin type 1 repeat
UIS	upregulated in infectious sporozoites

UTR	untranslated region
VWA	von Willebrand factor type A-like
WT	wild type

## 1 Introduction

### 1.1 Malaria

Malaria is a parasitic infectious disease that is transmitted by mosquitoes. It occurs mostly in tropical and subtropical regions where climatic conditions are ideal for the development of the parasite and its vector. Malaria has been affecting humanity for thousands of years and remains a major global health problem, with nearly half of the world's population living at risk of infection (1). In 2012, more than 200 million people contracted malaria and an estimated 627 000 people died from it, mainly young children and pregnant women (1). The causative agents are protozoan parasites of the genus *Plasmodium* belonging to the phylum Apicomplexa. There are over 250 *Plasmodium* species infecting a variety of reptiles, birds and mammals, with each species having a narrow host range (2). Five are known to infect humans: *P. falciparum*, *P. vivax*, *P. ovale*, *P. malariae* and *P. knowlesi*, a zoonotic species that primarily parasitizes Southeast Asian macaques (3). Most malaria deaths are attributed to *P. falciparum* which is predominantly found in sub-Saharan Africa, while *P. vivax* is globally widespread and is the major cause of malaria morbidity outside Africa (1).

### 1.2 The *Plasmodium* life cycle

*Plasmodium* is an obligate intracellular parasite. Its life cycle is composed of an asexual phase in the vertebrate host and a sexual phase in the mosquito which is therefore the definitive host.

Malaria infection begins when an infected female mosquito bites a host to take a blood meal (Figure 1). During probing for blood, the mosquito injects saliva along with infectious sporozoites into the extravascular portion of the host's skin (4,5). The sporozoites actively move through the tissue in order to reach a blood vessel and invade it (6,7). Once in the blood stream, sporozoites are transported to the liver where they cross the sinusoidal barrier to enter the liver parenchyma and infect hepatocytes. During hepatocyte invasion, the sporozoite causes the hepatocyte plasma membrane to invaginate and thereby creates a compartment termed the parasitophorous vacuole (PV)(8). The intrahepatic elongated sporozoite then transforms into a round liver stage which grows greatly in size and undergoes repeated nuclear divisions without cytokinesis (schizogony), yielding a large multi-nucleated syncytium (schizont). Once nuclear divisions are completed, the parasite plasma membrane starts to invaginate to

form thousands of daughter cells termed merozoites. The PV membrane (PVM) eventually breaks down and merozoites are released into the blood stream as packages (merosomes) wrapped in the plasma membrane of the dying host cell (9,10). The intrahepatic development of the parasite is asymptomatic and takes about one week in humans and remarkably only two days in rodents. *P. vivax* and *P. ovale* additionally form dormant liver stages (hypnozoites) which can persist in the liver for weeks, months or even years before reactivating to generate merozoites (11,12). Upon egress from merosomes, merozoites invade red blood cells and thereby initiate the cyclic intra-erythrocytic phase of infection which causes all clinical symptoms of malaria. Within the PV, merozoites grow and multiply by schizogony to form new merozoites, which takes approximately 18-24 h or 48-72 h in species infecting rodents and humans, respectively. Once development is complete, merozoites egress from erythrocytes and invade new erythrocytes. Some merozoites, however, invade erythrocytes and then develop into nonpathogenic male or female gametocytes which are ingested by a blood-feeding mosquito (13). Within the mosquito midgut, the gametocytes are activated by the drop of temperature and other factors, and escape from the red blood cell (14-16). Within 10-15 min, each male gametocyte produces four to eight motile flagellated microgametes in a process called exflagellation (17). Each microgamete seeks a female gamete (macrogamete) and fuses with it to form a diploid zygote which then differentiates into a motile ookinete. The ookinete leaves the blood meal by crossing the peritrophic membrane enclosing it, and traverses the midgut epithelium to come to reside between the epithelial cells and the basal lamina (18). Here, the ookinete transforms into a round sessile oocyst that grows and replicates to produce hundreds to thousands of sporozoites over a period of 10-14 days. The sporozoites actively egress from the oocyst into the hemolymph (19) and invade the salivary glands where they await transmission to a new host.

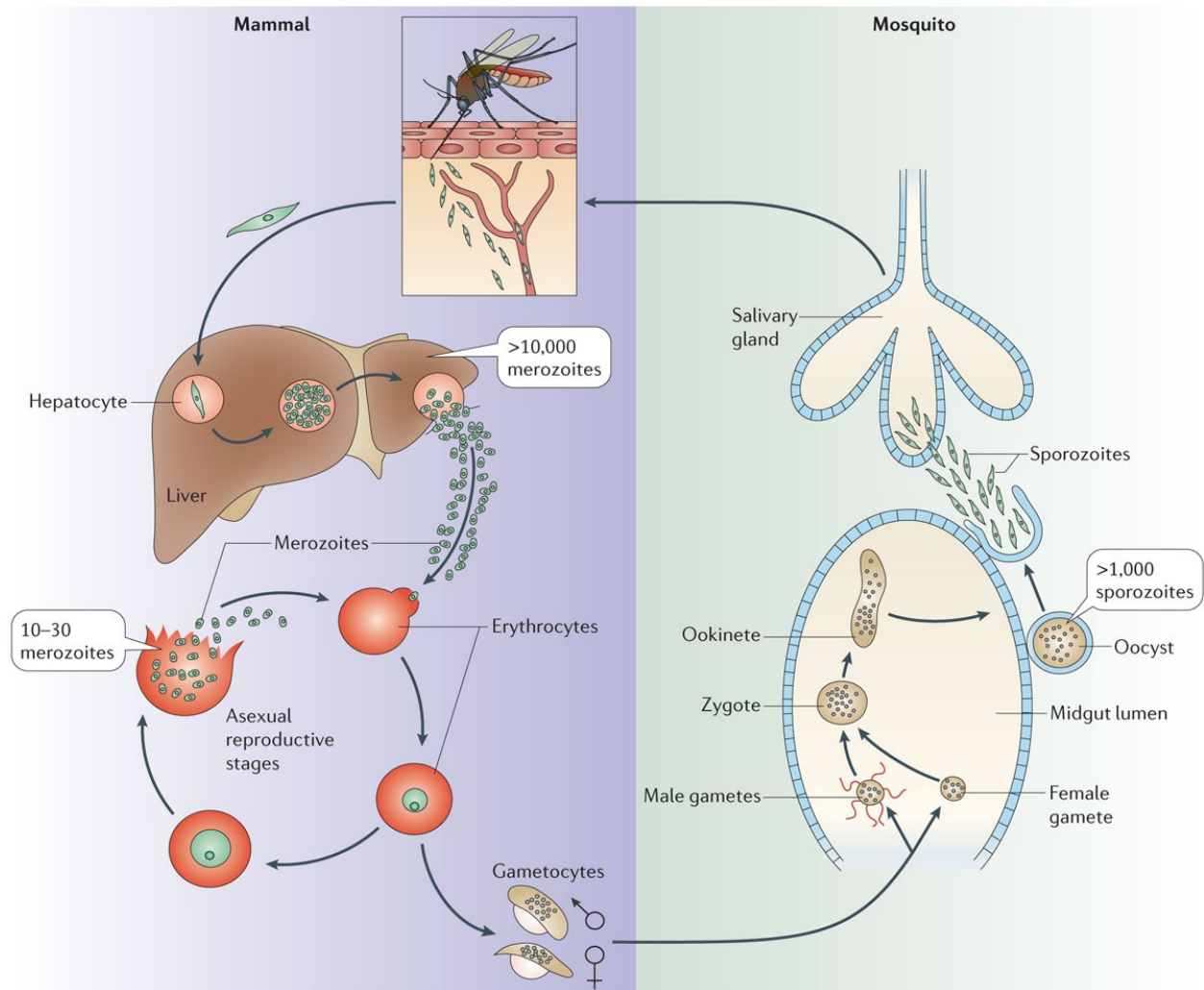


**Figure 1.1** The life cycle of mammalian *Plasmodium* spp. (20). Sporozoites are inoculated into the skin of the mammalian host by an infected mosquito. Sporozoites actively enter the blood circulation and are carried to the liver where they infect hepatocytes and develop into liver stages. Each liver stage produces thousands of merozoites which are released into the blood stream. Merozoites invade erythrocytes, replicate and release new merozoites that initiate a new asexual cycle. Some merozoites develop into gametocytes which are ingested by a mosquito during a blood meal. Male and female gametes escape from erythrocytes and fuse to form a zygote which transforms into a motile ookinete. The ookinete traverses the midgut epithelium, settles beneath the basal lamina and differentiates into an oocyst which produces sporozoites. Once mature, sporozoites actively egress from oocyst into the hemolymph and invade the salivary glands.

### 1.3 Pathology and immunity

All symptoms associated with malaria are caused by asexual blood stage parasites, while the pre-erythrocytic phase of infection is clinically silent. Symptoms of uncomplicated malaria infection are non-specific and often resemble those of viral infections such as fever, chills, sweats, nausea, headache, fatigue and muscle pain. Fever corresponds to the rupture of infected erythrocytes which release merozoites and

waste substances that cause inflammation (21). Severe forms of malaria are generally associated with *P. falciparum* infections. The parasites express adhesive proteins on the surface of the infected erythrocyte which mediate adhesion to vascular endothelial cells (cytoadherence), to uninfected erythrocytes (rosetting) and to other infected erythrocytes via platelets (clumping) (22–24). Sequestration of infected erythrocytes in the microvasculature leads to local inflammation, endothelial dysfunction and blood flow obstruction, and can cause life-threatening complications (25). Additionally, *P. falciparum* invades erythrocytes of all ages resulting in high parasite densities, whereas *P. vivax* mainly invades reticulocytes which are a minor subset of erythrocytes (26). Severe malaria manifests as organ failure, severe anemia, metabolic acidosis, hypoglycemia, and acute encephalopathy characterized by seizures, paralysis, impaired consciousness and coma. The latter neurological complications are known as cerebral malaria, a common cause of death (27).

The course of malaria infection depends on many factors, e.g. parasite virulence (cytoadherence, drug resistance), age, genetics (blood disorders) and immune status of the host. Individuals living in malaria-endemic regions develop immunity to malaria in an age- and exposure-related manner. This naturally acquired immunity (NAI) protects against severe disease and death, but it is never complete and wanes quickly upon cessation of exposure to malaria (28). Protection against clinical malaria is partially mediated by antibodies that block cytoadherence and merozoite invasion. Because the parasite proteins involved in cytoadherence undergo extensive antigenic variation (29), immunity is only slowly acquired and requires repeated exposure to the different variants. But in areas with stable malaria where transmission is high, immunity develops during the first five years of life and is highly protective against severe disease by the onset of puberty, followed by protection against mild clinical episodes (28). Additional immunity that restricts parasite density develops progressively with age, such that adults often have low-level asymptomatic parasitemia. Acquisition of NAI to malaria is not well understood and, unfortunately, no single immune correlate of protection against clinical malaria has been identified to date (30). Malaria-exposed individuals also mount immune responses to pre-erythrocytic stages. Antibodies against sporozoites are common in exposed individuals but their contribution to protective immunity is unclear (31).

### **1.4 Approaches to control malaria**

Malaria is preventable and curable, yet causes significant morbidity and mortality. Over the past 15 years, malaria control has received great attention from the international community. Current control strategies focus on prompt diagnosis and treatment, and reduction of transmission through vector control (32). There are several antimalarial drugs available which can be used for prophylaxis and treatment. They inhibit development of asexual blood stage parasites by interfering with different metabolic pathways (33–35). Only two commercial drugs kill liver stages, with one of them being active against the dormant liver forms of *P. vivax* (36,37). A major problem in treatment of malaria is the emergence of resistance to nearly all currently used drugs (38). Another approach to fight malaria is vector control. A reduction of mosquito populations can be accomplished through drainage of breeding grounds and through insecticides. Insecticide-treated bed nets and spraying indoor surfaces of houses with insecticides can greatly reduce transmission. However, similar to drug resistance of malaria parasites, mosquitoes develop resistance to insecticides. More than 60 countries have reported resistance of mosquitoes to at least one insecticide used for malaria control (1). While these global control efforts have led to a reduction of malaria mortality by 42 % between 2000 and 2012, it is clear that new intervention strategies are needed in order to reach the long-term goal of global malaria eradication (1,39).

A malaria vaccine is highly desirable, but despite many years of intense research, there is currently no commercial vaccine available. Research into malaria vaccines generally focuses on targeting either asexual blood stage parasites, sexual stages (transmission-blocking vaccines), or sporozoites and liver stages (pre-erythrocytic vaccines). Blood stage vaccines aim to reduce parasite density and severe disease but do not prevent infection. The classical approach is the immunization with recombinant parasite proteins to induce invasion-blocking or sequestration-blocking antibodies. Progress in the development of such a vaccine has been slow, mainly due to the poor understanding of the mechanisms underlying protective immunity. Other factors that limit progress are difficulties in expressing recombinant plasmodial proteins, the inability to induce long-lived immune responses, the presence of polymorphisms in vaccine antigens, and the parasite's ability to use alternative invasion pathways (40). To date, no experimental blood-stage vaccine has proven efficacy.

Transmission-blocking vaccines induce antibody responses to surface proteins of the sexual stages which become vulnerable once emerged from the erythrocyte in the mosquito midgut. While this strategy does not directly protect the vaccinated individual, it prevents transmission to other individuals by inhibiting the parasite development (i.e. oocyst formation) within the mosquito (41).

Interrupting the parasite life cycle at the clinically silent pre-erythrocytic stages is the most attractive goal as it prevents blood stage infection, and thus disease, and also disrupts transmission. Several decades ago, it was found that immunization with gamma-irradiated *Plasmodium* sporozoites can confer sterile protection against challenge with live sporozoites in animal models and humans (42–45). Irradiation of sporozoites is believed to induce random mutations into the parasite's genome which likely lead to a multifaceted attenuation. The sporozoites are capable of invading hepatocytes but arrest early in liver stage development and thus fail to infect the blood. Protection is primarily mediated by cytotoxic T cells which are active against infected hepatocytes (46,47). More recently, attenuation of parasites has been accomplished by deleting parasite genes that are critical for liver stage development (48–50). Similar to irradiated sporozoites, vaccination with these genetically attenuated parasites (GAPs) induces protective immunity (50,51). GAPs that arrest late during liver stage development were furthermore shown to induce superior protection over early arresting GAPs or irradiated sporozoites in mice (52). This is explained by the broader and more varied cytotoxic T cell response to late-arresting GAPs which are much larger in size and express many more antigens than early-arresting parasites (53). It was recently demonstrated in mice and humans that repeated exposure of wild type sporozoites under chemoprophylaxis can also induce sterile immunity (54–56). Live sporozoite vaccines are currently the only fully protective experimental malaria vaccine. However, major technical and logistical hurdles must be overcome in order to deploy such vaccines (57).

The most clinically advanced vaccine candidate is RTS,S<sup>®</sup>, a subunit vaccine that targets pre-erythrocytic stages. The vaccine is based on the *P. falciparum* circumsporozoite protein (CSP) which is the major sporozoite surface protein. RTS,S<sup>®</sup> consists of the hepatitis B surface antigen fused to a highly immunogenic portion of CSP. The vaccine has entered Phase III trials in 2009 and involves more than 15,000 children in 7 African

countries (58). Unfortunately, RTS,S<sup>®</sup> conferred only partial and short-lived protection involving humoral and cell-mediated immunity (59). Vaccine efficacy against clinical malaria was 68 % shortly after vaccination (0-6 months), and decreased to 26 % after 12-18 months (44).

### 1.6 Malaria research

Malaria research has been transformed by the completion of the genome sequence of different *Plasmodium* species within the past 12 years (62-67), and by the development of genetic tools that allow genetic manipulation of the parasite (68-71).

The haploid *Plasmodium* genome is 23-27 Mbp in size and is organized into 14 chromosomes. It is extremely AT-rich (~ 80 % in *P. falciparum* and rodent species) and encodes 5000-6000 genes, with roughly half of them encoding proteins for which no functional information is available (62,63). The characterization of a particular gene and its product usually requires the targeted manipulation of the parasite's genome (72). This typically involves the deletion of the gene of interest to analyze its importance in the parasite life cycle, or its fusion to other sequences such as epitope tags to study protein localization. The generation of transgenic or gene knockout parasites is time- and resource-intensive, but remains the most straight-forward approach for assessment of gene function.

Advances in high-throughput technologies such as microarrays and mass spectrometry-based proteomics have led to a wealth of data, especially for *P. falciparum* blood stages as they can be cultured *in vitro* and are thus readily accessible. Sporozoites and liver stages are more difficult to obtain in sufficient quantity and purity for high-throughput analyses. Only few laboratories rear *Anopheles* mosquitoes and sporozoites are isolated from mosquito salivary glands by manual dissection. Liver stages of *P. falciparum* are impossible to study in humans and *in vitro* systems have not efficiently supported liver stage development until recently, but sporozoite infection rates are low (0.07 %) (73). Much of our understanding of parasite transmission and liver infection has come from studies in animal models of malaria. The most commonly used parasites are *Plasmodium yoelii* and *Plasmodium berghei*, sibling species that naturally infect African thicket rats. They have been adapted to grow in laboratory rodents and allow the maintenance of the entire parasite life cycle *in vivo* (74). An important recent achievement has been the development of chimeric mice engrafted with human hepatocytes which now allow for analysis of *P. falciparum* liver stages *in vivo* (75).

## **1.5 The *Plasmodium* sporozoite**

*Plasmodium* sporozoites are the most versatile stages of the malaria parasite as they invade two different tissues in different hosts – the salivary glands in the mosquito and the liver in the mammalian host. In order to reach and invade a hepatocyte, sporozoites must cover long distances and cross biological barriers, processes for which sporozoites are adequately equipped.

### **1.5.1 Morphology and organelles**

Sporozoites are slender, elongated and highly polarized cells with a crescent shape, measuring 10–15  $\mu\text{m}$  in length and less than 1  $\mu\text{m}$  in width (Figure 1.2). Sporozoites possess the typical eukaryotic organelles such as a nucleus, mitochondrion, endoplasmic reticulum, Golgi apparatus, but also a relict plastid called the apicoplast (76). The defining structural feature of the phylum Apicomplexa is the apical complex. It consists of an apical polar ring, which serves as microtubule-organizing center, and specialized secretory organelles termed micronemes and rhoptries (77). Micronemes are small oval organelles that are present in large numbers. They are found throughout the sporozoite cytoplasm but concentrate at the apical end. Rhoptries are paired club-shaped organelles that can be divided into two sections, the neck and the bulb which each contain a distinct set of proteins and phospholipids. The contents of micronemes and rhoptries are important for sporozoite motility, host cell recognition, host cell invasion and formation of the parasitophorous vacuole (PV). The contents of a third type of secretory organelles termed dense granules are thought to modify the PV for optimal parasite development. Sporozoites are surrounded by a three-layered pellicle that consists of the plasma membrane and the closely apposed inner membrane complex (IMC), which is made up made up of flattened vesicles (alveoli). The pellicle is supported by a network of interwoven filaments and microtubules that help to maintain cell shape.

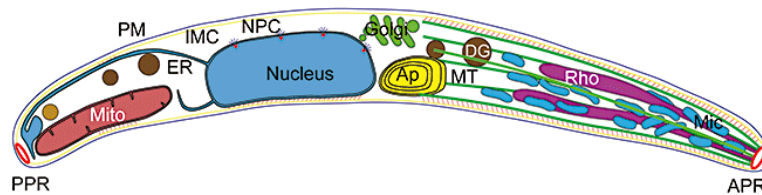


**Figure 1.2** *Plasmodium* sporozoite morphology. Ap, apicoplast; APR, apical polar ring; DG, dense granule; ER, endoplasmic reticulum; IMC, inner membrane complex; Mic, micronemes; Mito, mitochondrion; MT, microtubule; NPC, nuclear pores; PM, plasma membrane; PPR, proximal polar ring; Rho, rhoptries. From (78).

### 1.5.2 Gliding motility

Like many extracellular stages of apicomplexans, sporozoites move rapidly over solid substrates despite the lack of cilia, flagella or pseudopods. This unique form of active locomotion is termed gliding motility, a trait that is acquired during sporozoite maturation (79). Sporozoites typically move in a circular manner on solid substrate without a change in cell shape (80). Gliding motility is believed to be powered by the glideosome that consists of an actomyosin motor and surface adhesion proteins (81). The actomyosin motor is located between the plasma membrane and the underlying IMC. Myosin A (MyoA), which is an unconventional myosin unique to Apicomplexa, is firmly anchored to the IMC via myosin A tail interacting protein (MTIP) and the glideosome-associated proteins 45 and 50 (GAP45, GAP50). During gliding, type I transmembrane adhesins are apically secreted from micronemes and get incorporated into the sporozoite plasma membrane. The extracellular adhesive domains of these proteins bind to the substrate while their cytoplasmic tails are connected to actin filaments, presumably via tetramers of the glycolytic enzyme aldolase. The stationary MyoA pulls on actin filaments and thereby translocates the actin-aldolase-adhesin complex toward the posterior end of the sporozoite. Since the adhesin is bound to the substrate, this rearward translocation results in forward movement of the parasite (Figure 1.3). At the posterior end of the sporozoite, the interaction between the substrate and the parasite is disengaged through intra- or juxtamembrane cleavage of the adhesin by proteases (82). The cleaved portion of the adhesin is left behind in the trails of the gliding sporozoite (83,84).

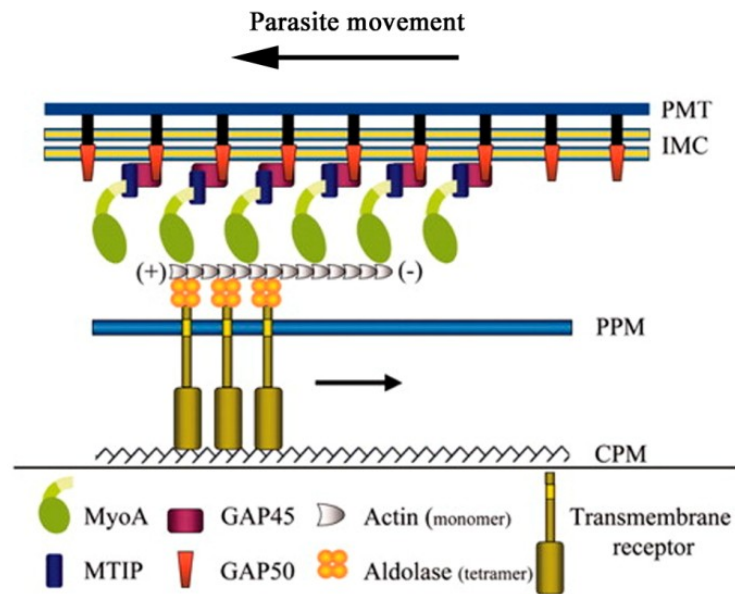


**Figure 1.3** Schematic representation of the *Plasmodium* glideosome. MTIP is tethered to the IMC via interaction with GAP45 and the integral protein GAP50. The MyoA tail binds to MTIP while the head domain interacts with actin filaments. Actin is linked to the cytoplasmic domain of a transmembrane adhesin via an aldolase tetramer. The adhesin binds to the host cell membrane. As the head domain of MyoA pulls on actin filaments, the actin–aldolase–adhesin complex is translocated toward the posterior end of the parasite (black arrow), leading in forward movement of the parasite. GAP45 and GAP50, glideosome-associated protein 45 and 50; PMT, parasite microtubules; IMC, inner membrane complex; PPM, parasite plasma membrane; CPM, cellular plasma membrane; MTIP, MyoA-tail interacting protein; MyoA, myosin A. Adapted from (85).

Adhesion proteins involved in gliding motility belong to the thrombospondin-related anonymous protein (TRAP) family, which is found throughout Apicomplexa (77). TRAP family proteins are characterized by one or more extracellular adhesive domains, i.e. von Willebrand factor type A-like (VWA) domains and/or thrombospondin type I repeat (TSR) domains. VWA and TSR are evolutionarily ancient domains that are present in a variety of eukaryotic proteins involved in cell-cell and cell-extracellular matrix interactions (86,87). The cytoplasmic tail of TRAP family proteins contains multiple negatively charged residues and a penultimate tryptophan residue that appears to be critical for the binding to aldolase (83,88–90). The founding member *Plasmodium* TRAP, also known as sporozoite surface protein 2 (SSP2) (91), is expressed in oocyst and salivary gland sporozoites where it is found in micronemes and on the cell surface. TRAP is essential for sporozoite infectivity; disruption of TRAP abrogates the sporozoite's ability to glide and invade cells (83,92,93).

The major surface protein CSP has been also implicated in gliding motility (94,95), although it is unclear if or how CSP interacts with the actomyosin motor as it is predicted to be attached to the plasma membrane by a glycosylphosphatidylinositol (GPI) anchor. CSP is unique to the *Plasmodium* genus. The overall structure of CSPs from different *Plasmodium* species is conserved and consists of a central species-specific repeat region that is N-terminally flanked by a highly conserved 5-amino acid sequence termed region I, and C-terminally by a TSR-like domain (96). During gliding motility on a solid substrate, CSP is continuously secreted at the apical end of the sporozoite and is translocated to the posterior where it is shed into the gliding trail (94,97). Decades ago, it was observed that incubation of live sporozoites with immune sera from mice vaccinated with irradiated sporozoites inhibits sporozoite motility and leads to the formation of a thread-like precipitate at the sporozoite's posterior end (42,95,98). This process is known as the CSP precipitation reaction and describes the shedding of the cross-linked CSP surface coat.

### **1.5.3 Host cell invasion**

Most of our knowledge about host cell invasion comes from studies in *Toxoplasma* tachyzoites and *Plasmodium* merozoites. The invasion process can be divided into 5 phases: initial attachment to the host cell, apical contact with the host cell plasma membrane, tight junction formation, active invasion with formation of the parasitophorous vacuole membrane (PVM), and sealing of the PVM (99). Initial attachment of the parasite to the host cell is likely mediated by surface proteins and results in a low-affinity binding to the host cell. The parasite then reorients itself to bring its apical tip in direct contact with the host cell membrane which is followed by a calcium-regulated discharge of micronemes (100). It was shown that, in addition to calcium, cyclic adenosine monophosphate is involved in exocytosis of micronemes in *Plasmodium* sporozoites (101). Following discharge of micronemes, rhoptries release their contents. Proteins from both organelles mediate intimate attachment to the host cell membrane and the formation of a ring-shaped tight junction, termed the moving junction (MJ) (102,103). The parasite then starts to actively propel itself into the cell by rearward translocation of the MJ complex thought to be driven by the actomyosin motor (104). Simultaneously, the parasite induces the host cell plasma membrane to invaginate, which results in the formation of the parasitophorous vacuole (PV). During the invasion process, receptor-ligand interactions are continually disrupted to allow

invasion to proceed (82). Finally, upon entry into the host cell, the parasitophorous vacuole membrane is sealed.

It has been widely accepted that host cell invasion is driven by the same actomyosin motor that powers gliding motility (105). However, recent genetic studies demonstrated that key components of the motor machinery can be deleted without abolishing host cell invasion, suggesting that the current model of invasion is in need of revision and/or that alternative invasion mechanisms exist (106–108).

### **1.5.4 Cell traversal**

Sporozoites are able to migrate through cells, but the mechanism is poorly understood. During this so-called cell traversal, sporozoites do not enter the cell with concomitant PVM formation but breach the cell's plasma membrane (109,110). The sporozoite then glides through the cytosol and exits the cell, again, by wounding the plasma membrane. Cell traversal allows the sporozoite to cross biological cell barriers such as the vascular endothelium, and it was shown to play a role in escaping destruction by phagocytic cells (111). Sporozoites also traverse cells within its target organ, the liver (110). It is unclear why sporozoites display this behavior but studies with cell traversal-deficient sporozoites demonstrated that it is not a prerequisite for successful hepatocyte infection (112–114).

## **1.6 Parasite proteins involved in the sporozoite's journey through its hosts**

### **1.6.1 Into the salivary gland**

Sporozoites are formed through sporogony within oocysts which are lodged between the mosquito midgut epithelium and the basal lamina. Oocyst development takes 10–14 days and the sporozoite surface protein CSP is essential for this process. Parasites lacking CSP are able to form oocysts which however fail to produce sporozoites (115). After completion of sporogony, sporozoites egress into the mosquito hemocoel in a protease-dependent process (19). The hemolymph carries the sporozoites throughout the mosquito circulatory system, even to the legs and wings (116). Sporozoites eventually encounter the salivary glands and attach to it. Salivary gland invasion by sporozoites is qualitatively different from cell traversal and host cell invasion. Sporozoites breach the basal lamina and invade the secretory acinar cells by forming a moving junction and a parasitophorous vacuole that however rapidly disintegrates and

leaves the sporozoites free in the cell cytoplasm (Figure 1.4). During exit of the acinar cell, sporozoites again form a transient vacuole and enter the salivary gland secretory cavity (117).

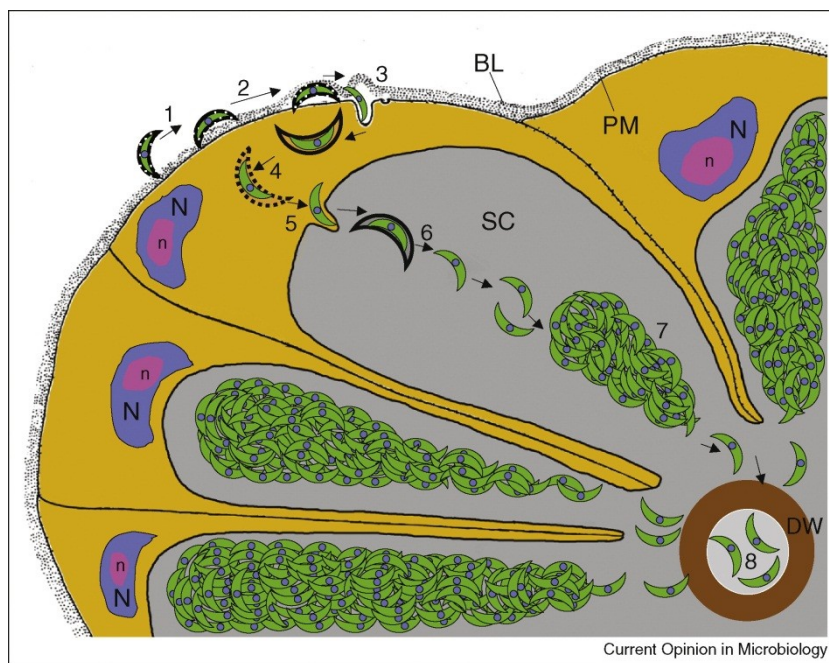


**Figure 1.4** Progression of sporozoite invasion of the salivary gland. (1) The sporozoite attaches to the basal lamina; (2) sporozoite passage to the space between the basal lamina and the basal epithelial cell plasma membrane, a process associated with the loss of the sporozoite's thick coat; (3) penetration of the basal plasma membrane; the sporozoite resides within a vesicle; (4) release of the sporozoite from the surrounding membrane by an unknown mechanism; (5) invasion of the apical membrane and entry into the secretory cavity; (6) sporozoites are released from the surrounding membrane by an unknown mechanism; (7) sporozoites assemble into bundles within the secretory cavity; and (8) a small number of sporozoites enter the secretory duct by an unknown mechanism. BL: basal lamina; DW: duct wall; N: nucleus; n: nucleolus; PM: plasma membrane; SC: secretory cavity. Figure and caption from (117).

Several proteins have been identified to play a role in attachment and/or invasion of salivary glands. CSP is thought to mediate initial attachment of the parasite to the salivary glands. Recombinant CSP was shown to preferentially bind to salivary glands over other mosquito organs, and a CSP-derived peptide was demonstrated to inhibit sporozoite invasion (118,119). Another protein involved in salivary gland invasion is the apical membrane antigen/erythrocyte binding-like (MAEBL) protein. MAEBL is a type I transmembrane protein that contains extracellular cysteine-rich domains which

are also present in merozoite proteins involved in erythrocyte invasion (120). MAEBL localizes to micronemes and the sporozoite surface, and when disrupted renders sporozoites unable to attach to salivary glands while gliding motility is unaffected (120,121). TRAP is essential for salivary gland invasion, which is mediated by its extracellular adhesive domains and its cytoplasmic tail that connects to the actomyosin motor (83,92,93). Sporozoites with mutations in either the TSR or the VWA domain of TRAP are less invasive, and those with mutations in both domains are non-invasive while gliding motility is normal (93). Another TRAP family protein involved in salivary gland invasion is TRAP-related protein (TREP), also known as sporozoite-specific gene 6 (S6) or upregulated in oocyst sporozoite gene 3 (UOS3) (122–124). It is found in secretory organelles and on the surface of sporozoites and its extracellular portion contains a single TSR domain. Disruption of S6/UOS3/TREP impairs the sporozoites' capacity to glide and invade salivary glands (122–124). The cysteine repeat modular proteins (CRMP) 1 and 2 (125) also play a role in salivary gland invasion. These proteins are very large multi-pass transmembrane proteins with cysteine-rich domains expressed on the surface of sporozoites (125).

Once in the salivary glands, sporozoites become highly infectious to the mammalian liver, but they irreversibly lose infectivity for salivary glands (126). This transformation coincides with significant changes in gene expression (127). A set of more than 120 genes has been identified to be upregulated in infectious sporozoites (UIS) when compared to oocyst sporozoites (123,127). UIS proteins are believed to be important for infection of the vertebrate host. In fact, several of them were shown to be essential for establishing the parasite's intrahepatic replication niche and for liver stage development (e.g. P52, UIS3, UIS4) (48,50,51). Sporozoites lacking these essential UIS genes have been successfully used as GAP vaccines in rodent models (48,50,51).

### **1.6.2 From the skin to the liver**

When a mosquito probes for a blood source, it inoculates saliva along with sporozoites into the skin of the mammalian host. While mosquitoes can harbor thousands of sporozoites in their salivary glands, they generally inoculate relatively small numbers at a rate of  $\sim 1$ –2.5 sporozoites per second (5). Sporozoite transmission therefore constitutes a major bottleneck in the parasite life cycle. Most sporozoites are deposited in the extravascular portion of the skin and not directly into the blood stream (Figure

1.5) (4,6). Albumin and potentially other factors trigger vigorous gliding motility and sporozoites randomly migrate through the skin until they encounter and invade a blood vessel (7,79,128). It has been previously thought that sporozoites rapidly enter the circulatory system but it was recently shown that sporozoites leave the inoculation site in a slow trickle over a period of several hours (129). Some sporozoites (~ 20 %) enter the lymphatic system and end up in lymph nodes where most of them are degraded (7,129). Sporozoites in the blood stream, however, are transported to the liver where they arrest, likely through interaction of CSP with heparin sulfate proteoglycans (HSPGs) present on the surface of hepatocytes (96). Hepatocyte HSPGs protrude into the liver sinusoids through the fenestration of the endothelial cells (Figure 1.5). While HSPGs are expressed on the surface of multiple cell types, those on hepatocytes are more sulfated than HSPGs on dermal or endothelial cells (96). It has been proposed that sporozoites use the degree of HSPG sulfation to navigate through the mammalian host (130). Once in the liver, the majority of sporozoites cross the sinusoidal endothelium by traversing endothelial cells or Kupffer cells which are the liver-resident macrophages that line the sinusoidal wall (111).

In this initial phase of infection, sporozoites rely on their ability to glide and traverse cells in order to reach the liver (103). Four proteins have been shown to play a role in host cell traversal: sporozoite microneme protein 1 (SPECT1), SPECT 2 (also known as perforin-like protein 1; PLP1), cell-traversal protein for ookinetes and sporozoites (CelTOS), and a phospholipase (PL) (112–114,131,132). These proteins are soluble secreted proteins that are stored in micronemes except for PL which associates with the sporozoite surface by an unknown mechanism. Sporozoites lacking either of these proteins display a defect in cell traversal activity *in vitro* and are poorly infective *in vivo*. SPECT 1 and CelTOS have no similarity to known proteins. SPECT2/PLP1 contains a membrane attack complex/perforin-like domain, and recombinant PL was shown to have membrane-lytic activity (113,131,132). These two proteins likely mediate pore formation in plasma membranes of non-permissive cells. While PL appears to be only involved in cell traversal within the skin, SPECT1 and SPECT2/PLP1 are also important for crossing the sinusoidal cell layer in the liver. Recently, the TRAP family adhesin TLP (TRAP-like protein) has been also implicated in traversal of the dermal tissue (133,134).

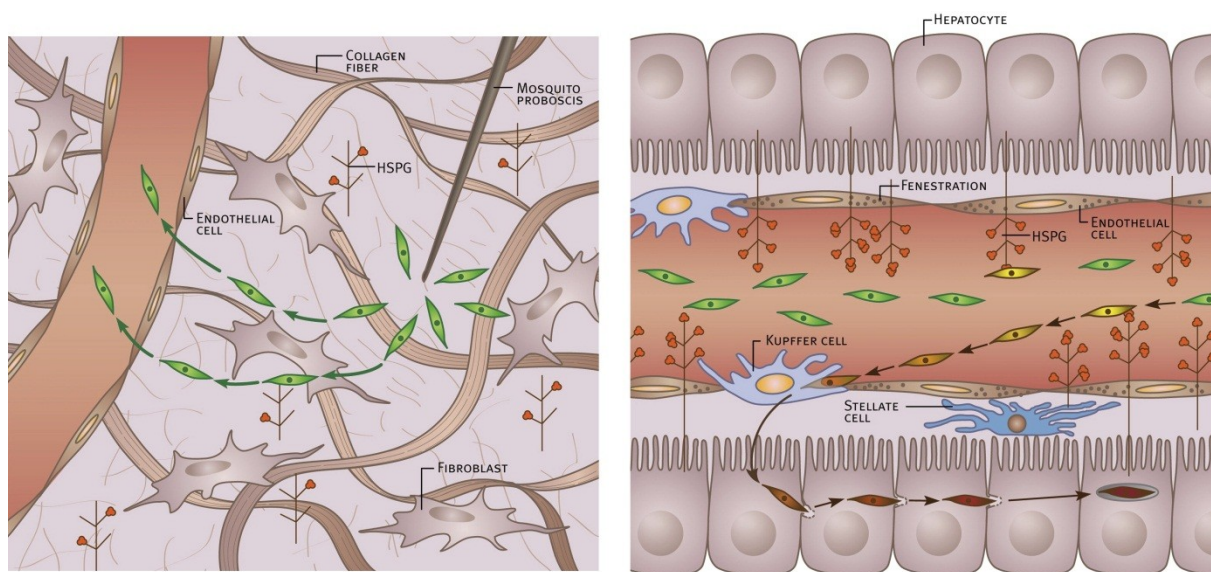


**Figure 1.5** The *Plasmodium* sporozoites' journey from the skin to the liver. *Plasmodium* sporozoites (green) are inoculated into the extravascular dermis of the vertebrate host by a mosquito. Sporozoites migrate through the dermal tissue, which does not express highly sulfated HSPGs, until they reach and invade a blood vessel. Once in the liver, sporozoites arrest through interaction with highly sulfated hepatocyte HSPGs that protrude into the sinusoidal lumen. Sporozoites then cross the sinusoidal layer by traversal of Kupffer cells or through other routes, and enter the liver parenchyma. Following traversal of several hepatocytes, the sporozoite productively invades a target host hepatocyte with formation of a parasitophorous vacuole. Figure from (135).

### 1.6.3 Into the hepatocyte

In addition to targeting the sporozoite to the liver, CSP is also involved in the hepatocyte invasion process itself. It was shown that binding of CSP to highly sulfated HSPGs on hepatocytes promotes CSP cleavage, which importantly appears to trigger the switch from cell traversal to cell invasion mode (130,136). CSP is cleaved within region I by a parasite cysteine protease and, when inhibited, invasion of hepatocytes is blocked (136). Like CSP, TRAP has multiple functions in the sporozoite's life. It is not only involved in salivary gland invasion but also in hepatocyte entry. The extracellular adhesive domains of TRAP are required for hepatocyte invasion but not for attachment (93). Another protein implicated in hepatocyte invasion is the thrombospondin-related sporozoite protein (TRSP), a type I transmembrane protein with an extracellular TSR domain (137). It potentially localizes to rhoptries, and sporozoites deficient in TRSP were shown to invade hepatocytes less efficiently (138). Productive invasion of hepatocytes involves the formation of the moving junction and the parasitophorous vacuole membrane (PVM). The rhoptry neck protein 4 (RON4) has been shown to be essential for junction formation and hepatocyte invasion (139). RON4 is a soluble

secreted protein that is conserved among apicomplexan parasites. Studies in *Plasmodium* merozoites and in *Toxoplasma* tachyzoites suggest that RON4 is translocated from the rhoptry neck to the cytosolic side of the host cell membrane where it in complex with additional RONs interacts with the host cell cytoskeleton and serves as anchor for other parasite proteins involved in invasion (140–142). A protein that was shown to bind to this RON complex is apical membrane antigen 1 (AMA-1) (141,142). AMA-1 is a micronemal type I transmembrane protein that is conserved among Apicomplexa. It translocates from micronemes to the parasite surface during invasion and has long been thought of as essential for junction formation and host cell invasion (143). However, it was recently demonstrated that AMA-1 has no role in *Plasmodium* sporozoite invasion of hepatocytes (139). As the sporozoite enters the cell, it forms a parasitophorous vacuole and two proteins have been implicated in this process, P52 and P36 (50,144). These proteins belong to the *Plasmodium* 6-Cys family, which is described in more detail in section 1.7. The proteins UIS3 and UIS4 are expressed in salivary gland sporozoites but do not play a role until after hepatocyte invasion (48,51). Parasites lacking UIS3 or UIS4 arrest early in liver stage development and thus fail to transition to blood stage. UIS3 and UIS4 localize to the PVM of liver stage parasites (48,145). UIS3 belongs to the family of early transcribed membrane proteins (ETRAMPs) and the C-termini of these proteins face the host cell cytoplasm (146,147). Using a yeast-two-hybrid system, Mikolajczak and colleagues showed that UIS3 binds to liver fatty acid binding protein (L-FABP), suggesting that UIS3 may be involved in lipid acquisition from the host (145). A few other proteins have been implicated in hepatocyte invasion based on their surface localization in sporozoites and on the fact that antibodies against them can inhibit hepatocyte invasion. These proteins include the secreted protein with altered TSR domain (SPATR), sporozoite and liver stage antigen (SALSA), sporozoite threonine-asparagine-rich protein (STARP), sporozoite-associated protein 1 and 2 (SIAP1,2) (148–153).

### **1.7 The 6-Cys protein family**

The *Plasmodium* genome encodes a family of ten proteins that are characterized by domains with six positionally conserved cysteine residues that form three disulfide bonds (154,155). These 6-Cysteine (6-Cys) or s48/45 domains are structurally related to the surface antigen 1 (SAG)-related sequence (SRS) fold in the *Toxoplasma* SAG surface proteins (156–158). SAG proteins are predicted to mediate attachment to the

host cell, likely through binding to glycans present on the host cell surface (159,160). The 6-Cys proteins are conserved across the *Plasmodium* genus. Eight of them are encoded by genes that form paralogous gene pairs that are organized in a head-to-tail manner within the genome. Most 6-Cys proteins are expressed in distinct stages of the parasite life cycle, i.e. merozoites, gametes, sporozoites (161–163). About half of them are predicted to be soluble, secreted proteins whereas the remaining 6-Cys proteins contain a putative GPI anchor. Several 6-Cys proteins have been implicated in cell-cell interactions (161,164,165). The gamete-expressed proteins P48/45 and P230 form a complex on the parasite surface and were shown to play an essential role in the recognition and/or attachment of gametes, which makes these proteins attractive targets for transmission-blocking vaccines (164–166). Indeed, monoclonal antibodies against P48/45 and P230 were demonstrated to reduce oocyst formation by inhibiting zygote formation (167–170). The paralog of P48/45, P47, is expressed on the surface of female gametes and plays an important role in fertilization in the rodent parasite *P. berghei*, but is interestingly dispensable in the human parasite *P. falciparum* (164,171). The blood stage-expressed proteins P12 and P41 were shown to localize to the merozoite surface in *P. falciparum* (161,172). P12 is attached to the merozoite plasma membrane by a GPI anchor and forms a complex with the soluble protein P41. Both proteins are strongly recognized by immune sera from individuals living in malaria-endemic countries, but neither P12 nor P41 was found to be involved in erythrocyte attachment or invasion (172,173). The sporozoite-specific protein P52 (also known as P36p) and its paralog P36 are both important for liver infection (49,164,174). P52 has a putative GPI anchoring sequence and appears to localize to micronemes in salivary gland sporozoites in *P. berghei* (49). P36 is a putative secreted protein. Gene disruptions of *P52* or *P36* in *P. berghei* resulted in sporozoites that were impaired in liver stage development (49,50). In *P. yoelii*, the simultaneous deletion of both genes, *P52* and *P36*, yielded sporozoites that failed to form and/or maintain a PVM and aborted liver stage development soon after hepatocyte invasion (144). A comparable phenotype was observed in *P. falciparum* sporozoites lacking these genes, which led to the production of the first live GAP vaccine for use in human clinical trials (174,175). Another 6-Cys protein expressed in sporozoites is P38 (176). Unlike most members, P38 is not restricted to a single stage of the parasite life cycle, but is also expressed in gametocytes and asexual blood stages (161,177). In *P. falciparum*, P38 was shown to

localize to apical secretory organelles and the surface of merozoites (161). Recently, P38 was disrupted in *P. berghei* which had no effect on blood stage growth, gametocyte production or fertilization (164). However, the localization or importance of P38 in sporozoites has not yet been analyzed.

### **1.8 Aims and outline of the thesis**

Despite the key role of sporozoites in initiating malaria infection, relatively little is known about their unique biology. This thesis aims to expand our knowledge of sporozoite surface and secreted proteins, as they play a potential role in host-parasite interactions in the initial phase of malaria infection. The first part of the thesis addresses the localization and function of the 6-Cys protein P38 in sporozoites, which belongs to a family of surface and secreted proteins involved in cell-cell interactions. The second part describes the identification of novel sporozoite surface proteins in the rodent malaria model *P. yoelii* and the clinically relevant parasite *P. falciparum*, using biochemical surface labeling and mass spectrometry. In the third part, three so-identified putative surface proteins are investigated for their role in sporozoite infectivity. The fourth part focuses on the characterization of a novel type I transmembrane protein identified in the sporozoite surface proteome.

## 2 Materials and methods

### 2.1 Materials

#### 2.1.1 Chemical and biological reagents

Reagent	Manufacturer/Distributor
1 kb DNA Ladder	Promega
4',6-diamidino-2-phenylindole (DAPI)	Pierce
Accudenz® powder	Accurate Chemical & Scientific Corp.
Agarose, SeaKem® LE	VWR
Alsever's solution	Sigma
Ampicillin sodium salt	Thermo Scientific
BioMix™ Red	Bioline
Blue/Orange loading dye, 6x	Promega
Bovine serum albumin (BSA)	Sigma
BupH Tris-Glycine Transfer Buffer	Pierce
BupH Tris-HEPES-SDS Running Buffer Packs	Pierce
Cellulose powder, CF11	Whatman
cComplete™ Protease inhibitor cocktail tablets, Mini	Roche
Dextran, AlexaFluor®488-labeled, lysine fixable, MW 10,000	Thermo Scientific
DIG Easy Hyb™ solution	Roche
Dimethyl sulfoxide (DMSO)	Sigma
Dynabeads® MyOne™ Streptavidin T1	Invitrogen
Ethidium bromide solution, 0.625 µg/ml	VWR
EZ-Link® Sulfo-NHS-LC-Biotin	Thermo Scientific
Fetal bovine Serum (FBS)	Sigma
Formalin solution, 10 % neutral-buffered	Sigma
Gentamycin 50 mg/ml	Mediatech
Giemsa stain	Sigma
Glutaraldehyde	Polysciences
Glycerol	MP Biomedicals
Heparin sodium salt	Thermo Scientific
Isopropanol	Sigma
Lane Marker Sample Buffer, Non-reducing, 5x	Pierce
LB agar powder	VWR
LB broth powder	Fisher
Methanol	BDH
M-PER® Mammalian Protein Extraction Reagent	Pierce
PageRuler™ Plus Prestained Protein Ladder	Pierce

Paraformaldehyde solution, 16 %, methanol-free	Thermo Scientific
PBS without calcium and magnesium	MP Biomedicals
Phusion® High-Fidelity DNA Polymerase	New England Biolabs
Potassium permanganate	Fisher
Power SYBR® Green Master Mix	Applied Biosystems
ProLong® Gold Antifade Reagent	Thermo Scientific
Pyrimethamine	MP Biomedicals
Restore™ Western Blot Stripping Buffer	Pierce
Restriction enzymes	New England Biolabs
RPMI 1640	Sigma
Saline-sodium citrate (SSC) buffer, 20x	Thermo Scientific
Saponin	Sigma
Skim milk powder, Difco™	BD
Sodium dodecyl sulfate (SDS)	Fisher
Streptavidin-HRP	Pierce
SuperSignal™ West Pico Chemiluminescent Substrate	Pierce
T4 DNA ligase	Roche
TAE buffer, 50x	Thermo Scientific
Triton X-100	MP Biomedicals
TRIzol® reagent	Thermo Scientific
Trypsin EDTA solution	Thermo Scientific
Tween20	Sigma
Urea	Fisher
VectaShield® HardSet™ Mounting Medium	Vector Laboratories
β-mercaptoethanol	MP Biomedicals

### 2.1.2 Equipment

Other than common laboratory equipment, the following instruments were used:

Type	Model	Manufacturer
Clinical microscope	Eclipse 50i	Nikon
Dissecting microscope	Stemi DV4	Zeiss
Electroporator	Nucleofector™ device	Lonza
Flow cytometer	LSR II	BD Biosciences
Fluorescence microscope	Eclipse E600	Nikon
Fluorescence microscope with deconvolution software	DeltaVision® microscope system based on an Olympus inverted 1X70 microscope	Applied Precision
Fluorescent Western Blot imager	Odyssey® Imaging System	LI-COR
Microcentrifuge	5415R	Eppendorf
Real-time thermal cycler	7300 Real-time PCR system	Applied Biosystems
Spectrophotometer	NanoDrop® 1000	NanoDrop

Thermal cycler	2720	Applied Biosystems
Thermal cycler	Mastercycler® nexus	Eppendorf
UV crosslinker	UV Stratalinker® 1800	Stratagene
Vibratome	Microslicer™ DTK-1000	Ted Pella

### 2.1.3 Commercial kits

Name	Manufacturer
Amaxa® Human T Cell Nucleofector® Kit	Lonza
DIG DNA Labeling and Detection Kit	Roche
DIG Wash and Block Buffer Set	Roche
Direct-zol™ RNA MiniPrep Kit	Zymo Research
HiSpeed® Plasmid Maxi Kit	Qiagen
QIAamp® DNA Blood Mini Kit	Qiagen
QIAprep® Spin Miniprep Kit	Qiagen
QIAquick® Gel Extraction Kit	Qiagen
QIAquick® PCR purification Kit	Qiagen
QuantiTect® Reverse Transcription Kit	Qiagen

### 2.1.4 Antibodies

Primary antibody	Species	Manufacturer/Distributor
Digoxigenin-alkaline phosphatase	sheep	Roche
Pf CSP (2A10), monoclonal	mouse	MR4 (MRA-183A)
Py CSP (2F6), monoclonal	mouse	In-house
Py CSP (2F6)-AlexaFluor®647 conjugate		In-house
HA (12C5A), monoclonal	mouse	Roche
HA (Y-11), polyclonal	rabbit	Santa Cruz Biotechnology
Py MSP-1 (83a) monoclonal	mouse	Dr. Lawrence W. Bergman
Py MTIP, polyclonal	rabbit	In-house
Myc (9E10), monoclonal	mouse	Santa Cruz Biotechnology
Myc (SC-789), polyclonal	rabbit	Santa Cruz Biotechnology
Py S23, polyclonal	mouse	In-house
Py TRAP (clone F3B5), monoclonal	mouse	In-house
Py UIS4, polyclonal	rabbit	In-house

Secondary antibody	Species	Manufacturer/Distributor
Anti-mouse Alexa Fluor®488/594	goat	Molecular Probes
Anti-rabbit Alexa Fluor®488/594	goat	Molecular Probes
Anti-mouse HRP, stabilized	goat	Pierce
Anti-rabbit HRP, stabilized	goat	Pierce
Anti-mouse IRDye® 800CW	donkey	LI-COR Biosciences
Anti-rabbit IRDye® 680RD	donkey	LI-COR Biosciences

### 2.1.5 Cells and organisms

Cell/organism	Manufacturer/Distributor
One Shot® TOP10 Chemically Competent <i>E. coli</i>	Invitrogen
DH5α <i>E. coli</i>	In-house
Mouse Hepa1-6 hepatoma cells	Dr. Ana Rodriguez (New York University)
<i>Plasmodium yoelii</i> 17XNL clone1.1	In-house
<i>Anopheles stephensi</i>	In-house
BALB/c mice, 6-8 weeks, female	Jackson Laboratory
BALB/cBy mice, 6-8 weeks, female	Jackson Laboratory
Swiss Webster mice, 6-8 weeks, female	Harlan Laboratories

### 2.1.6 Solutions

Solution	Composition
Cryopreservation solution for <i>P. yoelii</i> -infected blood	Alsever's solution with 10 % glycerol; mix 1 volume of blood with 2 volumes of cryopreservation solution
<i>P. yoelii</i> culture medium	140 ml RPMI 1640 w/ L-glutamine and 25 mM HEPES 35 ml heat-inactivated FBS 50 µl gentamicin (50 mg/ml)
Accudenz® stock solution	27.6 g Accudenz® powder in 100 ml of: 5 mM Tris-HCl (pH 7.5) 3 mM KCl 0.3 mM EDTA
Pyrimethamine 100x	7 mg/ml pyrimethamine in DMSO

## 2.2 Molecular biology techniques

### 2.2.1 Polymerase chain reaction

The polymerase chain reaction was developed by Kary B. Mullis (Saiki et al., 1985) for which he was awarded the Nobel Prize for Chemistry in 1993. The PCR principle is the oligonucleotide primer-directed *in vitro* amplification of a known DNA sequence with a thermostable DNA polymerase, and involves repeated cycles of template DNA denaturation, primer annealing and primer extension. In this study, cycles were repeated between 30 and 35 times. Primers were synthesized by Thermo Fisher Scientific, Inc. and were stored as 100 µM stock solutions at -20 °C. Primers were used at a final concentration of 1 µM. PCR cycling conditions were set according to the primers, DNA polymerase and amplicon size. Extension time was 1 min per kb of target per cycle. Extension temperature was set to 62 °C or 68 °C due to the low GC content of the *Plasmodium yoelii* genome.

### **2.2.2 Sequence overlap extension PCR**

Sequence overlap extension PCR was used to fuse two PCR products for subsequent cloning into *P. yoelii* transfection plasmids. First, each DNA fragment was amplified by PCR with primers that added restriction sites to facilitate directional cloning. The reverse primer of DNA fragment #1 and the forward primer of DNA fragment #2 were designed to contain the same restriction site and additional overlapping complementary sequences. The PCR products were gel purified and an aliquot of each was added to the second PCR mixture to serve as template. The overlapping complementary sequences allowed annealing of the two PCR products to each other, producing a continuous template which was amplified with the forward primer of DNA fragment #1 and the reverse primer of fragment #2. The resulting DNA fragment was gel purified (178).

### **2.2.3 Colony PCR**

Colony PCR was used to quickly screen transformants for the plasmid insert. Single colonies were picked with sterilized toothpicks and each suspended in 20 µl of deionized water, 3 µl of which were added to the PCR mixture. Prior to PCR cycling, samples were heated to 95 °C for 10 min to lyse cells.

### **2.2.4 Agarose gel electrophoresis**

DNA fragments were separated on 0.8-1 % agarose gels, depending on the size of DNA fragments. To load and track DNA samples, they were mixed with 6x Blue/Orange loading dye (Promega). Samples were run at 110 V for 25 min. A 1 kb DNA ladder (Promega) was used as molecular weight marker. Bands were visualized by UV illumination at 302 nm and photographed using the Alphamager® HP (ProteinSimple).

### **2.2.5 Agarose gel DNA extraction**

Separated DNA fragments were visualized with long wave UV light. The band of interest was excised and DNA was extracted and purified using the QIAquick® Gel Extraction kit according to the manufacturer's instructions.

### **2.2.6 Restriction digest of DNA**

DNA was digested with appropriate restriction endonucleases (0.4-5 U/g of DNA) in 20-70 µl reactions containing a compatible buffer, recommended and supplied by the enzyme manufacturer (New England Biolabs). DNA was digested for at least 1 h at the recommended temperature. PCR products were purified prior to restriction digest. Vectors that were digested for subsequent cloning were treated with 1 U of Shrimp

Alkaline Phosphatase for 1 h at 37 °C to dephosphorylate the 5'-ends. For downstream ligation, reactions were purified using the QIAquick® PCR purification kit.

### **2.2.7 DNA ligation**

Ligation reactions were set up in a volume of 10 µl, using 1 ul of T4 DNA ligase (5 U/µl). DNA concentration of cut vector and insert was estimated by gel electrophoresis of 3 ul of each, with a standard. Vector:insert ratios of 1:2 to 1:4 were used. Ligations were incubated for 1 h at RT or overnight at 15 °C. Double-digested and SAP-treated vector served as negative control.

### **2.2.8 Bacterial transformation**

DH5α or OneShot® TOP10 chemically competent *E. coli* cells were thawed on ice. Each ligation reaction (10 µl) was mixed with 12.5-50 µl of cells and incubated on ice for 5-10 min. Cells were heat-shocked for 30 s at 42 °C in a water bath and immediately cooled on ice for 2 min, followed by a recovery period in 250 µl warm SOC for 1 h at 37 °C and 220 rpm. The cell suspension was spread on LB agar plates containing 100 µg/µl ampicillin and incubated overnight at 37 °C.

### **2.2.9 Plasmid isolation**

Single colonies were picked, transferred into 4 ml of LB broth containing 100 µg/µl ampicillin and grown overnight at 37 °C and 220 rpm. Plasmid DNA from 3 ml of overnight *E. coli* culture was isolated using the QIAprep® Spin Miniprep Kit according to the manufacturer's protocol. Plasmid DNA was eluted in 50 µl water and stored at -20 °C. To prepare bacterial stocks, 800 µl of *E. coli* overnight culture were mixed with 200 µl of 75 % glycerol and stored at -80°C. For large-scale plasmid isolation from 200 ml of overnight *E. coli* cultures, the HiSpeed® Plasmid Maxi Kit was used. DNA concentration was determined with a NanoDrop® spectrophotometer. Plasmids were stored at -20 °C.

## **2.3 Animal work**

All animal work was conducted in accordance with Institutional Animal Care and Use Committee-approved protocols.

### **Injections**

Intraperitoneal (IP) injections were performed with 27-gauge needles. Intravenous injections were administered to lateral tail veins, using a Tailveiner® restrainer

(Braintree Scientific) and 1-ml insulin syringes with 29-gauge 1/2-inch needles. Prior to injection, mice were pre-warmed with a heat lamp for 5-10 min to promote venodilation. To prepare a blood smear, the tail vein was punctured with a 27-gauge needle and a small drop of blood was placed on a slide. Intradermal injections were performed by vivarium technicians.

#### **Anesthesia and euthanasia**

Mice were anesthetized by intraperitoneal injection of a ketamine/xylazine mixture (5 ml of 100 mg/ml Ketamine, 500  $\mu$ l of 100 mg/ml Xylazine, 34.5 ml of sterile PBS). A volume of 80  $\mu$ l per 10 g bodyweight was administered. Mice were kept on a heating pad until recovered from anesthesia or were subsequently euthanized by carbon dioxide exposure for several minutes.

#### **Terminal blood collection**

Cardiac puncture was used for terminal blood collection. It was performed quickly on freshly euthanized mice, either open- or close-chested using a heparinized 1-ml insulin syringe with a 27-gauge 5/8-needle.

### **2.4 *P. yoelii* methods**

#### **2.4.1 Giemsa staining**

To visualize blood-stage parasites, a thin smear of tail blood from an infected mouse was prepared and air-dried. The smear was fixed with 100 % methanol, air-dried, and stained with 10 % Giemsa stain in water for 20 min. The slide was rinsed with water, dried, and examined with a 100x oil immersion objective.

#### **2.4.2 Cryopreservation of *P. yoelii*-infected blood**

To prepare blood stocks, one volume of infected blood was mixed with two volumes of freezing solution (10 % glycerol in Alsever's solution) and stored in liquid nitrogen.

#### **2.4.3 Maintenance of the *P. yoelii* life cycle**

The entire life cycle of *P. yoelii* 17XNL parasites was reproduced by cycling between SW mice and female *Anopheles stephensi* mosquitoes.

*Anopheles stephensi* mosquitoes were from Seattle BioMed's internal insectary and were reared and maintained by the insectary staff. Adult mosquitoes were held in mesh-covered paper cups and were maintained on sugar water at a temperature of 24.5 °C, humidity of 70 % and with a photoperiod of 12.5 h light: 11.5 h dark.

To infect mosquitoes with *P. yoelii* parasites, a donor SW mouse was injected IP with infected blood from a thawed aliquot of cryopreserved stock. At a parasitemia between 2 % and 4 %, blood was collected, diluted with RPMI 1640 to 1 % parasitemia and injected IP into 2-3 naïve SW mice (200 µl per mouse). After three days, a drop of tail vein blood was examined for exflagellation of microgametocytes by microscopy at a 400x magnification.

Uninfected mosquitoes were fed on mice when at least 3 exflagellation events per field of view were observed. Mosquitoes were allowed to feed on anesthetized mice for 30 min. Subsequently, mice were euthanized. On day 14 or day 15 post infection, sporozoites were isolated from mosquito salivary glands and injected IV into naïve mice to keep the cycle going. Alternatively, infected mosquitoes were allowed to transmit sporozoites during a blood meal on anesthetized naïve mice.

#### **2.4.4 Evaluation of sporozoite loads in mosquitoes**

Ten days after the infectious blood meal, approximately 30 female mosquito midguts were dissected to evaluate the prevalence of oocysts and to determine mean numbers of oocyst-derived sporozoites per mosquito. Mosquitoes were collected in 70 % ethanol to kill and surface-sterilize them, followed by extensive rinsing with PBS. Dissection was performed on RPMI 1640-covered slides under a stereo microscope using syringe needles. Midguts were collected in cold RPMI 1640, ground with a polypropylene pestle and centrifuged at 800 rpm for 3 min at 4 °C to pellet mosquito debris. The supernatant containing the sporozoites was collected and kept on ice. A 10-µl aliquot of the supernatant was diluted 1:5 with RPMI 1640 and loaded into a hemocytometer. Sporozoites were allowed to settle for 10 min and were then counted using a phase-contrast microscope at 400x magnification. On day 14 or day 15 post infectious blood meal, salivary glands of at least 30 infected mosquitoes were isolated and sporozoite numbers were determined in the same manner as described above.

#### **2.4.5 Generation of transgenic *P. yoelii* parasites**

To generate transgenic *P. yoelii* parasites, the protocols of (179) and (180) were followed. The procedure is summarized in Figure 2.1 and is explained in detail in the following subsections.

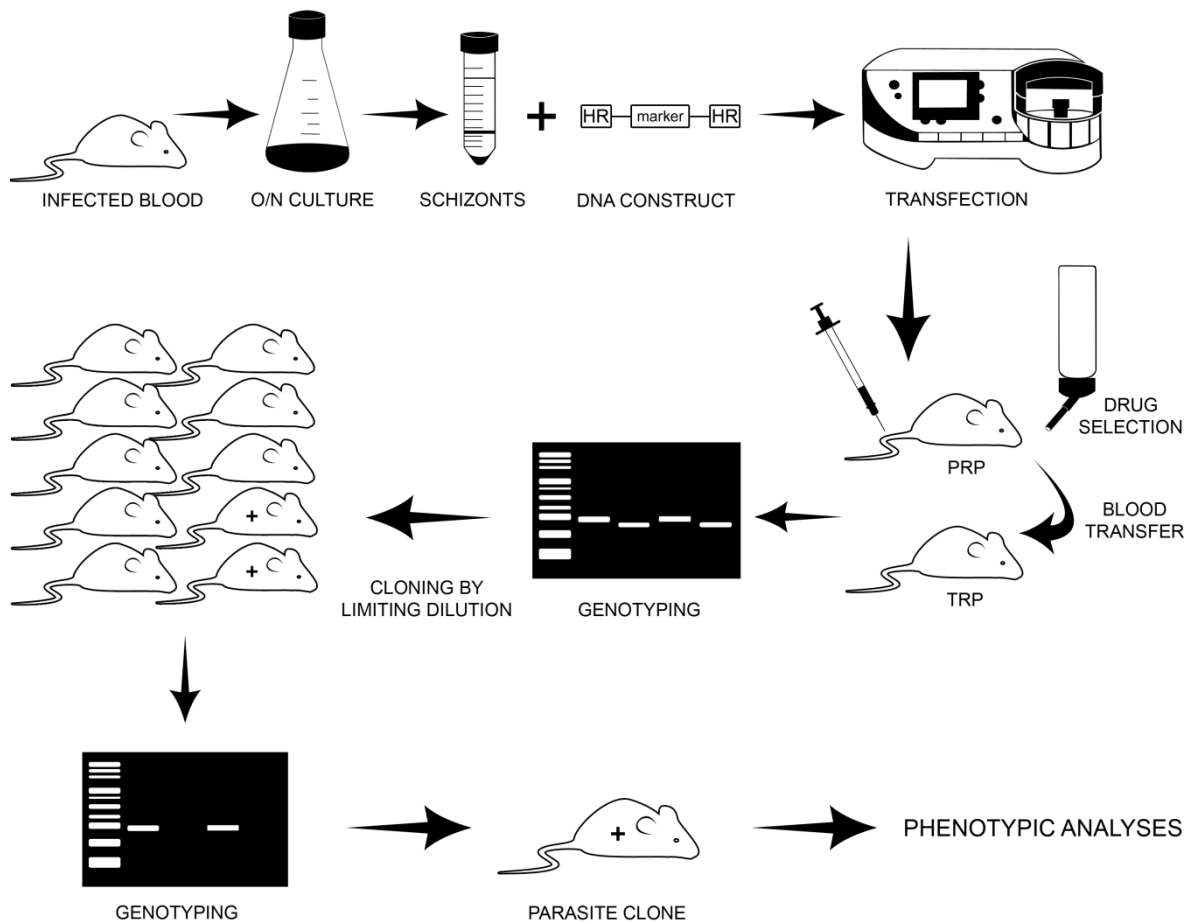


**Figure 2.1** Schematic procedure for the generation of transgenic *P. yoelii* parasites. *P. yoelii*-infected blood is cultured overnight (O/N). Mature schizonts are collected by density gradient centrifugation and transfected with a linear DNA construct containing a positive selectable marker cassette and homologous regions (HR) to the target locus. Transfected parasites are injected into the tail vein of mice. Transgenic parasites are selected by drug-administration in drinking water. The parental resistant population (PRP) is transferred to a new mouse to yield a rapidly expanding transfer resistant population (TRP). TRPs are drug-treated as well. Drug-resistant parasites are analyzed by PCR genotyping. Populations that contain a good proportion of transgenic parasites are used to isolate clones by limiting dilution cloning. Genomic DNA of clonal populations is analyzed by PCR. Clonal transgenic parasites are then studied.

#### 2.4.5.1 Cloning of transfection plasmids

Transfection plasmids used for this thesis were derived from plasmid pL0001 (MR4: MRA-770) and pL0005 (MR4: MRA-774), both originally created by Dr. Andy Waters (University of Glasgow, United Kingdom) and designed for targeted gene deletion and gene modification by single- or double-crossover recombination. pL0001 contains a selectable marker cassette that consists of a mutated version of the dihydrofolate thymidylate synthase (DHFR/TS) gene from *T. gondii* which confers resistance to pyrimethamine. The marker is constitutively expressed under the control of 5' and 3'

regulatory sequences of the *P. berghei* DHFR/TS gene. pL0005 contains a mutated version of the human DHFR gene which confers resistance to pyrimethamine and WR 99120. Marker expression is controlled by elongation factor 1  $\alpha$  promoter of *P. berghei* and 3' regulatory elements of the *P. berghei* DHFR/TS gene.

Generally, transfection plasmids were designed to replace the endogenous gene via double crossover homologous recombination. Two regions of the *P. yoelii* target locus were amplified by PCR with primers that added specific restriction sites and that contained overlapping complementary sequences to enable fusion of the fragments in a subsequent SOE PCR (178). The resulting DNA fragment was gel-purified, digested with the appropriate restriction enzymes, ligated into the cut vector and transformed into *E.coli*. Single colonies were screened by colony PCR. Colonies that tested positive were grown overnight in LB broth. Plasmid DNA was extracted and digested to confirm the presence of the insert. Plasmids were then sequenced. A clone with the correct DNA sequence was grown in a larger volume of LB broth to yield a sufficient quantity of plasmid DNA for parasite transfection.

#### 2.4.5.2 Plasmid preparation for transfection

Plasmid DNA was cut at a unique restriction site designed within the targeting sequence to yield a linear DNA construct with terminal regions that were homologous to the target. Sixty micrograms of plasmid DNA were digested overnight in a 500- $\mu$ l reaction containing the appropriate restriction enzyme and buffer. Linearized plasmid DNA was precipitated by adding 50  $\mu$ l of 3 M sodium acetate buffer solution and 500  $\mu$ l of isopropanol. The tube was inverted several times and then centrifuged at 13,200 rpm for 10 min at 4 °C. The DNA pellet was washed with 70 % ethanol and spun as above. Ethanol was carefully aspirated. The DNA pellet was briefly air-dried and then dissolved in 40  $\mu$ l of water. DNA concentration was measured. DNA was stored at -20 °C until transfection.

**Table 2.1** Primers used for cloning the targeting constructs. Restriction endonuclease (RE) sites are underlined.

Primer Name	Primer Sequence (5' → 3')	RE
<b>P38KO cloning</b>		
P38KO 3'F	AT <u>GATATCA</u> ACATCATAATAAAAGATGGGATGA	EcoRV
P38KO 3'R	TTTACAAAATATTATC <u>GGGCC</u> CATGGGAGTACTCCCTTTTACAATTA	Apal
P38KO 5'F	AGGGAGTACTCCCAT <u>GGGCC</u> GATAATTTGTAAAATGAGTGTGTGGT	Apal

## Materials and methods

P38KO 5'R	TACCGCGGATATTGTTGCTTAGGAGGATGAACA	SacII
<b>P38HA cloning</b>		
P38 prom F	TAATCCGCGGGATAATATTTGTAAAATGAGTGTGTGGT	SacII
P38 ORF no GPI R	TAATACCGGTTCTATAGTAAGATGTAGTTGAAACTTCT	AgeI
P38 GPI F	TAATATCGATTTCAGAGAGAACAACACTAGTAATGGTTTTGTTTTATTTTTAGT	Clal
P38 short 3'R	ATATGATATCATGGGAGTACTCCCTTTTTACAATTA	EcoRV
<b>2432KO cloning</b>		
2432KO 3'F	TAATGGTACCAGCAAACAATAAACACTTACGT	KpnI
2432KO 3'R	TAATTGGGCCCATTTGGAACACCCAAACGAAACA	Apal
2432KO 5'F	CCAATGGGCCCAATTAGCTGTTTGCATTTCGTA	Apal
2432KO 5'R	ATTAGCGGCCGCAACACTTGATTGGACATTGTA	NotI
<b>2432N-HA cloning</b>		
2432KO 3'F	TAATGGTACCAGCAAACAATAAACACTTACGT	KpnI
2432KO 3'R	TAATTGGGCCCATTTGGAACACCCAAACGAAACA	Apal
2432KO 5'F	CCAATGGGCCCAATTAGCTGTTTGCATTTCGTA	Apal
2432N-HA 5'R	TATTACCGGTCATTGTAAATGGATTTTTATTATATGATAT	AgeI
2432N-HA ORF F	TAATCTCGAGATGTCCAATCAAGTGTTAGAAACA	XhoI
2432 ORF stop R	TAATCTCGAGTTAAGGAAAAACTATAGCAGTAGGA	XhoI
<b>5332KO cloning</b>		
5332KO 3'F	ATCCGCGGTAAATAAACATTCATATTTATTTATTATATTC	SacII
5332KO 3'R	CTAAAAATAAGTGGCGGCCGCTTCGGCAGGTATGCCATATACG	EagI
5332KO 5'F	CCTGCCGAAGCGGCCGCCACTTATTTTTAGTATCATATCAATTC	EagI
5332KO 5'R	ATACTAGTAAAATATAGACATAATAAATGTTCCAATAAAAAATTG	SpeI
<b>5332C-HA cloning</b>		
5332HA 3'F	TAATCCGCGGTGCATTTCACACTTATTCATTT	SacII
5332HA 3'R	TACTTATCGGCCGTGGTACGTCGTTTGGTACATAA	EagI
5332HA mid ORF F	TACCACGGCCGATAAGTAAAGTTGGAATAGACGA	EagI
5332HA ORF no stop R	GTTCACTAGTTATTTCTGCTTCTTGTACTTTTTGAT	SpeI
<b>6766KO cloning</b>		
6766KO 3'F	TAATGGTACCAGAAACAAAATGACTACAAGGCA	KpnI
6766KO 3'R	ATGCGGGCCCATCCGAATTCGCATAAGTGTA	Apal
6766KO 5'F	GGATGGGCCCTCCTTAAACATAAAAATCAGATAGCTT	Apal
6766KO 5'R	ATTAGCGGCCGCATAGCAAAACAACATAATACAGCA	NotI
<b>6766C-HA cloning</b>		
6766HA 3'F	CCGGTACCGCCTATGAGCGTAATATTTCTCATATTTCTTTTTGTTGGTATTC	KpnI
6766HA 3'R	TTTCGTGGGGCCAGCTAGCGATTATAGGTATGTGAATTTACCGTAATGGGATTTTCCC	Apal
6766HA 5'F	TCGCTAGCTGGGCCCCACGAAAACATTTTGTATGAATGTATATGTATATATTAAGAC	Apal
6766HA ORF R	GGICTAGATGCCTTGTAGTCATTTTGTCTGTCTGATTATCAACTATCTTC	XbaI
<b>S23C-Myc cloning</b>		
1796myc 3'F	ATCCGCGGGATTCCATAGAACATGCAAATAATGG	SacII
1796myc 3'R	CATTTACTAATGGGCGGCCGATAAATTGTATAGAAACATGATTCGTAC	EagI
1796myc 5'F	GTTTCTATACAATTTATCGGCCGCCATTAGTAAATGAAACAGATATTA	EagI
1796myc 5'R	ATACTAGTTTTAATATTTGTATCGTAAGAAATGAAAG	SpeI

## Materials and methods

<b>S23nHA-cMyc cloning</b>		
1796myc 3'F	ATCCGCGGGATTCCATAGAACATGCAAATAATGG	SacI
1796nHA 3'R	GGGTATAGGCGGCCGATAAATTGTATAGAAACATGATTCGTAC	EagI
1796nHA 5'F	ACAATTTATCGGCCGCTATACCCCAAATGTTTCGGTG	EagI
1796nHA SP R	TAATACCGGTATCCCCTTTGACAGGGGTATAAAAAATA	AgeI
1796nHA ORF F	TAATCTCGAGGGATATATATGTGACTTTTCTGCAGA	XhoI
1796myc 5'R	ATACTAGITTTAATATTTGTATCGTAAGAAATGAAAG	SpeI
<b>S23KO cloning</b>		
1796KO 3'F	GCGGTACCTTCCATAGAACATGCAAATAATGGA	KpnI
1796KO 3'R	AATTTGTTTACTGTCAGGCACATCACATAATATGCAAATGGG	SbfI
1796KO 5'F	ATGTGATGTGCCTGCAGGTAAACAAATTATATCGAATCATTTTCAG	SbfI
1796KO 5'R	CGGCGGCCGCGCCGAAATTTATATTAATATACACAG	NotI

**Table 2.2** Primers used for genotyping transgenic parasites.

Primer Name	Primer Sequence (5' → 3')	Primer Pair
<b>P38KO genotyping</b>		
P38KO test 1 F	TTAGCTATCTCATTGGACATGCA	Test 1
T7 R (b3D)	TAATACGACTCACTATAGGG	
P38KO test 2 R	TGTTTGACACTTATACATATTATGTCT	Test 2
Tg F (b3D)	GGCTACGTCCCGCACGGACGAATCCAGA	
P38 test wt F	ACAGTCGATTTAGCCACTTATGAGAA	Test wt
P38 test wt R	ACCATCCATGGTTATAGCTGTAGATGT	
<b>P38HA genotyping</b>		
P38KO test 1 F	TTAGCTATCTCATTGGACATGCA	Test 1
MCS-1 (pDEF)	AGCTCGAATTCAGTGGCCGT	
P38KO test 2 R	TGTTTGACACTTATACATATTATGTCT	Test 2
MCS-4 (pDEF)	TACCGCACAGATGCGTAAGGAG	
P38KO test 1 F	TTAGCTATCTCATTGGACATGCA	Test wt
P38KO test 2 R	TGTTTGACACTTATACATATTATGTCT	
<b>2432KO genotyping</b>		
2432 test 1 F	GCGTCTATTTCAATGTTCTTATAT	Test 1
pDEF-GFP662 R	TGCCATTAACATCACCATCTA	
2432KO test 2 R	ATAATGTAATTCAACCAGTAGAGA	Test 2
pDEF3790 F	AGGAGAAAGGCATTAAGTACA	
2432 test wt F	ATAATGAACATGAATCGTCCA	Test wt
2432 test wt R	GAAGTTTTGCTTCCATTCTCAT	
<b>2432N-HA genotyping</b>		
2432KO test 1 F	GCGTCTATTTCAATGTTCTTATAT	Test 1
MCS-4	TACCGCACAGATGCGTAAGGAG	
2432KO test 2 R	ATAATGTAATTCAACCAGTAGAGA	Test 2
pDEF3790 F	AGGAGAAAGGCATTAAGTACA	
2432 test wt F	ATAATGAACATGAATCGTCCA	Test wt
2432KO 3'R	TAATTGGGCCATTGGAACACCCAAACGAAACA	
<b>5332KO genotyping</b>		

## Materials and methods

5332 test 1 F	GTAATATGTATCGTGAAATGACAC	Test 1
pDEF-GFP662 R	TGCCATTAACATCACCATCTA	
5332KO test 2 R	GCAAAAATAATCAGTAATAATAAGCTG	Test 2
pDEF3790 F	AGGAGAAAGGCATTAAGTACA	
5332 test wt F	AATAGTCAGTAATGCCTGTCTGGC	Test wt
5332 test wt R	GCCCCAACAACTTTATATTCTTCTG	
<b>5332C-HA genotyping</b>		
5332 test wt F	AATAGTCAGTAATGCCTGTCTGGC	Test 1
MCS-4	TACCGCACAGATGCGTAAGGAG	
5332HA test 2 R	TAAAGTTTGTATTATTTTCTCCCT	Test 2
pDEF3790 F	AGGAGAAAGGCATTAAGTACA	
5332 test wt F	AATAGTCAGTAATGCCTGTCTGGC	Test wt
5332KO test 2 R	GCAAAAATAATCAGTAATAATAAGCTG	
<b>6766KO genotyping</b>		
6766KO test 1 F	ATGTTTGTTTAATTCAGGACGT	Test 1
pDEF-GFP662 R	TGCCATTAACATCACCATCTA	
6766KO test 2 R	TAACAACTTAGTTATTCCATCGAGT	Test 2
pDEF3790 F	AGGAGAAAGGCATTAAGTACA	
6766 test wt F	ATCATTTATTCTTATTTTGGTGCT	Test wt
6766 test wt R	TCAACTATCTTCTTTCTCCTTACT	
<b>6766C-HA genotyping</b>		
6766KO 5'F	GGATGGGCCCTCCTTAAACATAAAATCAGATAGCTT	Test 1
MCS-4	TACCGCACAGATGCGTAAGGAG	
pDEF3790 F	AGGAGAAAGGCATTAAGTACA	Test 2
6766HA test R	GGTTACGAATAATTGACACTAACTGATGGAGTGTTTTATAAACTATTAACATCGAAAGC	
6766KO 3'F	TAATGGTACCCAGAACAAAATGACTACAAGGCA	Test wt
6766HA 3'R	TTTCGTGGGGCCAGCTAGCGATTATAGGTATGTGTAATTTACCGTAATGGGATTTCCC	
<b>S23C-Myc genotyping</b>		
1796KO 5'F	ATGTGATGTGCCTGCAGGTAACAAATTATATCGAATCATTTTCAG	Test 1
MCS-4	TACCGCACAGATGCGTAAGGAG	
pDEF3790 F	AGGAGAAAGGCATTAAGTACA	Test 2
1796myc test 2 R	AAGTTGGGAACTGCAATATGA	
1796 wt test F	TATGTGAGCATGAAATAGGGAAT	Test wt
1796myc test 2 R	AAGTTGGGAACTGCAATATGA	
<b>S23nHA-cMyc genotyping</b>		
1796nHA 5'test F	TGGTTATGCAATAATAACAGAAGACA	Test 1
3rdHA R	AGCGTAATCTGGAACGTCGT	
1796nHA test 2 R	AAGTTGGGAACTGCAATATGA	Test 2
pDEF3790 F	AGGAGAAAGGCATTAAGTACA	
1796nHA wt test F	AATAATGTTCAATATACTGAGCAAGGA	Test wt
1796nHA test 2 R	AAGTTGGGAACTGCAATATGA	
<b>S23KO genotyping</b>		
1796KO test 1 F	CCTATACCCCAAATGTTTCGGTG	Test 1

pDEF-GFP662 R	TGCCCATTAACATCACCATCTA	
1796KO test 2 R	TAAATTGTATAGAAACATGATTTCGTAC	Test 2
pDEF3790 F	AGGAGAAAAGGCATTAAGTACA	
1796 wt test F	GGATATATATGTGACTTTTCTGCAG	Test wt
1796 wt test R	AAATGAAAGGGTTAGAAGGTTTCAC	
<b>Real-time PCR</b>		
Py18S F	GGGGATTGGTTTTGACGTTTTTGCG	18S
Py18S R	AAGCATTAAATAAAGCGAATACATCCTTAT	
Mouse GAPDH F	CCTCAACTACATGGTTTACAT	GAPDH
Mouse GAPDH R	GCTCCTGGAAGATGGTGATG	

#### 2.4.5.3 Preparation of recipient *P. yoelii* parasites

Three to five naïve SW mice were infected with *P. yoelii* parasites. Blood was collected by cardiac puncture when parasitemia was between 1 % and 3 % and was immediately transferred to a 50 ml falcon tube containing 10 ml of culture medium (section 2.1.6) and 0.25 ml heparin solution (200 U/ml), pre-warmed to 37 °C. The suspension was centrifuged for 8 min in a swinging bucket centrifuge at 200 g at RT. The RBC pellet was carefully resuspended in 50 ml warm culture medium and transferred to a 1000 ml polycarbonate Erlenmeyer flask (Corning) containing 100 ml of pre-warmed culture medium. Parasites were cultured with a gas mixture of 10 % O<sub>2</sub>, 5 % CO<sub>2</sub> and 85 % N<sub>2</sub>, and were gently shaken (80 rpm) at 37 °C for 12 h, during which the majority of the parasites mature into schizonts. The intraerythrocytic cycle of *P. yoelii* takes 18-20 h but mature schizonts do not rupture *in vitro* thus leading to an enrichment of schizonts. The quality of the *in vitro* culture was evaluated by a Giemsa-stained blood smear. Mature schizonts were separated from uninfected erythrocytes by Accudenz® density gradient centrifugation. Thirty milliliters of Accudenz® stock solution were mixed with 20 ml of magnesium- and calcium-free PBS to obtain a 60 % density gradient solution. The culture suspension was split into four 50 ml falcon tubes (~35 ml each) and 10 ml of gradient solution were carefully added to the bottom of each tube and centrifuged for 25 min in a swinging bucket rotor at 200 g (no brake) at RT. Schizonts were collected at the interphase with Pasteur pipettes and pelleted by centrifugation for 10 min at 200 g. Schizonts were resuspended in 10 µl culture medium per transfection.

#### 2.4.5.4 Transfection of *P. yoelii* schizonts

Transfection was performed using the Nucleofector® device and the Human T Cell Nucleofector® kit. One hundred microliters of Nucleofector® solution pre-warmed to RT

were mixed with 5-10 µg of linearized plasmid DNA and 10 µl of schizont suspension. The mixture was transferred to a cuvette and parasites were transfected using Nucleofector® program U-33. Subsequently, 50 µl of pre-warmed (37 °C) culture medium were added. Quickly, the solution was injected into the tail vein of a naïve female Swiss Webster mouse.

#### **2.4.5.5 Parasite selection**

Starting 24 h post transfection, pyrimethamine was administered to mice in drinking water (70 µg/ml) to select for transfected parasites. Blood was daily examined for parasites by microscopy. On the day of detection of parasites (generally between day 4 and day 6 post transfection), blood was collected by cardiac puncture and 50-100 µl were transferred to a naïve SW mouse to yield a rapidly expanding transfer resistant population. Mice were treated with pyrimethamine until terminal bleeding.

#### **2.4.5.6 Parasite cloning**

Transgenic parasites were cloned by limiting dilution to obtain single clones. A SW mouse was infected with the transfer resistant population and was bled at a parasitemia of 0.4 – 1 %. The number of parasites per microliter mouse blood ( $\sim 7 \times 10^6$  RBCs/µl) was calculated and blood was diluted with RPMI 1640 by serial 10-fold dilutions to obtain a solution that contained less than 0.1 parasite/µl. Ten to fifteen SW mice were injected intravenously each with 1-2 parasites in a volume of 100 µl. Starting 4 days after injection, blood smears were examined for parasites. Blood stage-positive mice were euthanized at a parasitemia of more than 1 % to prepare frozen stocks and to extract genomic DNA for PCR genotyping or Southern blot analysis.

#### **2.4.6 Extraction of genomic DNA from *P. yoelii* blood stages**

Blood of an infected mouse was mixed with 10 ml PBS. To remove white blood cells, the suspension was loaded onto a CF11 cellulose column and allowed to pass through by gravity flow. The column was washed with PBS to obtain a final filtrate volume of approximately 10 ml. To lyse red blood cells, 1 ml of 2 % saponin in PBS was added to the filtrate. Lysis was allowed to proceed for 10 min at RT. Liberated parasites were pelleted by centrifugation for 10 min at 3,000 rpm. The pellet was repeatedly washed with PBS until supernatant was clear. The resulting parasite pellet was resuspended in 200 µl or 400 µl of PBS, depending on the pellet size. Parasite lysis and DNA extraction

were performed using QIAamp® DNA Blood Mini Kit according to the manufacturer's protocol. Parasite genomic DNA was eluted with 200 µl water and stored at -20 °C.

DNA of transgenic parasites was analyzed by PCR using the primers listed in Table 2.1. To test if the transfection construct had integrated, primer combinations were chosen that were specific to the recombinant locus. More specifically, a primer that annealed within the vector backbone was combined with a primer that annealed upstream or downstream of the regions used for homologous recombination. Primers specific to the wild type locus were used to test for residual wild type parasites within the pyrimethamine-resistant parasite population. Genomic DNA from wild type parasites served as control.

#### **2.4.7 Southern blot of genomic DNA from *P. yoelii* blood stages**

Genomic DNA (1-5 µg) from *P. yoelii* blood stages was digested with selected restriction enzymes and separated by gel electrophoresis on a 0.8 % agarose gel overnight at 15 V. The gel was stained with ethidium bromide for 10 min to visualize DNA, imaged, and subsequently destained with water for 15 min. To depurinate DNA, the gel was submerged in 0.125 M HCl and incubated for 20 min with gentle shaking, followed by treatment with 1.5 M NaCl/0.5 M NaOH for 30 min to denature DNA. To neutralize the DNA, the gel was submerged in 0.5 M Tris-HCl (pH8.0)/1.5 M NaCl and incubated for 30 min with gentle shaking. DNA was transferred onto nylon membrane (Roche) via capillary forces using paper towels and 20x saline-sodium citrate (SSC) buffer. Following transfer, the membrane was rinsed with 2x SSC and DNA was UV-crosslinked to the membrane with a UV Stratalinker® (auto-crosslink setting). Probes were digoxigenin (DIG)-labeled using the DIG DNA labeling kit from Roche. DIG-incorporation was evaluated by agarose gel electrophoresis of labeled and unlabeled probes. Successful DIG-incorporation resulted in a band shift. For hybridization of the probe, the membrane was first pre-incubated in DIG Easy Hyb™ buffer (Roche) for 15 min at 42 °C. Meanwhile, DIG-labeled probes were denatured at 95 °C for 5 min and were then immediately chilled on ice. Denatured probes were added to the hybridization buffer and membranes were hybridized overnight at 42 °C. Membranes were washed and blocked using the DIG Wash and Block Buffer Set (Roche) according to the manufacturer's instructions. Probes were immunodetected with an anti-digoxigenin antibody conjugated to alkaline phosphatase (Roche) and were visualized with the chemiluminescent substrate CSPD® (Roche).

## 2.5 Cell biological assays

### 2.5.1 Blood stage parasite growth curve

Blood from SW mice infected with *P. yoelii* parasites was harvested, diluted with RPMI 1640 and was used to infect naïve SW mice for blood stage growth analysis. One hundred  $\mu\text{l}$  of diluted blood containing  $1 \times 10^6$  infected red blood cells were injected intravenously into each SW mouse ( $n = 5$  per experimental group). Parasitemia was determined by counting parasites in Giemsa-stained thin blood smears daily until parasites were cleared by the mouse immune system.

### 2.5.2 Sporozoite gliding motility assay

Coverslips were precoated with anti-CSP antibodies ( $10 \mu\text{g/ml}$  in PBS) overnight at RT, and then washed three times with PBS. *P. yoelii* salivary gland sporozoites ( $3 \times 10^4$ ) were activated with 20 % FBS-RPMI 1640 and added to the precoated coverslips. Sporozoites were allowed to glide for 1 h at  $37^\circ\text{C}$ , the medium was then removed, and sporozoites were fixed with 4 % PFA for 10 min, washed with PBS, and blocked with 3 % BSA-PBS for 45 min. To visualize the CSP-containing trails, coverslips were incubated with Alexa Fluor<sup>®</sup>488-conjugated anti-CSP antibodies for 30 min. Sporozoites were washed with PBS and mounted with ProLong<sup>®</sup> Gold Antifade Reagent. Trails were analyzed using a fluorescence microscope. To evaluate gliding motility, the number of circles per trail associated with sporozoites was counted in random fields of view with a 60x objective. Trails were categorized into trails with 0-2 circles, 3-10 circles and more than 10 circles. At least 100 trails were analyzed. To assess if differences between control and transgenic sporozoites were significant, the two-tailed unpaired t-test was used.

### 2.5.3 Sporozoite cell traversal and invasion assay

Isolated salivary gland sporozoites were activated for 20 min in 20 % FBS-PBS at RT. One hundred thousand sporozoites per well were added to  $3 \times 10^5$  Hepa 1-6 cells in the presence of 1 mg/ml FITC-labeled dextran (10,000 MW, lysine-fixable; Invitrogen). Sporozoites were allowed to invade for 1.5 h at  $37^\circ\text{C}$ . Cells were then washed with PBS, trypsinized, fixed and permeabilized with Cytofix/Cytoperm buffer (BD Biosciences). Cells were washed with PBS and blocked with Cytoperm/Cytowash buffer (BD Biosciences) supplemented with 2 % BSA for 10 min. Cells were then stained with Alexa

Fluor®647-conjugated CSP antibodies in Cytoperm/Cytowash buffer for 1 h, washed, and analyzed by flow cytometry using a BD-LSRII flow cytometer (BD Biosciences).

Hepa1-6 cells were cultured under standard conditions by Alyse N. Douglass who also assisted with flow cytometry analysis.

#### **2.5.4 *In vivo* sporozoite infection assays**

Sporozoites were isolated from mosquito salivary glands at day 14 or day 15 post infectious blood meal. Sporozoites were injected either intradermally (ID) or intravenously (IV) into the tail vein of BALB/cJ mice. For delivery of sporozoites via infectious mosquito bite, BALB/cJ mice (n = 5) were anesthetized and individually exposed to the bites of 12-15 sporozoite-infected mosquitoes. Mosquitoes were allowed to feed for a total time of 7.5 min. Mice were rotated between mosquito cages every 1.5-2 min. Salivary glands of blood-fed mosquitoes were then isolated to reassure the presence of sporozoites and to determine sporozoite loads.

The time to blood stage patency was determined by microscopic analysis of approximately  $1 \times 10^4$  red blood cells in Giemsa-stained thin blood smears. Smears were considered positive when more than one parasite was detected.

#### **2.5.5 Liver stage burden by quantitative real-time PCR**

Female BALB/cJ mice (n = 5) were intravenously injected with  $1 \times 10^5$  salivary gland sporozoites. Livers were harvested 44 h post injection and homogenized in TRIzol® reagent (Invitrogen). Total RNA was extracted using the Direct-zol™ RNA MiniPrep Kit (Zymo Research). cDNA was synthesized from 1 µg total RNA using the QuantiTect® Reverse Transcription Kit (Qiagen) according to the manufacturer's instructions. Reactions in which reverse transcriptase was omitted served as negative control. Synthesized cDNA was diluted 1:5 with nuclease-free water, and 2 µl of diluted cDNA was used as template for quantitative RT PCR. PCR was carried out in triplicate on each cDNA sample using the POWER SYBR® green master mix and the 7300 real-time thermal cycler (both from Applied Biosystems). Parasite DNA was detected using primers specific to the *P. yoelii* 18s rRNA gene while mouse DNA was detected by primers that annealed within the glyceraldehyde-3-phosphate dehydrogenase (GAPDH) gene (181). PCR cycling conditions were as follows: 2 min at 50 °C, 15 min at 95 °C, 40 cycles of 15 s at 95 °C and 1 min at 60 °C, followed by a dissociation curve to verify

specific amplification. Relative transcript quantification was determined using the  $2^{-\Delta\Delta Ct}$  method.

## **2.5.6 Immunofluorescence assays**

### **2.5.6.1 Sporozoites**

The staining procedure was performed at RT. Isolated sporozoites were fixed with 4 % paraformaldehyde (PFA) for 10 min. Sporozoites were washed twice with PBS, permeabilized with 0.1 % Triton X-100 in PBS for 10 min and blocked with 3 % BSA in PBS for at least 45 min. Sporozoites were then incubated with blocking buffer containing the properly diluted primary antibodies for 1 h. Sporozoites were then washed three times with PBS and incubated with AlexaFluor®-conjugated secondary antibodies in blocking buffer for 30 min. Sporozoites were washed, incubated with 0.5 µg/ml DAPI in PBS for 5 min, washed again and mounted. In live stainings, live sporozoites were incubated with primary antibodies in 3 % BSA-RPMI for 1 h at RT. Sporozoites were then washed twice with PBS, fixed with 4 % PFA for 10 min, and blocked and stained as above.

### **2.5.6.2 Blood stages**

All of the following incubation steps were performed at RT with end-over-end rotation. Infected mouse blood was harvested and centrifuged for 30 s at 4,000 rpm to pellet red blood cells. Cells were washed twice with PBS and then fixed with 4 % PFA (methanol-free) and 0.0075 % glutaraldehyde in PBS for 30 min. Cells were washed twice with PBS, permeabilized with 0.1 % Triton X-100 in PBS for 10 min, washed with PBS and blocked with 3 % BSA in PBS for at least 1 h. Cells were stained with primary antibodies in blocking buffer for 1 h or overnight at 4 °C. After three washes with PBS, cells were incubated with AlexaFluor®-conjugated secondary antibodies for 30 min to 1 h. Nuclei were stained with DAPI for 5 min. Cells were washed, resuspended in PBS and applied to a glass slide. A drop of mounting medium was mixed with cells to homogeneity before adding a cover glass.

Fluorescent and differential interference contrast (DIC) images were acquired using either the Olympus IX70 DeltaVision microscope equipped with deconvolution software or the Nikon Eclipse E600 fluorescence microscope MetaMorph® software (Molecular Devices).

### **2.5.7 Immunoelectron microscopy**

Infected salivary glands were carefully isolated from mosquitoes by slowly pulling the head away from the thorax using syringe needles. Salivary glands attached to the head were then cut off and collected in cold PBS. Glands were fixed with 1 % PFA/0.2 % glutaraldehyde in PBS for 20 min on ice with frequent agitation. Glands were then washed with PBS (3x10 min) and stored in 4 % sucrose in PBS at 4 °C until shipped to Motomi Torii (Ehime University Graduate School of Medicine, Ehime, Japan) who processed the glands for immunoelectron microscopy and examined them. Briefly, glands were embedded in LR White resin (Polysciences). Ultra-thin sections were blocked for 30 min in PBS-milk-Tween 20 and were then incubated with primary antibodies (mouse anti-S23 or mouse anti-HA) in blocking buffer overnight at 4 °C. After multiple washes, sections were incubated for 1 h with blocking buffer that contained goat anti-mouse IgG conjugated with gold particles (15 nm diameter; British BioCell International). After staining with 2 % uranyl acetate and lead citrate, sections were examined with a JEM-1230 electron microscope (JEOL, Japan).

## **2.6 Biochemical techniques**

### **2.6.1 Western blot**

For sporozoite lysates, sporozoites were isolated from mosquito midguts or salivary glands. Sporozoites were pelleted at 13,200 rpm for 2 min and resuspended in lysis buffer (M-PER® buffer and protease inhibitors). Lysis was allowed to proceed for 30 min on ice. For blood-stage parasite lysates, infected blood was harvested, washed with PBS and red blood cells were pelleted by centrifugation at 4000 rpm (~1400 g) for 1 min. The pellet was resuspended in 0.2 % saponin in PBS to lyse red blood cells. Liberated parasites were pelleted at 4000 rpm for 2 min, resuspended in lysis buffer (as above) and incubated on ice for 30 min. The lysate was spun at 13,200 rpm for 10 min to pellet cell debris. A lane marker and 5 %  $\beta$ -mercaptoethanol were added to lysates and samples were boiled for 5 min at 95 °C. The addition of  $\beta$ -mercaptoethanol and the boiling step were omitted when samples were run under non-reducing conditions. Proteins were separated by SDS-PAGE on 4-20 % gradient gels (Precise™ Protein Gels, Pierce) for 45 min at a constant voltage of 120 V, using BupH Tris-HEPES-SDS running buffer (Pierce). Proteins were transferred onto PVDF membrane at a constant voltage of 30 V overnight, using BupH Tris-Glycine buffer (Pierce). The membrane was blocked

with 5 % milk in 0.1 % Tween20-PBS (PBST) for 1 h at RT with shaking. The membrane was then probed with primary antibodies diluted in blocking buffer for at least 1 h at RT or overnight at 4 °C. After multiple washes with PBST, the membrane was incubated with either IRDye® secondary antibodies (LI-COR Biosciences) or HRP-conjugated antibodies in blocking buffer for 1 h at RT. Proteins were visualized either by Odyssey Infrared Imaging System (LI-COR Biosciences) or by chemiluminescence. To strip and re-probe membranes, Restore™ Western Blot Stripping Buffer (Pierce) was used according to the manufacturer's instructions.

### **2.6.2 Surface biotinylation of sporozoites**

As described in (182), salivary gland sporozoites ( $4-6 \times 10^6$ ) purified over an Accudenz® cushion(183) were washed in cold PBS (pH 8.0 at 4 °C) and incubated with 2 mM EZ-Link Sulfo-NHS-LC-Biotin (Thermo Scientific) for 30 min at RT. The biotinylation reaction was quenched by adding glycine to a final concentration of 100 mM. Sporozoites were further washed in 100 mM glycine in cold PBS (pH 8.0 at 4 °C), and were lysed for one hour on ice in a solution comprised of 0.1 % SDS, 4 M Urea, 150 mM NaCl, 50 mM Tris-HCl (pH 8.0 at 22 °C) and protease inhibitors (Complete Mini, Roche). The lysate was centrifuged at 16,300 g for 10 min at 4 °C to pellet cell debris. The supernatant was diluted 10-fold with a similar solution as above, but which lacked urea. The lysate was incubated with Dynabeads MyOne™ Streptavidin T1 (Invitrogen) for one hour at 4 °C with end-over-end rotation. The beads were then washed in 0.1 % SDS, 400 mM Urea, 150 mM NaCl and 50 mM Tris-HCl (pH 8.0 at 22 °C). Proteins were eluted from the beads by boiling for 5 minutes in 1x sample buffer (25 mM Tris (pH 6.8 at RT), 2.5 % w/v SDS, 2.5 % v/v glycerol, 0.08 % w/v bromophenol blue, 5 % beta-mercaptoethanol (added fresh immediately before use)). Proteins were assessed for biotinylation by Western blotting using standard methods with streptavidin-conjugated horseradish peroxidase (HRP) or antibodies against PyCSP (monoclonal, 2F6) or PfCSP (monoclonal, 2A10) with an HRP-conjugated anti-mouse IgG secondary antibody. Samples were visualized by enhanced chemiluminescence (SuperSignal West Pico, Thermo Scientific). Samples were stored at -20 °C until processed further by mass spectrometry which was performed by Kristian Swearingen (Robert Moritz' group, Insitute for Systems Biology, USA). Data analysis was carried out by Kristian Swearingen and Scott E. Lindner (previously in the group of Stefan Kappe at Seattle BioMed; currently at Pennsylvania State University, USA).

### **2.6.3 Recombinant S23 expression and antiserum production**

Recombinant protein was produced in HEK293F cells by Noah Sather and colleagues (Seattle BioMed, USA). The putative endogenous leader peptide (amino acid residues 1-22) of PyS23 was removed and replaced with the human tissue plasminogen signal peptide (MDAMKRGLCCVLLLCGAVFVSPSAS) to optimize protein expression in mammalian cells. Additionally, the predicted transmembrane domain and the putative cytoplasmic tail were removed, leaving a final expression construct containing amino acid positions 23-386. For purification purposes, a glycine-serine linker, 6-Histidine tag, and AviTag (GGSGHHHHHGLNDIFEAQKIEWHE) were added to the C-terminus of the expressed sequence. The resultant sequence was codon-optimized for expression in mammalian cell culture and cloned into the pTT3 vector (184), placing the coding sequence under the control of the CMV promoter (185). The soluble protein was produced in HEK293F cells adapted for suspension culture under serum-free conditions, as previously described (186). PyS23-encoding DNA was transfected into HEK293F cells using 293-Free Transfection Reagent (Life Technologies). For one liter of production culture, 500 µg of plasmid DNA were mixed with 1 ml 293-Free Transfection Reagent in 40 ml PBS, which was allowed to complex for 15 min at 25 °C. The DNA/293-Free mixture was added to 1 l of HEK293F cells at a density of  $1 \times 10^6$  cells/ml in FreeStyle 293 Expression Medium (Life Technologies). The culture was allowed to grow at 37 °C with shaking for six days. After harvest, the cells were removed by centrifugation and imidazole was added to the supernatant at a final concentration of 10 mM. Protein was purified by a two-step chromatography protocol. First, the supernatant was passed over a HisTrap FF nickel affinity column (GE Healthcare) and the His-tagged proteins were eluted in 20 mM sodium phosphate, 0.5 M sodium chloride and 0.5 M imidazole. The proteins were separated by size exclusion chromatography on a HiLoad 16/60 Superdex 200 column (GE Healthcare). The fractions containing monomeric PyS23 were collected and concentrated for final storage in PBS at pH 7.4. The final purified protein products were analyzed by native-PAGE and SDS-PAGE for size and purity (Appendix C, Figure C.3).

For production of specific antiserum, 25 µg of purified PyS23 were suspended in TiterMax Gold adjuvant (Sigma-Aldrich) and subcutaneously injected into BALB/c mice. Two boosters of 25 µg each in TiterMax Gold adjuvant were given at two and six weeks after the first immunization. Two weeks after the second boost, blood was

collected and serum was isolated by centrifugation of blood at 9600 rpm for 10 min at 4 °C. Generation of antisera was performed by Brandon Sack (Seattle BioMed).

## 3 Results

### 3.1 Functional analysis of the 6-Cys protein P38 in *P. yoelii*

P38 is a member of the conserved *Plasmodium* 6-Cys protein family, which contains candidates for transmission-blocking vaccines and pre-erythrocytic GAP vaccines (50,144,166). P38 is a blood stage antigen of unknown function located on the surface of *P. falciparum* merozoites (161). P38 is also expressed in sporozoites (176,182) but its subcellular localization and function in these stages has not been previously analyzed. In this study, epitope-tagging and reverse genetics are used to fill this knowledge gap.

#### 3.1.1 *P. yoelii* P38

*P. yoelii* (Py) P38 is encoded by a single-exon gene (PlasmoDB ID: PY02738) and contains an N-terminal signal peptide (SP), followed by two 6-Cys domains and a hydrophobic region at the very C-terminus, which is potentially replaced by a glycosylphosphatidylinositol (GPI) anchor (161,187,188). The N-terminal 6-Cys domain contains only the last four positionally conserved cysteine residues whereas the second domain contains all six. The protein has a predicted molecular mass of approximately 34 kDa, excluding the SP and the GPI signal sequence. P38 is conserved throughout the *Plasmodium* genus; it shares 78 % amino acid identity with *P. berghei* P38 and 39 % and 40 % with the orthologs in the human parasites *P. falciparum* and *P. vivax*, respectively (Appendix A).

#### 3.1.2 Generation of parasites expressing epitope-tagged P38

In order to investigate the subcellular localization of P38 in *P. yoelii*, transgenic parasites were generated that express an epitope-tagged copy of P38. Because P38 potentially undergoes post-translational modification at the C-terminus, the tag was introduced upstream of the predicted GPI modification site (Figure 3.1A, Appendix A). The tagging vector was designed to integrate into the 5' untranslated region (UTR) of the *P38* open reading frame (ORF) via single crossover homologous recombination, yielding parasites with two copies of *P38* – the tagged and the endogenous copy (Figure 3.1B). To do this, a DNA fragment consisting of 720 bp of the 5' UTR of *P38* and the *P38* ORF without the GPI signal sequence was cloned into the transfection plasmid, which contains a pyrimethamine-resistance cassette. A triple hemagglutinin (HA) tag was then

added in frame to the truncated *P38* ORF, followed by the *P38* C-terminus and a part of its 3' UTR. To prepare the plasmid for parasite transfection, it was linearized with the endonuclease *PacI*, which cuts at a unique endogenous restriction site within the 5' UTR. After transfection of *P. yoelii* 17XNL (non-lethal) blood-stage schizonts and selection of pyrimethamine-resistant parasites, genomic DNA (gDNA) was extracted to test for the presence of the integrated plasmid. PCRs with primer pairs specific to the 5' and 3' integration sites resulted in DNA fragments of the expected size (Figure 3.1C). To test if the resistant parasite population contained residual wild type (WT) parasites, primers that annealed upstream and downstream of the *P38* target region were used. Theoretically, these primers could amplify the complete transgenic locus but the short extension time of the PCR allowed amplification only if the plasmid had not integrated. The PCR yielded the expected DNA fragment in the WT control but not in the transgenic *Py P38HA* parasites. These results showed that the plasmid had properly integrated and that there was no detectable contamination with WT parasites.

To test if the tagged copy of P38 is expressed by the parasite, a Western blot on lysates from *Py P38HA* mixed blood stages and salivary gland sporozoites was performed. Proteins were separated by SDS polyacrylamide gel electrophoresis on a 4-20 % gradient gel, transferred onto a polyvinylidene difluoride (PVDF) membrane and blotted with a monoclonal antibody against HA. A faint but specific band that migrated at the expected size of full-length P38HA (~ 43 kDa; 34 kDa plus the triple HA) was detected in lysates from *Py P38HA* parasites whereas no signal was observed in the WT control. Expression of P38HA in sporozoites seemed higher than in blood stages, relative to the loading control myosin A tail domain-interacting protein (MTIP) (Figure 3.1D).

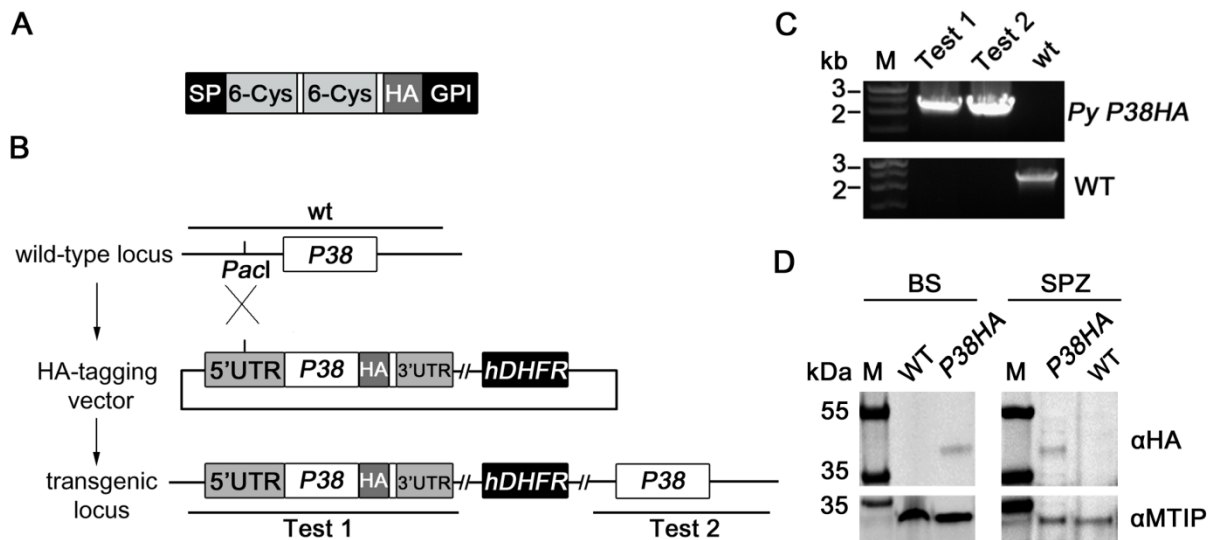


**Figure 3.1** Generation of *P. yoelii* *P38HA* parasites. (A) Predicted protein structure of HA-tagged P38. SP, signal peptide; 6-Cys, 6-Cysteine domain; GPI, glycosylphosphatidylinositol anchor. (B) Schematic of insertion strategy. The vector contained the HA-tagged copy of *P38* under the control of its own 5' and 3' regulatory elements, and a mutated human dihydrofolate reductase (hDHFR) gene that confers resistance to pyrimethamine. The tagging vector was linearized with *PacI* to integrate into the 5' untranslated region (UTR) of *P38* by single crossover homologous recombination, resulting in two copies of *P38* in the parasite genome. (C) PCR genotyping of *P38HA* gDNA with primers (bars in B) specific to the wild-type locus (wt) and the transgenic locus (Test 1 and Test 2) showed successful integration of the construct. Genomic DNA from wild-type parasites (WT) served as control. (D) Western blot analysis of lysates from *P38HA* mixed blood stages (BS) and salivary gland sporozoites (SPZ) probed with anti-HA antibodies revealed a specific band of the expected size (~43 kDa). Lysates from WT parasites served as negative control. Shown below is the same Western blot probed for MTIP as a loading control. M, marker.

### 3.1.3 P38 localizes to micronemes in sporozoites

The localization of P38 has been previously analyzed in *P. falciparum* blood stages by N-terminal GFP-tagging and immunofluorescence microscopy. It was found to localize in apical organelles and on the surface of mature schizonts/merozoites (161). To determine if this is also the case in *P. yoelii*, an immunofluorescence assay (IFA) on *P38HA* schizonts was performed. Parasites were stained with antibodies to HA and co-stained with antibodies to the merozoite surface protein 1 (MSP-1). The majority of schizonts exhibited a weak speckled P38HA pattern that partially co-localized with MSP-1 and was sometimes accompanied by a circumferential staining (Figure 3.2). The speckled pattern is suggestive of vesicular structures while the overlapping signals of P38HA and MSP-1 indicate that P38HA is present on the merozoite surface.

Next, it was analyzed where P38HA localizes in salivary gland sporozoites. To test if P38HA localized on the cell surface, sporozoites were stained with antibodies to HA and the sporozoite surface marker circumsporozoite protein (CSP). CSP showed the characteristic circumferential staining pattern while P38HA displayed a strong internal signal, except in the nuclear region (Figure 3.2B, top panel). Co-staining with the micronemal marker thrombospondin-related anonymous protein (TRAP) showed substantial overlap of the fluorescent signals, suggesting that P38HA localizes to micronemes in salivary gland sporozoites (Figure 3.2B, bottom panel).

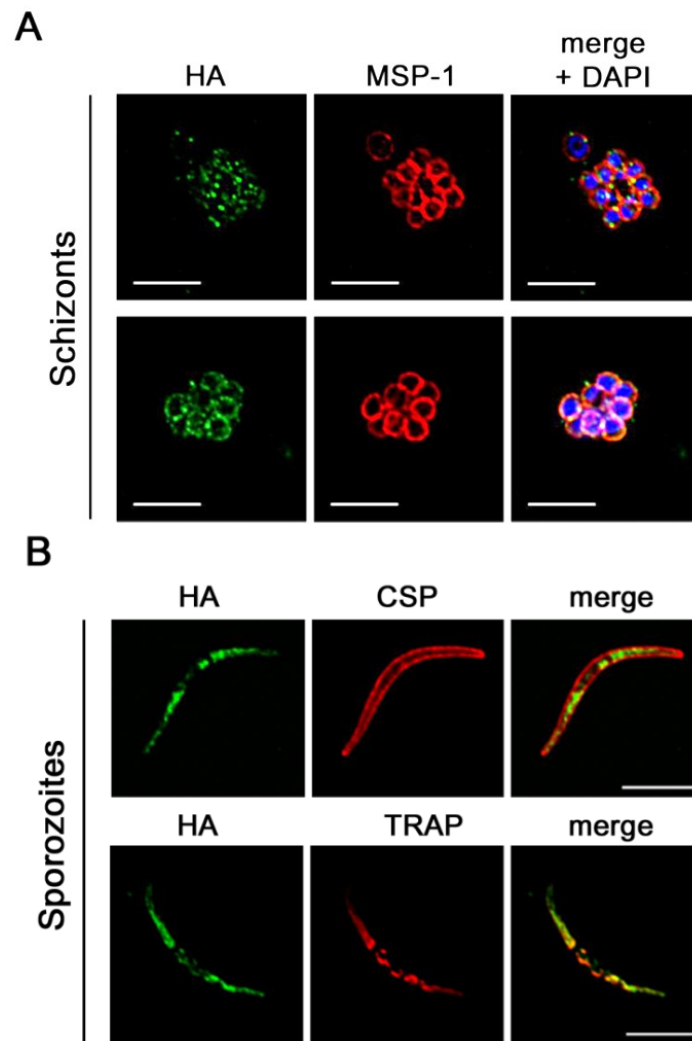


**Figure 3.2** Localization of P38HA in schizonts and salivary gland sporozoites. (A) The top panel shows a representative image of the P38HA pattern that was displayed by the majority of schizonts whereas the bottom staining was only sometimes observed. Co-staining with the merozoite surface protein 1 (MSP-1) resulted in partially overlapping signals. (B) P38HA did not localize on the sporozoite surface as determined by co-staining with the surface antigen CSP (top), but significantly co-localized with the micronemal marker TRAP (bottom). Scale bars are 5  $\mu\text{m}$ .

### 3.1.4 Generation of P38-deficient parasites

To determine if P38 is important for progression through the life cycle of *P. yoelii*, loss-of-function mutants were generated by targeted disruption of *P38*. The targeting vector contained DNA sequences homologous to the 5' UTR and 3' region of *P38* which flanked the pyrimethamine-resistant dihydrofolate reductase-thymidylate synthase (DHFR/TS) gene from *Toxoplasma gondii* (Figure 3.3A). Double crossover homologous recombination led to the replacement of the *P38* ORF with the selectable marker as determined by PCR genotyping of pyrimethamine-resistant parasites (Figure 3.3B). Transgenic parasites were then successfully subjected to limiting dilution cloning to obtain a clonal population of *p38*<sup>-</sup> parasites (Figure 3.3C). To further verify the absence of the *P38* ORF, a Southern blot was performed. Genomic DNA of blood stages was digested with BamHI and HindIII. BamHI cuts within the *P38* ORF or within the selectable marker, respectively, while HindIII cuts within the downstream neighboring gene. In WT gDNA, the restriction fragment is approximately 1 kb in length while it is 1.8 kb in *p38*<sup>-</sup> parasites. DNA fragments were separated by electrophoresis on a 0.8 % agarose gel, transferred to a nylon membrane and hybridized with a probe specific to the 3' region of *P38* which resulted in the expected band shift in *p38*<sup>-</sup> parasites (Figure 3.3D). These results confirmed that the gene was successfully deleted and furthermore demonstrated that P38 is dispensable for blood stage growth.

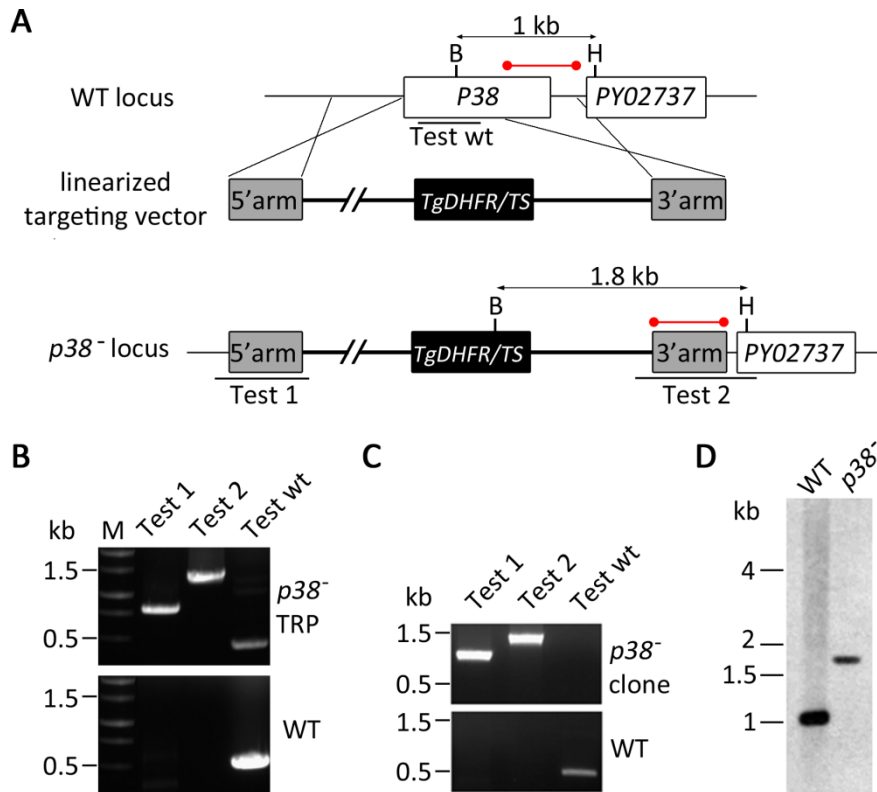


**Figure 3.3** Generation of P38-deficient *P. yoelii* parasites. (A) Schematic of targeting strategy for disruption of *P38*. Double crossover homologous recombination leads to replacement of *P38* with the selectable marker (*T. gondii DHFR/TS*), resulting in parasites that are deficient for *P38* (*p38*<sup>-</sup>). (B) PCR analysis of gDNA from transfer resistant parasites (TRP) with primers (bars in A) specific to the wild-type locus (Test wt) and the *p38*<sup>-</sup> locus (Test 1 and 2) revealed a mixture of recombinant and wild type (WT) parasites. (C) Limiting dilution cloning of the TRP led to the isolation of a *p38*<sup>-</sup> clone. (D) Deletion of *P38* in the clonal population was confirmed by Southern Blot analysis. Genomic DNA from blood stage parasites was digested with BamHI and HindIII ('B' and 'H' in A), blotted onto a nylon membrane and labeled with a probe (dumbbell bar in A) specific to the 3' region of *P38*. Sizes of the expected fragments are shown in A.

### 3.1.5 The lack of P38 does not affect blood stage growth or mosquito stage development

The successful generation of *p38*<sup>-</sup> parasites demonstrated that it is not essential for blood stage growth. However, the lack of P38 might affect the rate at which blood stages grow, given that the protein was found on the merozoite surface and thus might be involved in erythrocyte invasion. To test this, female Swiss Webster mice were intravenously injected with  $1 \times 10^6$  infected erythrocytes and parasitemia was determined daily by counting Giemsa-stained parasites in thin blood smears until the parasites were cleared by the mouse immune system. The growth rate of *p38*<sup>-</sup> parasites was similar to that of WT parasites with a peak parasitemia of 4.4 % and 4 %,

respectively, at day 9 post infection (pi) (Figure 3.4). Mice infected with WT parasites had resolved the infection by day 14 pi while there was a slight delay in clearance of *p38*<sup>-</sup> parasites.

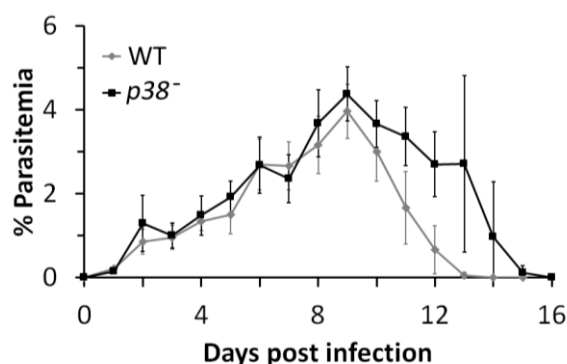


**Figure 3.4** Blood stage growth of *p38*<sup>-</sup> is similar to wild type *in vivo*. Swiss Webster mice (n = 5) were intravenously injected with  $1 \times 10^6$  infected erythrocytes. Parasitemia was determined daily from Giemsa-stained smears until infection resolved, and is plotted as mean  $\pm$  SD of data from each group. WT, wild type.

To investigate if the lack of P38 had an effect on the development within the mosquito, the capacity of *p38*<sup>-</sup> parasites to produce sporozoites was analyzed. Mice infected with *p38*<sup>-</sup> or WT parasites were fed to *Anopheles stephensi* mosquitoes. Mosquito midguts and salivary glands were isolated and analyzed on day 10 and 14 post infection, respectively (Table 3.1). Numbers of sporozoites derived from midgut oocysts and from salivary glands were similar between *p38*<sup>-</sup> and WT parasites. These results suggest that P38 is not important for any step during development within the mosquito, i.e. fertilization, oocyst and sporozoite formation, egress of sporozoites from oocysts and invasion of salivary glands.

**Table 3.1** *p38*<sup>-</sup> parasites show normal development in the mosquito vector. Mean numbers of midgut oocyst sporozoites (MG SPZ) and salivary gland sporozoites (SG SPZ) were calculated from three independent experiments, each with a minimum of 30 mosquitoes.

<i>P. yoelii</i> genotype	MG SPZ/mosquito (mean $\pm$ SD)	SG SPZ/mosquito (mean $\pm$ SD)
WT	75,573 $\pm$ 8950	39,434 $\pm$ 6830
<i>p38</i> <sup>-</sup>	62,361 $\pm$ 19,575	34,328 $\pm$ 16,053

### 3.1.7 P38-deficient sporozoites glide and traverse cells normally *in vitro*

Salivary gland sporozoites display continuous gliding on a solid substrate, during which they leave trails of shed CSP behind (97). To analyze if the lack of P38 affected gliding motility, sporozoites were added to glass coverslips in the presence of serum and incubated at 37 °C for 1 h (79). CSP trails were visualized by immunostaining with anti-CSP antibodies (Figure 3.5A). To quantify gliding motility of *p38*<sup>-</sup> sporozoites, the number of circles per trail associated with sporozoites was counted in at least 10 fields of view with a 60x objective. Trails were categorized into trails with 0-2 circles, 3-10 circles and more than 10 circles. No significant difference was found between trails produced by *p38*<sup>-</sup> and WT sporozoites with 64 % and 58 % of trails containing more than 10 circles, respectively (Figure 3.5B).

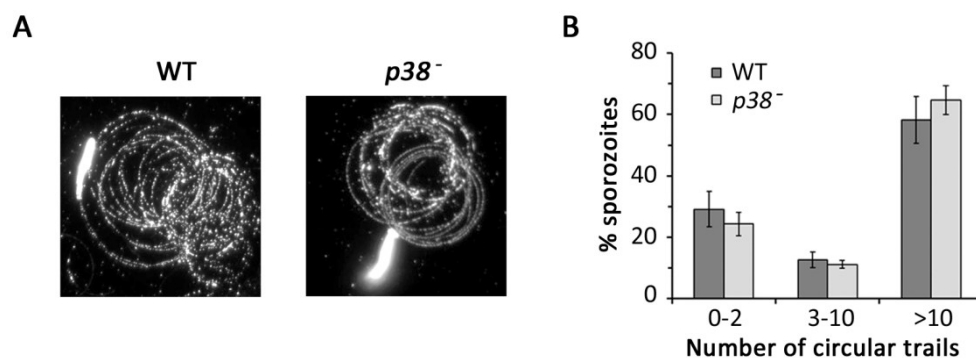


**Figure 3.5** *P. yoelii* *p38*<sup>-</sup> salivary gland sporozoites show normal gliding motility. (A) Sporozoite gliding trails were visualized with AlexaFluor<sup>®</sup>488-conjugated anti-CSP antibodies. (B) Quantification of gliding trails was performed in triplicate ( $n > 100$  per replicate). Shown is the mean percentage of sporozoites ( $\pm$  SD) displaying 0-2, 3-10 and >10 circular trails.

Next, it was tested if the lack of P38 impacted the sporozoites' cell traversal activity, a distinct parasite trait which is characterized by the wounding of the cell plasma membrane as the sporozoite enters and exits the cell (110). To analyze cell traversal activity, sporozoites were added to mouse hepatoma cells in the presence of cell-impermeable FITC-labeled dextran, and were allowed to traverse cells for 90 min. The membrane damage allows fluorescent dextran to leak into the cell where it gets trapped upon membrane repair (110). Cells were analyzed by flow cytometry and revealed that the percentage of traversed cells (FITC-positive) was similar between wells inoculated with *p38*<sup>-</sup> and WT sporozoites (Figure 3.6).

These results demonstrated that the lack of P38 did not affect sporozoite gliding motility or cell traversal activity.

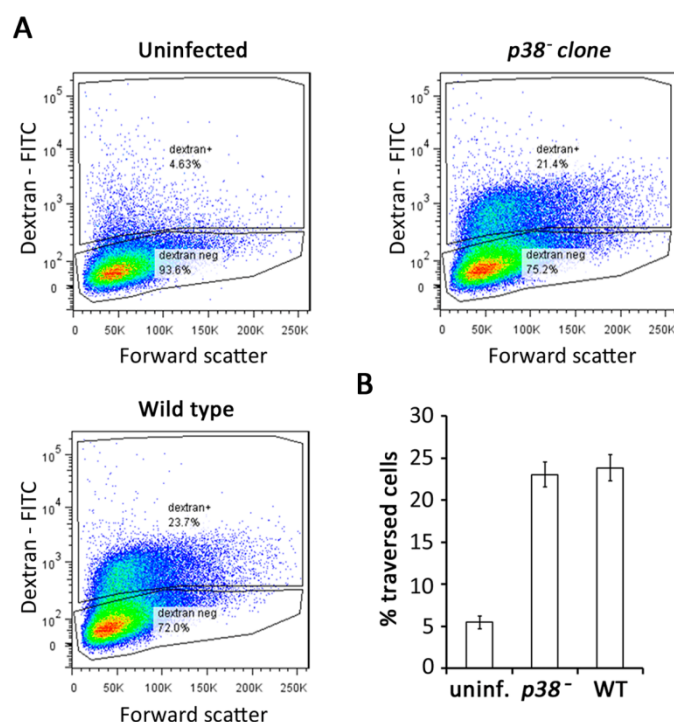


**Figure 3.6** *P. yoelii* *p38*<sup>-</sup> salivary gland sporozoites show normal cell traversal activity *in vitro*. (A) Hepa 1-6 cells were infected with either wild type (WT) or *p38*<sup>-</sup> sporozoites in the presence of cell-impermeable FITC-labeled dextran. Sporozoites were allowed to traverse cells for 90 min. Cells were then fixed and analyzed by flow cytometry. Shown are representative scatter plots of uninfected cells, wild type (WT)-infected cells and *p38*<sup>-</sup>-infected cells. The gating strategy used for identifying traversed cells is shown. (B) Bar graph shows mean percentages  $\pm$  SD of triplicate wells. uninf., uninfected control.

### 3.1.8 P38 is not required for sporozoite infectivity to the rodent host

Sporozoites lacking the 6-Cys proteins P52 and P36 fail to form a parasitophorous vacuole during hepatocyte invasion and abort liver stage development and thus do not infect the blood (49,50,144). To test if *p38*<sup>-</sup> sporozoites were similarly affected, their ability to establish blood-stage infection in mice was analyzed. BALB/cJ mice were intravenously injected with either  $1 \times 10^3$  or  $1 \times 10^4$  salivary gland sporozoites and were monitored for parasites by examining Giemsa-stained thin blood smears. A delay in the time to blood stage patency would indicate a defect during liver infection (189), either in recognition and invasion of hepatocytes or in intrahepatic development. Mice injected with *p38*<sup>-</sup> sporozoites became patent on day 3 and day 4 post injection, as did the WT- infected mice (Table 3.2), demonstrating that P38 is not required for liver infection. Intravenous injection of sporozoites completely bypasses the skin where sporozoites are deposited during natural transmission (4,6). To test if P38 played a role

## Results

during the skin phase of infection, mice were exposed to bites of infected mosquitoes. Again, all mice became patent on day 3 post infection, suggesting that P38 is not important for the migration of sporozoites from the skin to the liver. Overall, these results showed that P38 is dispensable for sporozoite infectivity to mice.

**Table 3.2** *P. yoelii p38<sup>-</sup>* sporozoites are able to establish blood stage infection in mice.

Parasite line	No. of inoculated sporozoites	No. of infected BALB/c mice	Median time to patency (days)
WT	$1 \times 10^3$	3/3	3.3
<i>p38<sup>-</sup></i>	$1 \times 10^3$	5/5	3.2
WT	$1 \times 10^4$	3/3	3
<i>p38<sup>-</sup></i>	$1 \times 10^4$	5/5	3
WT	Mosquito bite	3/3	3
<i>p38<sup>-</sup></i>	Mosquito bite	5/5	3

In summary, this study showed that HA-tagged P38 localizes to micronemes in salivary gland sporozoites of *P. yoelii* by IFA. This is in agreement with the reported micronemal localization of the 6-Cys sporozoite protein P52 (49). In contrast to P52 which is essential for liver infection, P38 plays no vital role in sporozoite infectivity. In fact, it is dispensable throughout the entire life cycle of *P. yoelii*.

### 3.2 Identification of putative sporozoite surface proteins

Transmission from the mosquito to the mammalian host is a critical phase for the malaria parasite. Upon inoculation into the host's skin, *Plasmodium* sporozoites must leave the bite site, find a blood vessel, enter the blood stream, exit it in the liver, and finally invade a suitable host hepatocyte. How sporozoites achieve this complex journey is largely unknown but proteins on the sporozoite surface are likely involved. Determining the sporozoite surface proteins is therefore of great importance, and could provide useful information for the development of antibody-based vaccines that aim to block infection by sporozoites and thus prevent malaria. Proteomic studies of sporozoites have been limited by difficulties in collecting material of sufficient quantity and purity (162,176,190). Here, we used a recently published improved sporozoite purification method in combination with cell surface biotinylation and mass spectrometry to identify novel proteins present on the surface of *P. yoelii* and *P. falciparum* sporozoites (182,183). This study is part of the following paper:

Lindner SE, Swearingen KE, Harupa A, Vaughan AM, Sinnis P, Moritz RL, et al. Total and putative surface proteomics of malaria parasite salivary gland sporozoites. *Mol Cell Proteomics MCP*. 2013 May;12(5):1127–43.

<http://dx.doi.org/10.1074/mcp.M112.024505>

#### 3.2.1 Surface biotinylation of live sporozoites

As described in (182), live salivary gland sporozoites from *P. yoelii* and *P. falciparum* were purified by density gradient centrifugation on a 17 % Accudenz cushion (183). Sporozoites were then incubated with a cell-impermeable amine-reactive biotin cross-linker to label N-termini and lysine side chains of surface-exposed proteins. Following lysis, labelled proteins were enriched by streptavidin-coated magnetic beads; untreated *P. yoelii* sporozoites served as negative control. To confirm protein biotinylation, a western blot was performed. Aliquots of biotinylated and untreated sporozoite samples were subjected to SDS polyacrylamide gel electrophoresis on a 4-20 % gradient gel, transferred to PVDF membrane, and probed with streptavidin-conjugated HRP. Multiple proteins were observed in the biotinylated *P. yoelii* and *P. falciparum* sporozoite samples whereas no bands were present in the non-biotinylated sporozoite control (Figure 3.1A). To confirm specific biotinylation of the major sporozoite surface protein CSP, the membrane was stripped and then incubated with monoclonal antibodies

specific to *P. yoelii* CSP. The characteristic double band was detected in the biotinylated *P. yoelii* sporozoite sample (Figure 3.1B) (136). To further confirm biotinylation of *P. falciparum* CSP, the membrane was stripped again and probed with anti-PfCSP antibodies which recognized a specific protein band at the expected size (Figure 3.1C).

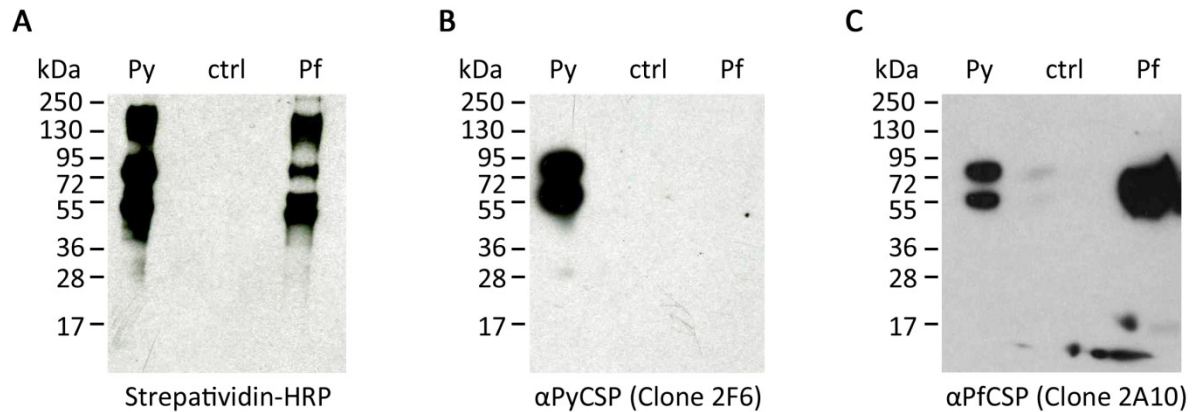


**Figure 3.7** Western blot analysis of biotinylated proteins using HRP-conjugated streptavidin (A), monoclonal antibodies against *P. yoelii* CSP (B) and monoclonal antibodies against *P. falciparum* CSP (C). Panel B and C are the same blot as Panel A, stripped and reprobed with indicated antibodies. Py: biotinylated *P. yoelii* salivary gland sporozoites; ctrl: untreated *P. yoelii* salivary gland sporozoites; Pf: biotinylated *P. falciparum* sporozoites. Note: detection of *P. yoelii* CSP in panel C likely resulted from incomplete stripping of bound anti-PyCSP.

After confirming successful biotinylation, the remainder of the protein samples was separated by 4-20 % SDS polyacrylamide gel electrophoresis, followed by treatment with Imperial Protein Stain to visualize protein bands. The gel was cut into four fractions and subjected to nanoscale liquid chromatography coupled to tandem mass spectrometry, which was performed in duplicate by Kristian E. Swearingen (Robert Moritz' group, Institute for Systems Biology). Analysis of mass spectrometry data was performed by Kristian E. Swearingen and Scott E. Lindner (previously in Stefan Kappe's group at Seattle BioMed; currently at Pennsylvania State University). For methodological details, please refer to the paper (182). For a complete list of all peptide spectrum matches and inferred protein identifications, please refer to the supplemental material of the paper (Table S1), available online at <http://www.mcponline.org/content/12/5/1127/suppl/DC1>.

### 3.2.2 Analysis of surface protein-enriched fractions

*P. falciparum* proteins captured by surface labeling yielded in 22 parasite-specific proteins whereas 27 parasite-specific proteins were identified in the *P. yoelii* sample.

Because of the erroneous annotation of the *P. yoelii* genome at the time of analysis, mass spectrometry data were also searched against the sibling species *P. berghei*. The combined *P. yoelii/P. berghei* search resulted in 35 unique proteins, 13 of which were shared with *P. falciparum* (Table 3.3). Among all of the surface-exposed proteins identified were multiple hypothetical proteins, heat shock proteins, transporters, and some known surface and secreted proteins such as CSP, TRAP and TRSP. However, several proteins that are highly unlikely to be found on the sporozoite surface were also detected (e.g. histones), as well as proteins associated with the inner membrane complex (IMC) that lies beneath the plasma membrane (discussed in section 4.2).

The datasets, while not exhaustive, provided a good starting point for the investigation of novel putative surface proteins and their role in sporozoite biology. Of the identified proteins, four previously uncharacterized proteins were selected for further analysis in *P. yoelii*. Selection was based on: the presence of the protein in the *P. falciparum* and *P. yoelii* dataset, available expression data ([www.PlasmoDB.org](http://www.PlasmoDB.org)) to exclude genes that might be important for proliferation of blood stages, and the presence of signals or domains that suggest membrane association. The selected proteins included three hypothetical proteins (PlasmoDB IDs: PY01796, PY02432, PY06766) and one putative sugar transporter (PY05332). The next sections describe the functional characterization of these proteins.

**Table 3.3** A selected group of surface-exposed sporozoite proteins identified via biotin-conjugated crosslinker addition and capture. The presence of predicted signal peptide sequences, transmembrane (TM) domains, and GPI anchor sequences is indicated. From (179), Table 2.

Protein	<i>P. falciparum</i> gene ID	Unique Peptides	Peptide Spectrum Matches	<i>P. yoelii</i> gene ID	Unique Peptides	Peptide Spectrum Matches	Signal Peptide	TM Domains	GPI Anchor
Hexose transporter	PF80210c	2	3	PY00899	2	3	No	Yes	No
CSP	PFC0210c	17	140	SBRIPIY_PFC0210c, SBRIPIY_PY07368	13	166	Yes	Yes	Yes
TRSP	PFA0200w	2	7	PY07092	4	14	Yes	Yes	No
TRAP	PF13_0201	1	1	PY03052	8	16	Yes	Yes	No
Sporozoite Conserved Orthologous Transcript	PF11_0545	2	6	PY02432	2	3	No	No	No
Sugar Transporter	PF10955w	1	2	PY05332	2	7	Yes	Yes	No
Sporozoite Conserved Orthologous Transcript	PF10_0112	2	4	PY06766	1	2	No	Yes	No
AMA1	PF11_0344	2	5	PY01581	-	-	Yes	Yes	No
Sporozoite Conserved Orthologous Transcript	PFL0650c	2	5	PY05921	-	-	No	No	No
Sporozoite Conserved Orthologous Transcript	PF08_0088	1	1	PY01796	1	3	Yes	Yes	No
GEST	PF14_0467	-	-	PY05966	1	4	Yes	No	No
conserved Plasmodium membrane protein, unknown function	PFL1825w	1	3	PY03591	-	-	No	Yes	Yes
conserved Plasmodium protein, unknown function	MAL7P1.67	-	-	SBRIPIY_MAL7P1.67	1	2	Yes	Yes	No
conserved Plasmodium protein, unknown function	PFL0370w	1	1	PY04162	-	-	No	No	No

### 3.3 Functional analysis of UIS surface proteins

The putative sporozoite surface proteins PY02432, PY06766 and PY05332 are encoded by genes that were previously found to be upregulated in infectious sporozoites (UIS) by microarray analysis of oocyst-derived and salivary gland sporozoites (123). UIS proteins are believed to be important for infection of the mammalian liver. Indeed, some of them were shown to be essential for liver infection, i.e. the 6-Cys protein P52 and the PVM proteins UIS3 and UIS4 (48,50,51). Parasites lacking these proteins are arrested in liver stage development and, thus, do not infect the blood. Here, it was tested if targeted deletion of PY02432, PY06766 and PY05332 had a similar attenuating effect on sporozoites. It was furthermore attempted to verify the proteins' localization on the sporozoite surface by epitope-tagging and immunofluorescence microscopy.

#### 3.3.1 PY02432 – a small tyrosine-rich protein

PY02432 is a small protein with a predicted molecular mass of ~17 kDa. Sequence homology searches identified orthologs in all *Plasmodium* species but not outside the genus, indicating that PY02432 is unique to *Plasmodium*. PY02432 shows no similarity to any known protein. It does not contain a signal peptide or a transmembrane domain but is predicted by the SecretomeP 2.0 server to be non-classically secreted (191,192). PY02432 furthermore contains a putative palmitoylation site at the cysteine residue 11 (Cys11) as predicted by the CSS-Palm 2.0 software with high confidence (score 31.5, cut-off 4.2) (193). Palmitoylation is a reversible post-translational lipid modification that mediates membrane association, among other processes (194). The *Plasmodium* palmitome was recently published and revealed that the parasite uses this modification extensively (195). All orthologs of PY02432 contain the conserved Cys11 palmitoylation site, except for *P. falciparum* which lacks the Cys11 but bears a putative palmitoylation site at position 2. An interesting feature of PY02432 is the high abundance of tyrosine residues (13.4 %) with a stretch of nine conserved tyrosines in the central region of the protein (Appendix B, Figure B.1).

#### 3.3.2 PY06766 – a conserved apicomplexan protein with four transmembrane domains

PY06766 is a small protein of ~20 kDa and has no similarity to known proteins. It is encoded by a UIS gene, which was previously found to be even more upregulated upon sporozoite activation, i.e. incubation at 37 °C in the presence of hepatocytes (123,153).

PY06766 was furthermore detected in the proteomes of gametocytes and oocyst-derived sporozoites in *P. berghei* and *P. falciparum* (176,177,196). Searching the amino acid sequence against a protein database yielded orthologous proteins in all *Plasmodium* species and also identified putative orthologs in *Toxoplasma*, *Eimeria* and *Neospora* (Appendix B, Figure B.2). Amino acid identity between PY06766 and the *P. falciparum* ortholog is 32 % and ranges from 22 to 30 % between PY06766 and the orthologs outside the genus. PY06766 contains four putative transmembrane domains with an intracellular N- and C-terminus. The N-terminal region contains three consecutive cysteine residues that are conserved among *Plasmodium* species and are predicted to be palmitoylated, using the CSS-Palm 2.0 software (193). The highest prediction score was obtained for Cys12 (score 34.6, cut-off 4.22), which lies immediately adjacent to the first putative transmembrane domain. Two additional putative palmitoylation sites are located within the second transmembrane domain. The cytoplasmic tail of PY06766 contains a stretch of residues that is conserved in all apicomplexan orthologs, suggesting that they might be of functional importance (Appendix B, Figure B.2).

### **3.3.3 PY05332 – a putative sugar transporter**

PY05332 is annotated as a putative sugar transporter of the Major Facilitator Superfamily (MFS) (123). As most members of the MFS family, it contains 12 putative transmembrane domains with the N- and C-terminus facing the cytoplasm. PY05332 is conserved amongst *Plasmodium* species and shares 50 % amino acid identity with its ortholog in *P. falciparum*. *Plasmodium* species express two more conserved putative sugar transporters (<http://PlasmoDB.org>). To date, only one has been characterized, that is the *Plasmodium* hexose transporter (HT). *Plasmodium* HT is homologous to the mammalian glucose transporters and is expressed throughout the parasite life cycle (197). It mediates uptake of glucose and fructose and is thought of as the principal sugar transporter in *Plasmodium* (197,198). HT is essential for blood stage growth and has been validated as a drug target in blood stages and liver stages (197,199). It was also detected in the surface proteomes of *P. yoelii* and *P. falciparum* sporozoites, but it is unknown if HT has an essential role in these stages (182). Multiple sequence alignment of PY05332 with *P. yoelii* HT (PY00899) and homologous glucose transporters from phylogenetically distant organism showed that several of the residues known to be of functional significance are not conserved in PY05332 (Appendix B, Figure B.3).

PY05332 is 22 % identical to PyHT and 18 % to the third putative sugar transporter in *P. yoelii* (PY00594).

#### **3.3.4 PY06766 and PY05332 localize to the periphery of sporozoites**

To analyze the localization of PY02432, PY06766 and PY05332, parasite lines that express a HA-tagged copy of the gene of interest were generated. PY02432 was tagged at its N-terminus (*PY02432N-HA*) because it contains a proline residue at the ultimate C-terminus, which is conserved among all *Plasmodium* species and might thus be important for protein function (Appendix B, Figure B.1). PY06766 and PY05332 were tagged at their C-termini (*PY06766C-HA* and *PY05332C-HA*). The endogenous gene of interest was replaced with the tagged version by double crossover homologous recombination, as depicted in Figure 3.8. Each tagged gene of interest was under the control of its endogenous promoter and the 3' regulatory elements of the *P. berghei* *DHFR/TS* gene. PCR genotyping of genomic DNA from recombinant parasites revealed that each tagging construct had successfully integrated (Figure 3.8).

## Results

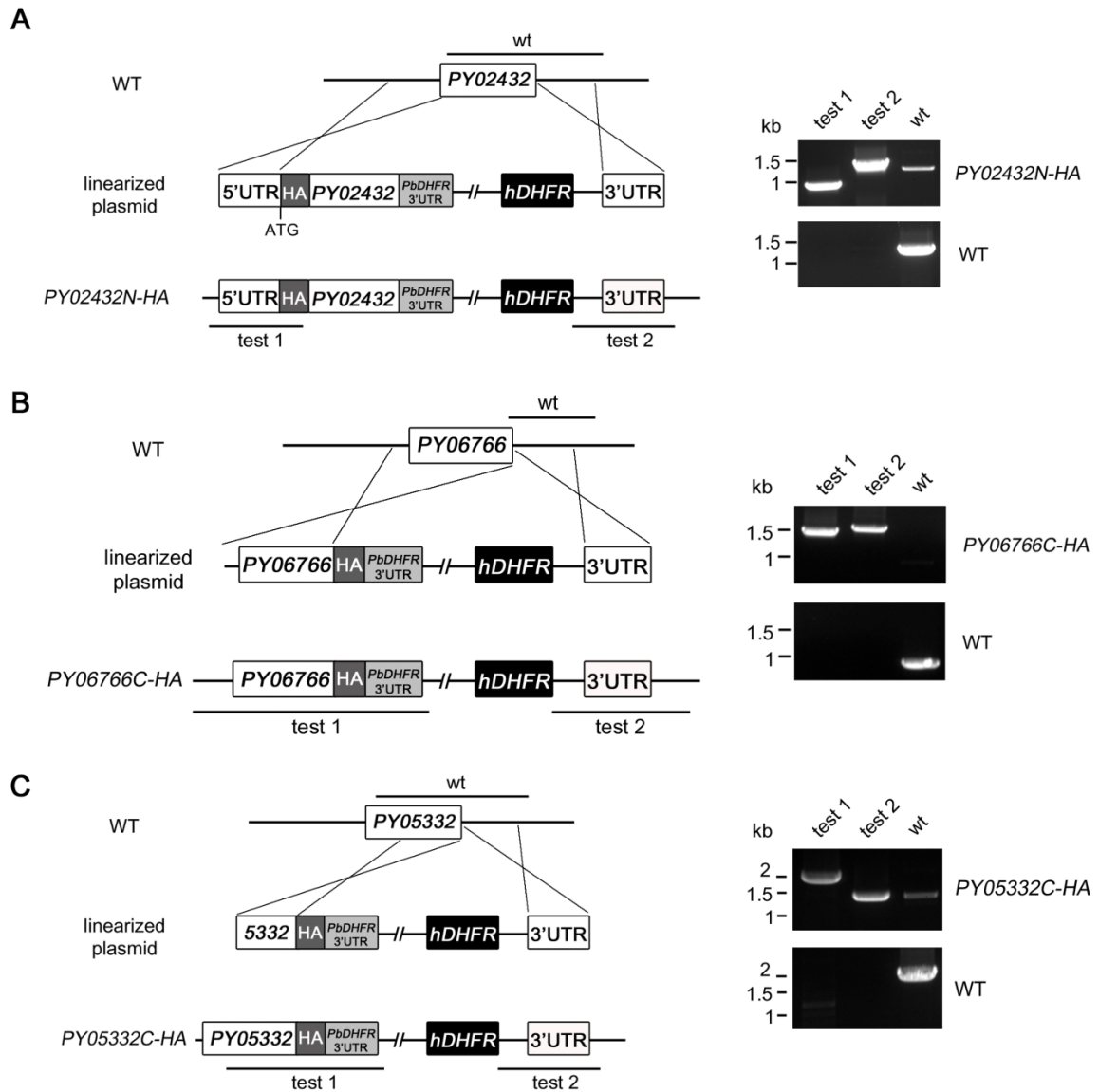


**Figure 3.8** HA-tagging of putative sporozoite surface proteins. Left panels show the schematic of the replacement strategy used to generate parasites that express N-terminally tagged PY02432 (A), C-terminally tagged PY06766 (B) or C-terminally tagged PY05332 (C), respectively. Right panels show the results of PCR genotyping of genomic DNA from transgenic parasites, using primer combinations specific to the transgenic locus (test 1 and test 2) and to the wild type locus (wt). Note: schematic is not drawn to scale.

To assess localization of the tagged proteins, sporozoites were subjected to IFAs with HA-specific antibodies. The vast majority of *PY02432N-HA* salivary gland sporozoites were not stained, which was unexpected since PY02432 was detected in the sporozoite surface proteome and thus is expressed in salivary gland sporozoites. To investigate if the transgenic *PY02432N-HA* locus contained the proper HA tag sequence, the region encompassing the 5'UTR, the tagged open reading frame and the downstream *P. berghei* *DHFR/TS* 3'UTR was amplified by PCR, purified, and sequenced. DNA sequencing

revealed that the HA tag was missing in the transgenic locus. Since the presence of the tag in the transfection plasmid was confirmed by sequencing prior to transfection, it appears that the tag was removed by the parasite. However, a minor fraction of parasites must have integrated the complete tagged copy because test primers annealing within the tag sequence generated a PCR product (Figure 3.8A). Since this minor genotype was below the detection limit of DNA sequencing, it was not attempted to clone these parasites. Another approach in which PY02432 was tagged internally within the C-terminal region yielded transgenic parasites that again lacked the tag (data not shown). Localization studies of PY02432 were therefore aborted. PY06766 was detected in oocyst and salivary gland sporozoites, and displayed a peripheral localization that overlapped with the surface marker CSP (Figure 3.9A). In contrast to PY06766, PY05332 was not observed in oocyst sporozoites but was strongly expressed in salivary gland sporozoites, where it co-localized with CSP (Figure 3.9B). These results suggest that PY06766 and PY05332 are indeed associated with the sporozoite surface whereas the localization of PY02432 remains to be determined.

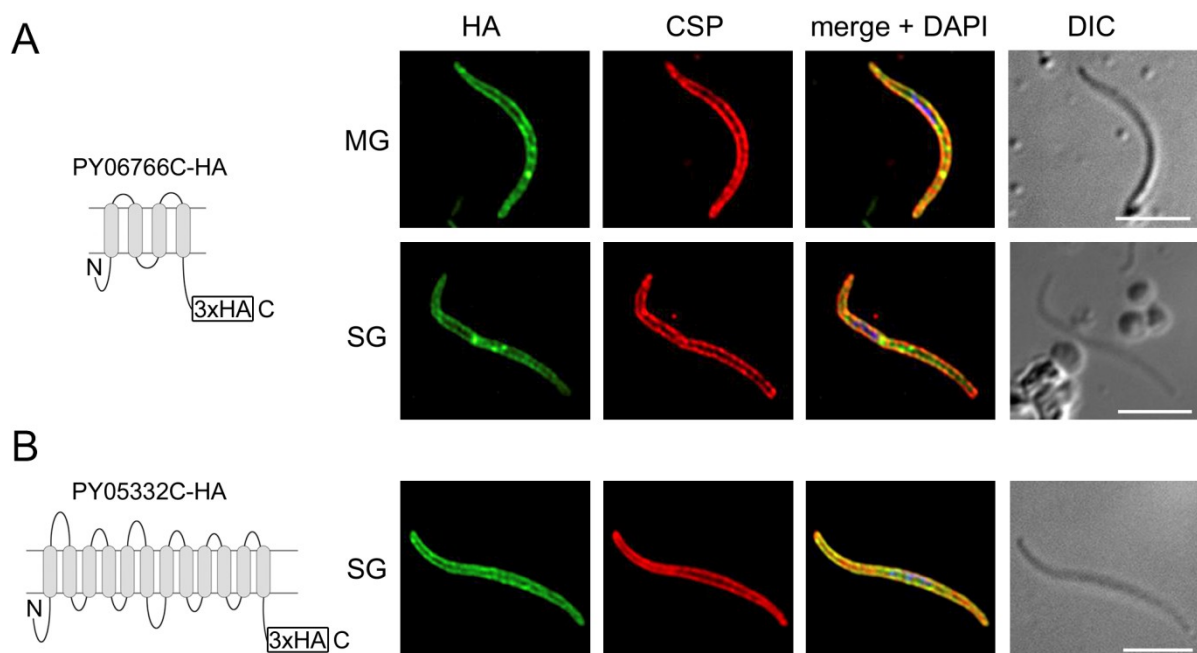


**Figure 3.9** Localization of PY05332 and PY06766 in sporozoites. (A) IFA of permeabilized sporozoites with HA-specific antibodies revealed a peripheral localization of PY06766 in midgut-derived (MG) oocyst sporozoites and salivary gland (SG) sporozoites that overlapped with the surface marker CSP. (B) PY05332 was not detected in MG sporozoites but was strongly expressed in SG sporozoites where it co-localized with CSP. Left panels show the predicted topology of the tagged proteins. Scale bars are 5 μm.

### 3.3.5 Generation of *UIS* knockout parasites

To assess whether PY02432, PY06766 and PY05332 are important for sporozoite infectivity to the mammalian host, each gene was deleted from the *P. yoelii* genome using the replacement strategy. The targeting vector contained a pyrimethamine-resistance cassette and 500-800 bp of the 5' and 3' UTR of the gene of interest to promote double crossover homologous recombination (Figure 3.10A). Following parasite transfection and selection with pyrimethamine, genomic DNA of resistant parasites was analyzed by PCR with primers specific to the recombinant locus. Populations that contained the desired recombinant parasites were then cloned by limiting dilution to isolate single clones of the gene knockout parasites. Each of the three genes was successfully deleted and at least one clone per target gene was obtained (Figure 3.10B). The successful generation of these gene knockout parasites demonstrated that the encoding genes are dispensable for blood stage proliferation.

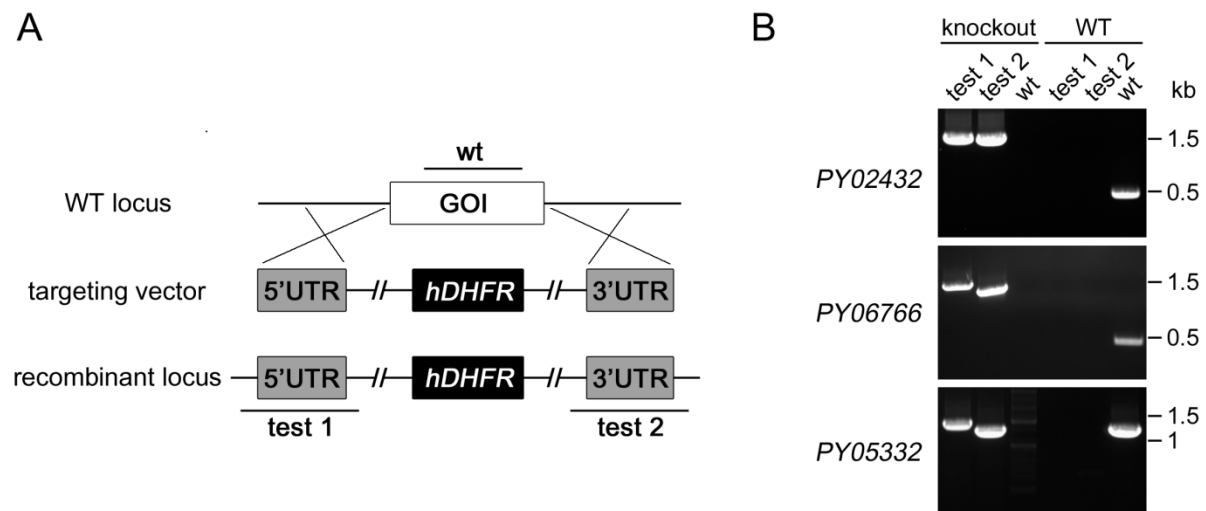


**Figure 3.10** Generation of gene knockout parasites. A) Schematic representation of replacement strategy. The gene of interest (GOI) was replaced with a positive selectable marker (human DHFR) by double crossover homologous recombination using the 5' and 3' untranslated regions (UTRs) of the GOI. (B) PCR genotyping of knockout clones with recombination-specific primer combinations (test 1 and test 2; bars in A) and primers specific to the wild-type locus (wt) shows successful integration of the construct and the loss of the GOI. Genomic DNA of *P. yoelii* wild-type (WT) parasites served as control.

### 3.3.6 *UIS* knockout sporozoites are infectious to mice

In order to determine if the knockout parasites were defective in mosquito stage development, numbers of sporozoites isolated from salivary glands were analyzed. Mice infected with knockout or control parasites were fed to *A. stephensi* mosquitoes. After

14 or 15 days, salivary glands from at least 30 mosquitoes per knockout parasite were isolated and the mean number of sporozoites per mosquito was determined in at least three independent experiments. Mean sporozoite loads were similar between control parasites and knockout mutants, although sporozoite numbers produced by *py02432*<sup>-</sup> and *py06766*<sup>-</sup> parasites varied considerably between experiments (Table 3.4). However, overall the results show that knockout parasites are able to produce sporozoites in similar numbers as WT.

**Table 3.4** Sporozoite (SPZ) numbers isolated from salivary glands (SG) are similar between wild type (WT) and knockout parasites. Mean numbers are derived from three independent experiments.

<i>P. yoelii</i> genotype	Mean no. of SG SPZ/mosquito ± SD
WT	32,482 ± 7,238
<i>py02432</i> <sup>-</sup>	33,094 ± 23,419
<i>py06766</i> <sup>-</sup>	19,462 ± 16,153
<i>py05332</i> <sup>-</sup>	29,385 ± 5,847

Next, it was tested if the knockout parasites are able to complete liver stage development as measured by the onset of blood stage patency. BALB/cJ mice were intravenously injected with  $1 \times 10^3$  salivary gland sporozoites of WT control or knockout parasites. Mice were monitored for parasites by analyzing Giemsa-stained thin blood smears. Unexpectedly, all mice became blood stage patent on day 3 post injection, suggesting that neither of the analyzed proteins is required for liver infection or intrahepatic development (Table 3.5). Since proteins on the sporozoite surface are potentially involved in host-parasite interactions during the initial phase in the skin, it was investigated if knockout sporozoites were able to establish blood-stage infection when transmitted by mosquito bite. Anesthetized BALB/cJ mice were exposed to the bites of 12-15 mosquitoes infected with control or knockout parasites. Mosquitoes were allowed to feed on mice for a total time of 7.5 min. Again, all mice developed blood stage parasitemia on day 3 post infection, suggesting that none of the analyzed proteins is critically involved in this initial phase of infection (Table 3.5).

## Results

**Table 3.5** Knockout sporozoites are able to infect the rodent host. SPZ, sporozoites.

<i>P. yoelii</i> genotype	No. of injected sporozoites	No. of infected BALB/cJ mice	Day of patency
WT	1 × 10 <sup>3</sup>	3/3	3
<i>py02432</i> <sup>-</sup>	1 × 10 <sup>3</sup>	3/3	3
<i>py06766</i> <sup>-</sup>	1 × 10 <sup>3</sup>	5/5	3
<i>py05332</i> <sup>-</sup>	1 × 10 <sup>3</sup>	3/3	3
WT	Mosquito bite (33,840 SPZ/mosquito)	5/5	3
<i>py02432</i> <sup>-</sup>	Mosquito bite (20,250 SPZ/mosquito)	5/5	3
<i>py06766</i> <sup>-</sup>	Mosquito bite (37,500 SPZ/mosquito)	5/5	3
<i>py05332</i> <sup>-</sup>	Mosquito bite (24,200 SPZ/mosquito)	5/5	3

In summary, this brief analysis showed that neither of the putative UIS surface proteins PY02432, PY06766 and PY05332 is required for any life cycle stage of the rodent parasite *P. yoelii*.

### 3.4 Characterization of the sporozoite surface protein S23

This section describes the characterization of PY01796, which was first identified in a screen for sporozoite-specific transcripts using suppression subtractive cDNA hybridization of *P. yoelii* salivary gland sporozoites and merozoites, and was thus previously named sporozoite-expressed gene 23 (S23) (200). Here, epitope-tagging and specific antibodies to S23 were used for detailed localization studies. The function of S23 in the parasite life cycle was investigated by using a reverse genetics approach. Parts of this study have been published:

Harupa A, Sack BK, Lakshmanan V, Arang N, Douglass AN, Oliver BG, Stuart AB, Sather DN, Lindner SE, Hybiske K, Torii M, Kappe SH. SSP3 is a novel *Plasmodium yoelii* sporozoite surface protein with a role in gliding motility. *Infect Immun.* 2014 Nov;82(11):4643–53. <http://dx.doi.org/10.1128/IAI.01800-14>

#### 3.4.1 S23 is a type I transmembrane protein with conserved cysteine residues

S23 is annotated as a hypothetical protein of unknown function with a predicted molecular mass of 50.4 kDa. It is predicted to be a surface-exposed type I transmembrane protein. Homology searches using BLASTP identified orthologs in all *Plasmodium* species (Appendix C, Figure C1), but did not yield any potential orthologs in other apicomplexan or non-apicomplexan organisms. S23 contains thirteen highly conserved cysteine residues, twelve of which are within the predicted ectodomain and one within the predicted transmembrane domain (Figure 3.11A). Structural homology searches using the HHpred web server (<http://toolkit.tuebingen.mpg.de/hhpred>) suggested that the N-terminal region of S23 is similar to the s48/45 domain of *Plasmodium* 6-Cys proteins (97 % confidence, PDB ID: 2YMO) (Figure 3.11B). The region upstream of the predicted transmembrane domain of S23 has some similarity to the fourth thrombospondin type 1 repeat (TSR) of F-spondin (55 % confidence, PDB ID: 1VEX) and to that of *Plasmodium* TRAP (64 % confidence, PDB ID: 4HQO). TSR domains are ~60 amino acids in length and have adhesive properties thought to be mediated by the motif WxxWSxCSxTCGxGxxxRxR (where 'x' can be any amino acid), which is partially conserved in S23 (Figure 3.11C) (201).

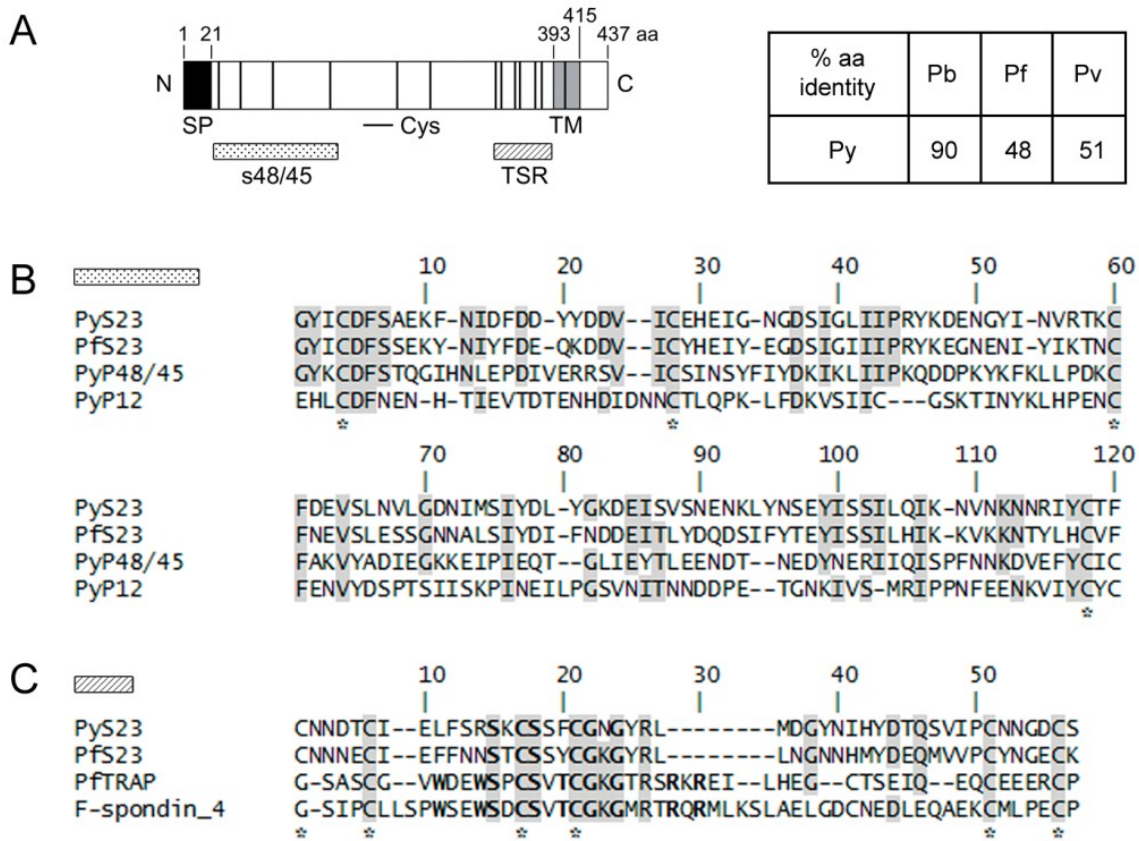


**Figure 3.11** Schematic of the predicted protein structure of PyS23 and sequence alignments. (A) Cartoon of S23 protein structure and amino acid (aa) sequence identities to its orthologs in *P. berghei* (Pb), *P. falciparum* and *P. vivax*. Black bars indicate conserved cysteine (Cys) residues. Boxes below mark regions of structural similarity to the indicated domains identified through HHpred search. SP, signal peptide; TM, transmembrane domain. (B) Sequence alignments of PyS23 and PfS23 with the s48/45 domain-1 of two representative members of the 6-Cys protein family and (C) with TSRs of PfTRAP and F-spondin. Conserved cysteine residues in S23 are marked by an asterisk. Identical residues are boxed gray. Invariant residues in most TSRs are highlighted in bold.

### 3.4.2 S23 localizes to the periphery in salivary gland sporozoites

To assess expression and localization of S23, a parasite line was created which expressed S23 C-terminally tagged with a quadruple Myc tag. Transgenic parasites were generated via double crossover homologous recombination to replace the endogenous open reading frame with the tagged version of S23 (Figure 3.12). Expression of *S23cMyc* was controlled by its endogenous promoter and the commonly used 3' regulatory elements of the *P. berghei DHFR/TS* gene.

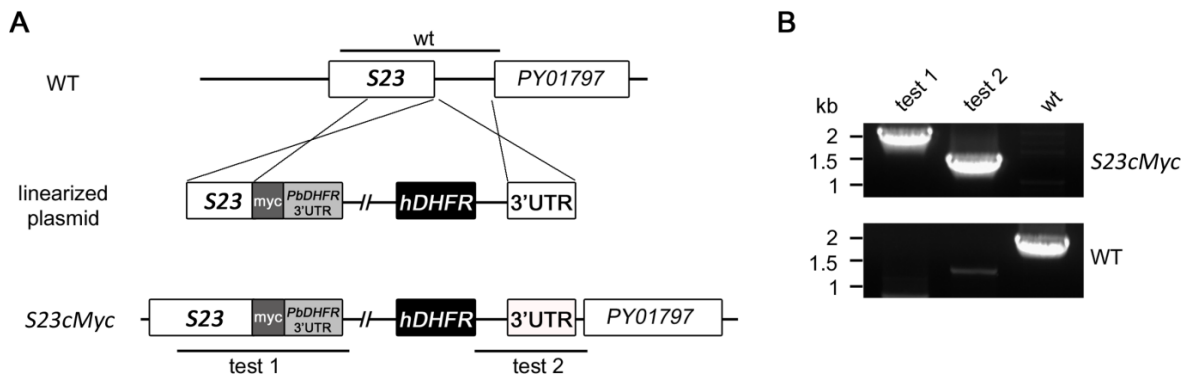


**Figure 3.12** Generation of *Py S23cMyc* parasites. (A) Schematic of the strategy used to replace the endogenous *S23* gene with the tagged copy and the selectable marker cassette (*hDHFR*) by double crossover homologous recombination. (B) PCR genotyping with primers (bars in A) shows proper integration of the tagging vector.

To analyze expression and localization of *S23*, immunofluorescence assays (IFAs) on sporozoites were performed. IFA of fixed and permeabilized oocyst sporozoites revealed an internal localization that partially overlapped with the luminal ER protein, binding immunoglobulin protein (BiP; Figure 3.13A, top panel). The observed signal for *S23* varied from faint to readily detectable, potentially marking sporozoites of different stages of maturation, possibly due to the asynchronous development of oocysts (80). In mosquito salivary glands, the majority of sporozoites showed a strong, circumferential localization of *S23* that co-localized with that of the surface protein CSP (Figure 3.13A, bottom panel), whereas some sporozoites exhibited *S23* expression within the sporozoite. This might be caused by differences in maturation, or could be due to a contamination with hemolymph sporozoites for which a strong internal localization for *S23* was observed (Figure 3.13A, middle panel). Expression of *S23* in sporozoites was further analyzed by Western blot using Myc-specific antibodies. A single specific band that migrated at the expected size of ~63 kDa (full-length *S23* plus the 4xMyc tag) was detected, suggesting that *S23* is not proteolytically processed (Figure 3.13B). In oocyst sporozoites, *S23* was barely detectable whereas *S23* was readily expressed in salivary gland sporozoites. *S23* was not detected in lysates of mixed blood stages, which is in agreement with the lack of *S23* in the previously published proteomes of asexual and sexual blood stages of *P. falciparum* and *P. berghei* (162,177,196,202,203). Overall, these data suggest that *S23* expression increases during sporozoite maturation and that it traffics through the secretory pathway to the periphery of sporozoites. Importantly, the number of *S23cMyc* sporozoites per mosquito was similar to wild type (WT) (Table

3.6), indicating that the addition of the epitope tag had no gross impact on parasite fitness.

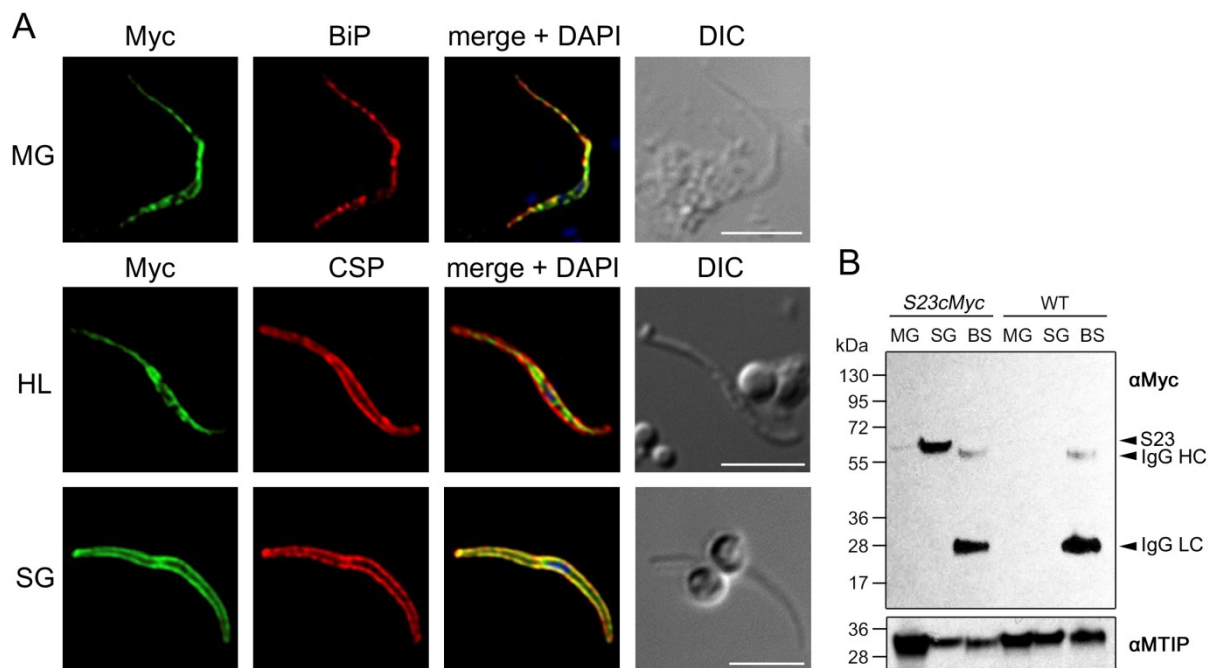


**Figure 3.13** Expression of S23 increases during sporozoite maturation. (A) IFA of *S23cMyc* sporozoites. S23 overlapped with the ER marker BiP in midgut oocyst sporozoites (MG). Hemolymph-derived sporozoites (HL) showed an internal staining pattern for S23 while salivary gland sporozoites (SG) showed a circumferential pattern that co-localized with the surface marker CSP. (E) Western blot analysis of lysates from *S23cMyc* sporozoites using mouse anti-Myc antibodies. S23 expression was minimal in midgut-derived sporozoites (MG) but increased in salivary gland sporozoites (SG). S23 was not detected in mixed blood stages (BS). Lysates of wild type parasites (WT) served as negative control. MTIP served as a loading control. Note that anti-mouse secondary antibodies detect endogenous mouse IgG present in the blood stage sample. HC, heavy chain; LC, light chain.

### 3.4.3 The ectodomain of S23 is not readily accessible to antibodies

To further characterize the subcellular localization of S23 and determine the orientation within the membrane, another parasite line was generated that expresses S23 N-terminally tagged with a triple hemagglutinin (HA) tag in addition to the C-terminal quadruple Myc tag (Figure 3.14A). Transgenic parasites were subjected to limiting dilution cloning, which resulted in the isolation of a single clone that was used for further analysis and is referred to as *S23nHA-cMyc* (Appendix C, Figure C.2). Expression of double-tagged S23 in salivary gland sporozoites was verified by Western blot using Myc- and HA-specific antibodies. A single protein species that migrated at ~70 kDa representing full-length double-tagged S23 was uniquely detected in transgenic

sporozoites (Figure 3.14B). Because S23 contains 13 conserved cysteine residues, it was tested whether these residues form disulfide bonds by analyzing the electrophoretic mobility of S23 under reducing and non-reducing conditions (omitting disulfide-reducing agent BME, no boiling). Indeed, a mobility shift was observed (Figure 3.14C), indicating the presence of intramolecular disulfide bonds.

IFA on permeabilized sporozoites with HA- and CSP-specific antibodies resulted in the expected overlapping staining pattern (Figure 3.14D, top panel). IFA with anti-HA and anti-Myc antibodies confirmed expression and co-localization of the tags (Figure 3.14D, bottom panel). To determine the orientation within the plasma membrane, IFAs on non-permeabilized salivary gland sporozoites were performed. Antibody staining with anti-Myc antibodies did not yield a signal (Figure 3.14E) indicating that the Myc tagged C-terminus of S23 might face the cytoplasm, which would be in agreement with its predicted topology. Unexpectedly however, only a few sporozoites stained positive when using antibodies against the N-terminal HA tag of S23 (Figure 3.14E). Thus, it appears that the N-terminus of S23 is not readily accessible to antibodies in non-permeabilized sporozoites.

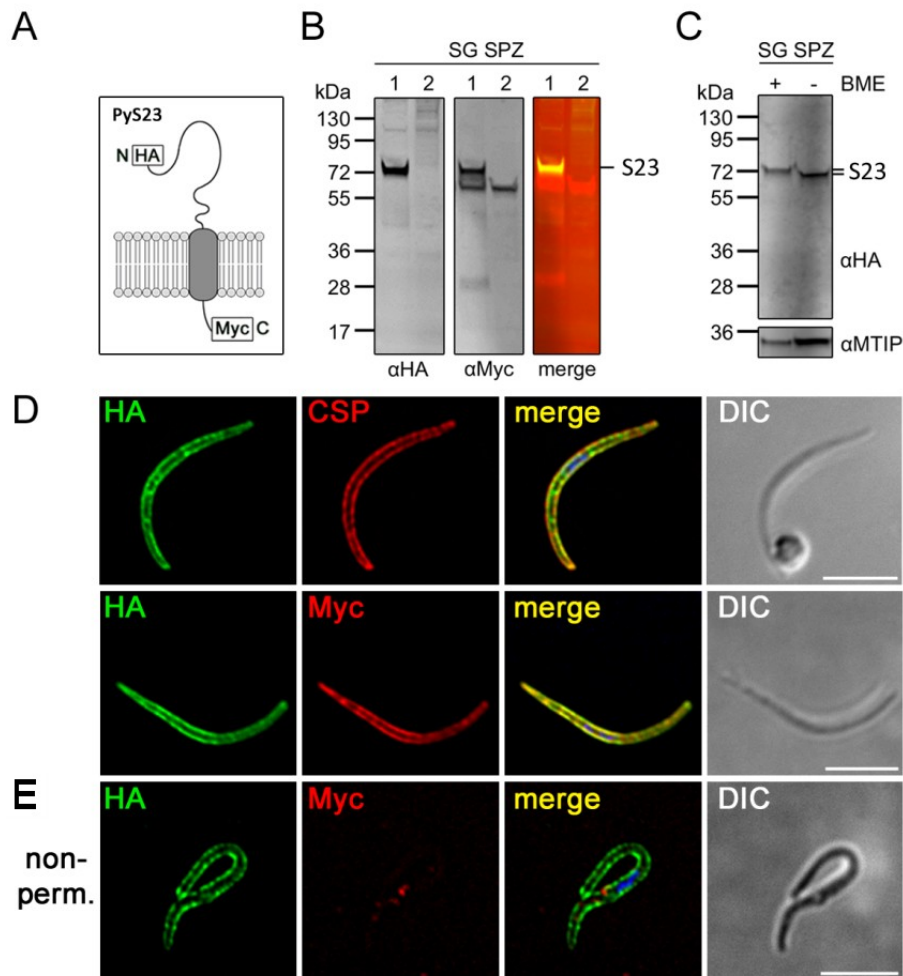


**Figure 3.14** Expression and localization of double-tagged S23 in *P. yoelii* sporozoites. (A) Schematic representation and predicted topology of S23 tagged with an N-terminal triple HA tag and a C-terminal quadruple Myc tag. Transgenic *P. yoelii* parasites expressing double-tagged S23 were generated by double-crossover homologous recombination (Figure S2). (B) Two-color western blot analysis of lysate from *Py S23nHA-cMyc* salivary gland sporozoites (lane 1) probed with anti-HA and anti-Myc shows expression of both tags. WT sporozoites (lane 2) were used as a negative control. Analysis was carried out using the Odyssey Infrared Imaging System. The blot is displayed for each channel in grayscale as well as in color when both channels are merged (HA in green, Myc in red). Note that anti-Myc antibody detects a non-specific band at ~55 kDa. (C) Lysate of *Py S23nHA-cMyc* sporozoites was run under reducing (+ BME) and non-reducing (- BME) conditions and revealed a mobility shift of S23. Incubation of the same blot with antibodies against Myosin A tail interacting protein (MTIP) served as a loading control. (D) IFA of salivary gland sporozoites. The majority of sporozoites displayed a peripheral pattern which overlapped with the surface protein CSP (top panel). The bottom panel shows the expected co-localization of the epitope tags. (E) IFA of non-permeabilized (non-perm.) salivary gland sporozoite. All scale bars are 5  $\mu$ m.

To further substantiate this finding, polyclonal antibodies against the putative ectodomain of S23 were generated by Noah Sather and Brandon Sack (Appendix C, Figure C.2). S23 antibodies were tested in Western blots of WT sporozoite lysates under

reducing and non-reducing conditions. A single band was observed in the non-reduced sample, suggesting that the S23 antibodies predominantly recognize conformational epitopes (Figure 3.15A). IFAs on permeabilized *S23nHAcMyc* sporozoites with anti-S23 and anti-Myc antibodies resulted in overlapping signals, demonstrating specificity of the S23 antibodies (Figure 3.16B, bottom panel). Staining of wild type sporozoites with anti-S23 yielded a similar peripheral pattern (Figure 3.16B, top panel). However, IFAs on non-permeabilized wild type sporozoites with anti-S23 antibodies did not yield a reliable signal; the majority of sporozoites was not stained (Figure 3.16C).

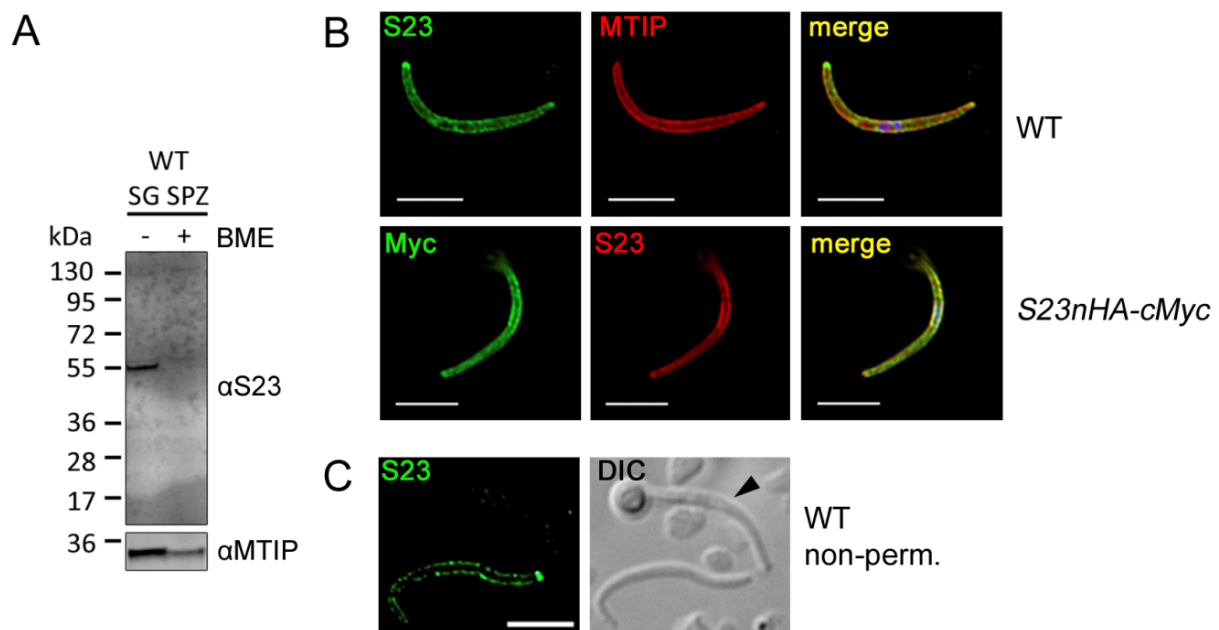


**Figure 3.15** IFA on sporozoites with polyclonal antibodies specific to PyS23. (A) Western blot analysis on lysate from WT salivary gland sporozoites (SG SPZ) under non-reducing (- BME) and reducing (+ BME) conditions. A specific protein band of the expected size was detected in the non-reduced sample, suggesting that anti-S23 antibodies predominantly recognize conformational epitopes. MTIP served as loading control. (B) Permeabilized WT sporozoites and sporozoites expressing tagged S23 showed peripheral staining pattern. (C) In non-permeabilized (non-perm.) wild type (WT) sporozoites, S23 was rarely detected. Most sporozoites did not stain positive for S23 (arrow). Bars are 5  $\mu$ m.

#### 3.4.4 Immuno-EM determines surface localization of S23

To further analyze the precise subcellular localization of S23, sporozoites were subjected to immuno-electron microscopy (IEM), conducted by Motomi Torii (Ehime University, Japan). Sections of *S23nHa-cMyc* sporozoite-infected salivary glands were stained with anti-HA antibodies or with anti-S23 antibodies followed by secondary antibodies conjugated to gold particles. S23 predominantly localized to the sporozoite

surface with gold particles closely associated with the plasma membrane. Interestingly, S23 appeared non-homogenously distributed as indicated by the frequent clustering of gold particles (Figure 3.16). A small amount of S23 was detected intracellularly within the sporozoite and might represent S23 trafficking through the secretory pathway to the periphery (Figure 3.16D and 3.16E). In addition to being detected on the sporozoite surface, S23 was less frequently localized to the space between the plasma membrane and the inner membrane complex (Figure 3.16E).

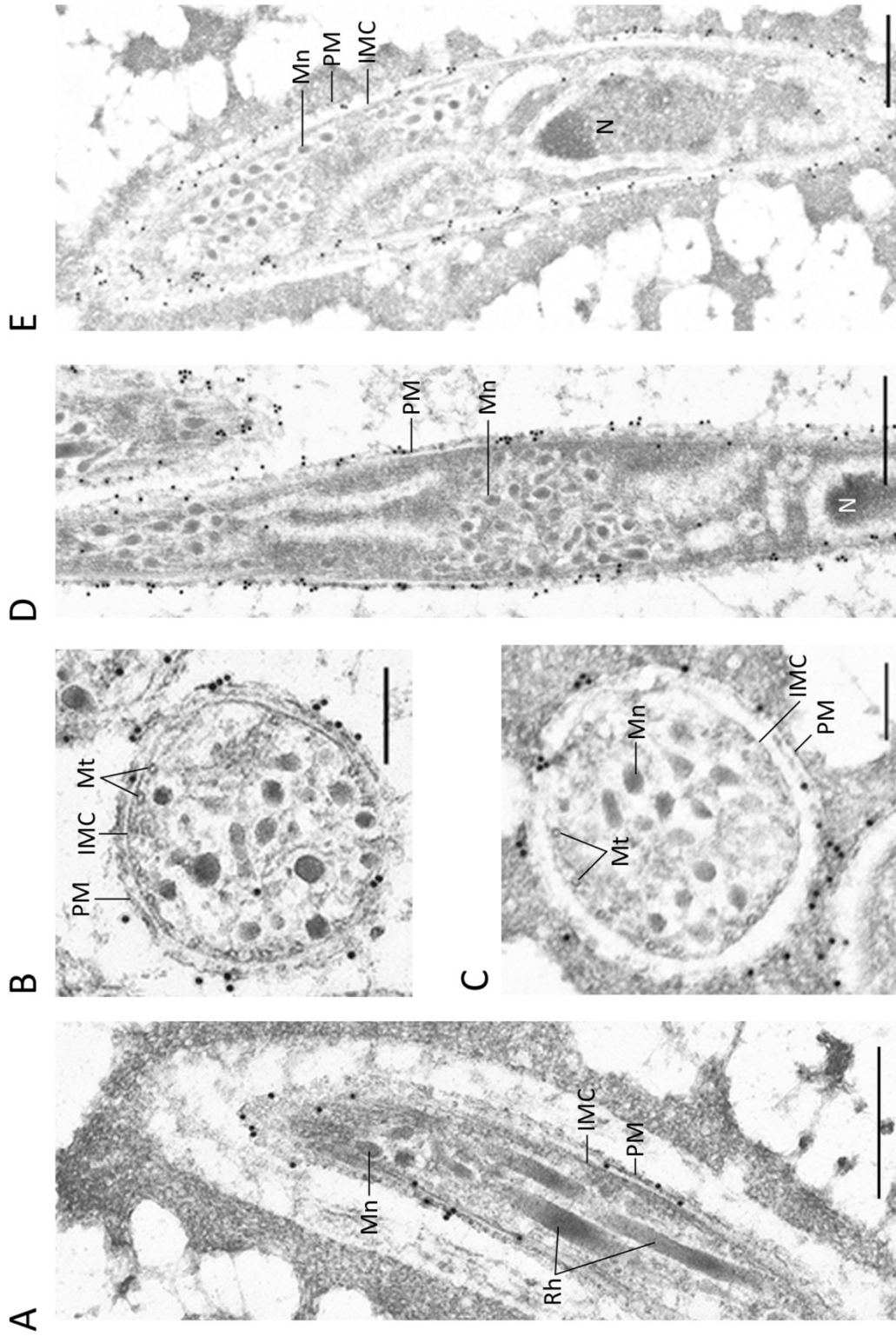


**Figure 3.16** Localization of PyS23 by immuno-electron microscopy. Ultrathin sections of mosquito salivary glands infected with *Py S23nHA-cMyc* sporozoites were incubated with either anti-HA antibodies (A and B) or with anti-S23 (C-E) followed by secondary antibodies conjugated to goldparticles. IMC, inner membrane complex; Mn, microneme; Mt, microtubule; N, nucleus; PM, plasma membrane; Rh, rhoptry. Scale bars in A, D and E are 500 nm; in B and C 250 nm.

### 3.4.5 S23 is not shed following sporozoite activation

Sporozoite surface proteins such as CSP and TRAP are shed in trails during gliding motility on a solid substrate (84,97). To investigate whether S23 is also shed in trails, *S23nHa-cMyc* sporozoites were allowed to glide on glass coverslips in the presence of serum for 1 h at 37 °C and were then stained with anti-CSP and anti-HA or anti-Myc antibodies. Gliding trails were clearly visible based on CSP staining, however S23 was not detected in trails as determined by the lack of staining of HA or Myc (Figure 3.17A). To corroborate the finding that S23 is not released upon gliding motility activation, the supernatant from preparations that contained activated sporozoites was analyzed by Western blot. S23 was not detected in the supernatant but only in the sporozoite pellet, whereas the micronemal protein TRAP was secreted and detected in the supernatant (Figure 3.17B). These results suggest that S23 is not released following sporozoite activation and is not shed during gliding motility.

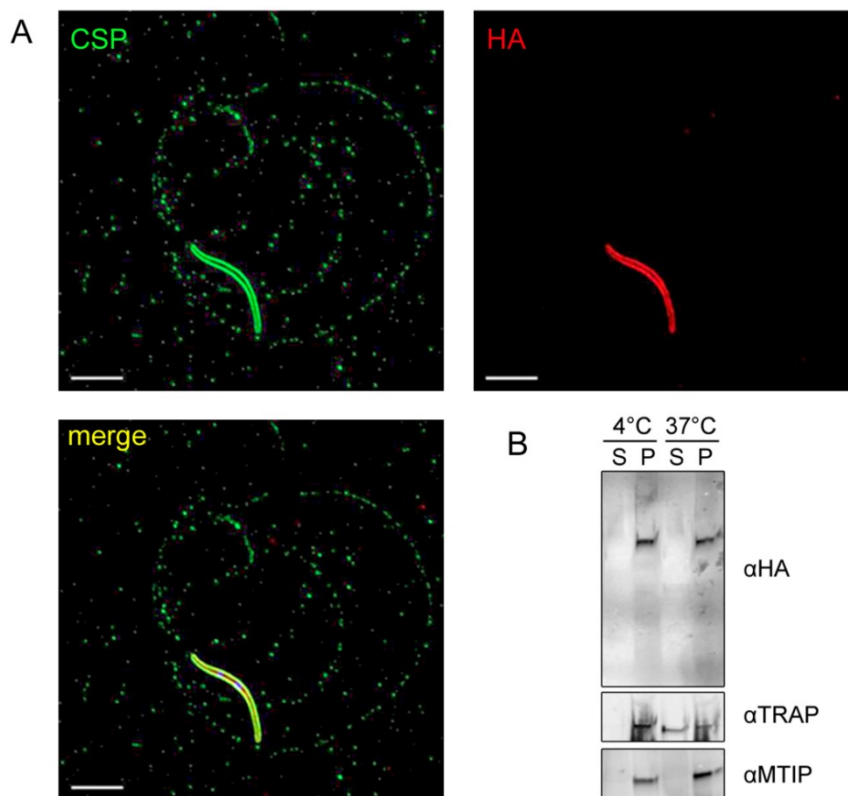


**Figure 3.17** S23 is not shed during sporozoite gliding motility. (A) Sporozoites were allowed to glide on CSP-coated glass coverslips for 1 h, fixed, permeabilized and stained with anti-HA and Alexa Fluor 488-conjugated anti-CSP to visualize trails. (B) To test whether S23 is shed into the supernatant upon activation, sporozoites were incubated in the presence of serum for 1 h on ice (control) and at 37 °C, respectively. Supernatants (S) and pellets (P) were subjected to SDS-PAGE, blotted and incubated with anti-HA; anti-MTIP and anti-TRAP served as controls. Scale bars are 5  $\mu$ m.

### 3.4.6 Accessibility to S23 on the sporozoite surface might be masked by CSP

S23 clearly localized to the surface of salivary gland sporozoites as determined by IEM, however S23 was not readily detected on the surface in non-permeabilized sporozoites using IFA. One reason for this could be that S23 is inaccessible to antibodies, potentially due to the dense coat of CSP that entirely covers the sporozoite surface. CSP is a putatively GPI-anchored protein that is shed when cross-linked by antibodies, a process known as the CSP precipitation reaction (42). To test whether S23 is accessible to antibodies upon shedding of CSP, live *S23nHa-cMyc* sporozoites were incubated with anti-CSP antibodies as well as anti-HA or anti-Myc to label S23. Sporozoites that had shed CSP were readily distinguished from non-shed either through the presence of the precipitate or through weaker fluorescence intensity of the CSP signal remaining on the sporozoite surface (Figure 3.18). While the majority of CSP-shed sporozoites still did not stain positive for S23, a strong circumferential signal for the N-terminal HA tag was observed in ~20 % of CSP-shed *S23nHa-cMyc* sporozoites (Figure 3.18, middle panel). As shown (Figure 3.14E), the C-terminal Myc tag was never detected in these experiments (Figure 3.18, bottom panel), further indicating that the C-terminus of S23 faces the sporozoite interior. Overall, these results suggest that S23 might be masked by CSP and is exposed and accessible to antibodies once CSP is shed.

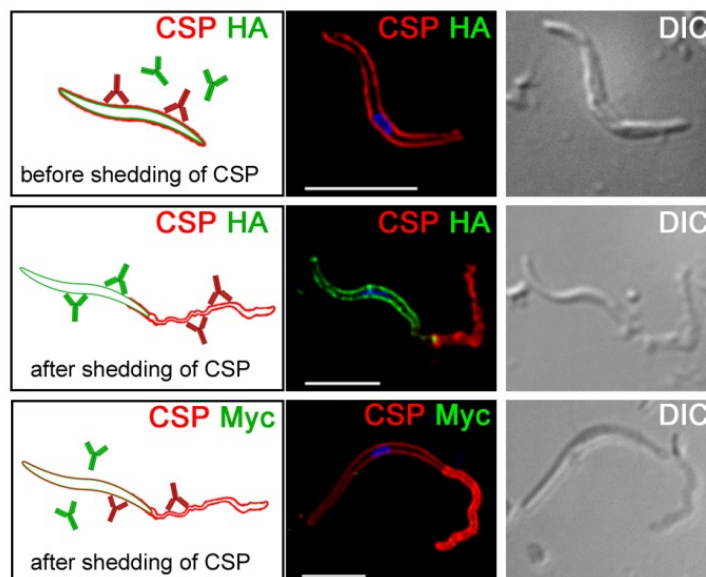


**Figure 3.18** S23 might be masked by CSP. Live *Py S23nHA-cMyc* sporozoites were incubated for 1 h with anti-CSP antibodies to induce shedding of CSP, and were simultaneously incubated with anti-HA or anti-Myc to label S23. Sporozoites were then washed, fixed and stained with secondary antibodies. Explanatory cartoons for the observed staining patterns are shown on the left. Scale bars are 5  $\mu\text{m}$ .

### 3.4.7 S23-deficient parasites are viable but are defective in gliding motility

To determine whether S23 is important for progression through the life cycle of *P. yoelii*, gene knockout parasites (*Py s23*<sup>-</sup>) were generated using the replacement strategy (Figure 3.19A). Recombinant parasites were cloned by serial dilution and the gene knockout was confirmed by PCR genotyping and Southern blot analysis (Figure 3.19B and 3.19C). The successful deletion of S23 in *P. yoelii* showed that it does not play a role for the growth of blood-stage parasites, which is in good agreement with the lack of S23 expression in these stages.

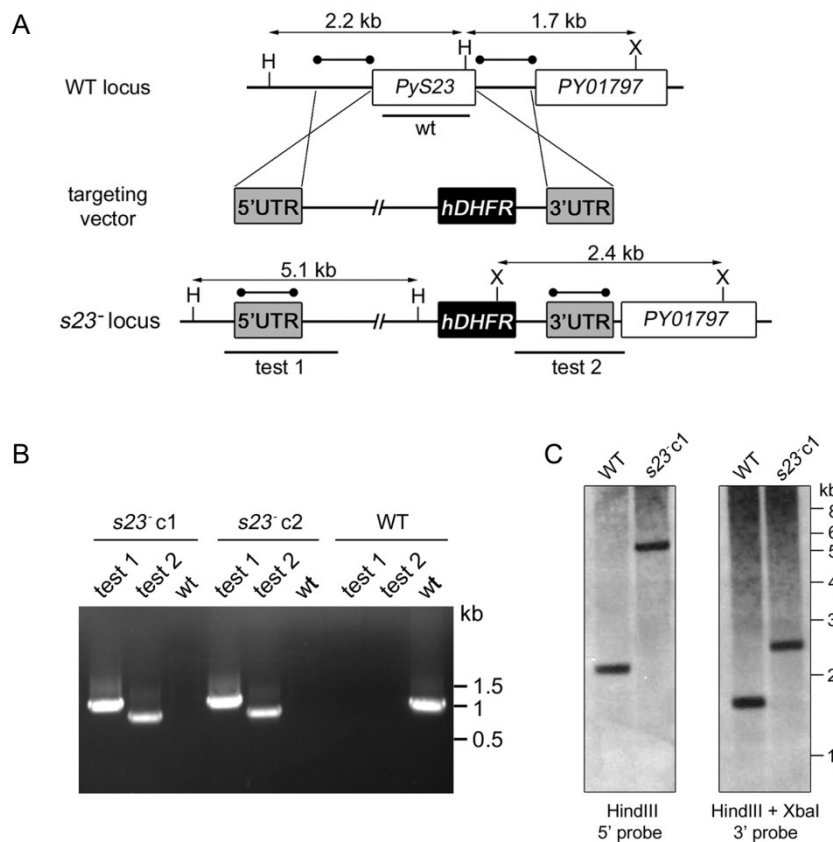


**Figure 3.19** Generation of *Py s23*<sup>-</sup> parasites. (A) Schematic of targeting strategy used to generate *Py s23*<sup>-</sup> parasites. The S23 open reading frame was replaced with the positive selectable marker human dihydrofolate reductase (*hDHFR*) by double crossover homologous recombination using the 5' and 3' untranslated regions (UTRs) of S23. (B) PCR genotyping of gDNA from two *s23*<sup>-</sup> clones with primers (bars in A) specific to the wild-type locus (wt) and to the transgenic locus (test 1 and test 2) shows proper integration of the construct. (D) Southern blot analysis of *s23*<sup>-</sup> clone 1. Digestion of *s23*<sup>-</sup> gDNA with HindIII and XbaI ('H' and 'X' in A) results in the expected band shift as compared to WT gDNA using probes (dumbbell bars in B) specific to the 5' and 3' UTRs of S23. Sizes of the expected fragments are shown in A.

## Results

To determine whether the deletion of *S23* affected the parasite life cycle stages within the mosquito, sporozoite numbers in midguts and salivary glands were determined. WT and *s23*<sup>-</sup> clones generated comparable numbers of oocyst and salivary gland sporozoites (Table 3.6). These results demonstrate that the deletion of *S23* does not affect sporogony, sporozoite egress from oocysts or invasion of salivary glands.

**Table 3.6** *P. yoelii s23*<sup>-</sup> show normal development in the mosquito vector.

<i>P. yoelii</i> genotype	MG SPZ/mosquito (mean ± SD)	SG SPZ/mosquito (mean ± SD)
<i>s23</i> <sup>-</sup> clone 1	50,085 ± 9,705	25,605 ± 5,767
<i>s23</i> <sup>-</sup> clone 2	59,933 ± 53,855	24,430 ± 25,270
<i>S23cMyc</i>	69,109 ± 8202	29,309 ± 10,487
<i>S23nHA-cMyc</i>	61,073 ± 33,999	26,143 ± 21,918
WT	69,236 ± 26,345	31,497 ± 4,746

Next it was tested whether the sporozoites' gliding locomotion is affected by the lack of *S23*. Productive gliding motility depends on adhesion to the substrate which is mediated by surface proteins including CSP and TRAP proteins (204,205). Adhesion is a multi-step process that involves an initial attachment with either the apical or the posterior end of the sporozoite, followed by attachment of the other end and finally adhesion of the central part (206). Sporozoites then start to move and leave trails of cleaved CSP and TRAP behind. To analyze motility of *s23*<sup>-</sup> parasites, salivary gland sporozoites were added to glass coverslips pre-coated with anti-CSP antibodies and trails were visualized using Alexa Fluor 488-conjugated anti-CSP antibodies. A significantly reduced number of trails were left behind by *s23*<sup>-</sup> sporozoites as compared to WT sporozoites (Figure 3.20). Gliding motility of *S23nHA-cMyc* sporozoites was analyzed as an additional control. WT and *S23nHA-cMyc* sporozoites showed typical circular gliding trails whereas the majority of *s23*<sup>-</sup> sporozoites did not produce any trails. We then performed video microscopy on live sporozoites. WT sporozoites exhibited continuous circular gliding motility whereas *s23*<sup>-</sup> sporozoites were often attached to the glass slide with only one end (please refer to the supplemental movies of the paper; <http://dx.doi.org/10.1128/IAI.01800-14>). It appeared that the adhesion steps following the initial attachment were unsuccessful and thus did not allow the sporozoite to initiate gliding. These results suggest that the motility defect in *s23*<sup>-</sup> sporozoites might result from the failure to properly attach to the substrate.

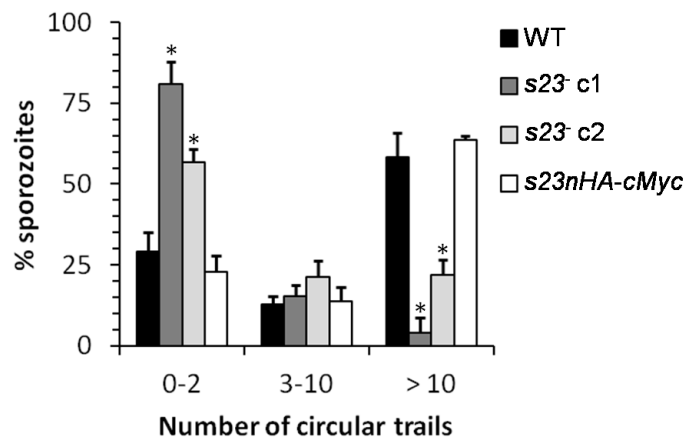


**Figure 3.20** *Py* s23<sup>-</sup> sporozoites show a gliding defect *in vitro*. Salivary gland sporozoites were allowed to glide on CSP-coated glass coverslips and trails were visualized using Alexa Fluor 488-conjugated anti-CSP antibodies. The number of circles per trail associated with a sporozoite was counted for at least 100 trails per experiment. s23<sup>-</sup> sporozoites showed significantly less trails that consist of more than 10 circles (\*  $p < 0.001$  when compared to WT; unpaired t test). Error bars represent SD of three biological replicates for WT and s23<sup>-</sup> clone 1, and three technical replicates for s23<sup>-</sup> clone 2 and S23nHA-cMyc.

#### 3.4.8 S23 is not required for cell traversal and invasion

Next it was analyzed whether the observed motility defect of s23<sup>-</sup> sporozoites translates into a defect in cell traversal and hepatocyte invasion by using a flow cytometry-based cell wounding- and invasion assay (110,207,208). Sporozoites were added to hepatoma cells in the presence of cell-impermeable Alexa Fluor 488-conjugated dextran and incubated for 90 min. Traversing sporozoites migrate through cells by disrupting the membrane which leads to uptake of dextran that gets trapped inside the cell once the membrane is resealed (110). Intracellular sporozoites were detected by staining of infected cells with CSP-antibody. Surprisingly, WT and s23<sup>-</sup> sporozoites showed no significant differences in their capacity to traverse and invade hepatoma cells *in vitro* (Figure 3.21A and 3.21B).

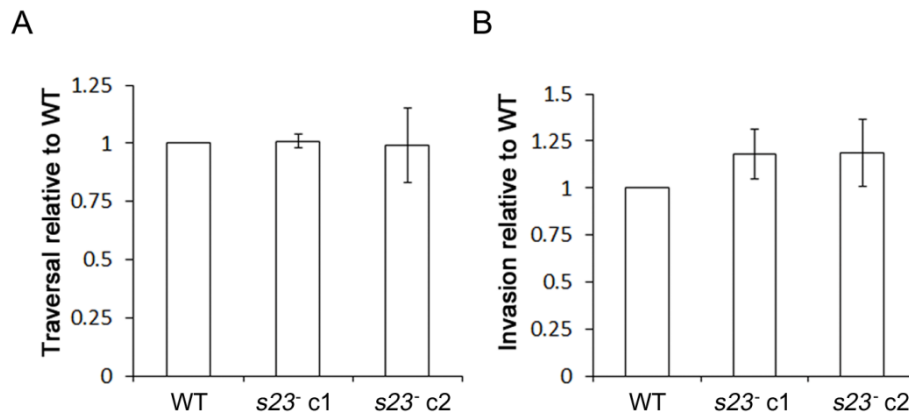


**Figure 3.21** *Py s23<sup>-</sup>* sporozoites show normal cell traversal and invasion *in vitro*. (A) *In vitro* traversal and (B) infection assay. Salivary gland sporozoites were added to Hepa 1–6 cells in the presence of cell-impermeable Alexa Fluor 488-dextran. Cells were trypsinized 90 min post infection, fixed, stained with Alexa Fluor 647-conjugated anti-CSP antibodies and subjected to flow cytometry analysis. Error bars represent SD of technical triplicates

It was then tested whether the lack of S23 affected the transmission of sporozoites from mosquito to mouse *in vivo* and whether *s23<sup>-</sup>* sporozoites are able to infect the liver and ultimately establish blood-stage infection. One thousand *s23<sup>-</sup>* sporozoites were intravenously injected into BALBc/J mice and the onset of blood-stage infection (patency) was monitored by analyzing Giemsa-stained thin blood smears. To analyze the ability of *s23<sup>-</sup>* sporozoites to exit the dermal tissue, mice were inoculated with  $1 \times 10^3$  or  $1 \times 10^4$  *s23<sup>-</sup>* sporozoites intradermally (ID) and via infectious mosquito bite. All mice became blood-stage patent on day 3 post infection (Table 3.7) except for mice that received the low-dose ID injection. One of five mice injected with  $1 \times 10^3$  *s23<sup>-</sup>* ID did not develop blood-stage parasitemia, while the other mice of this group became patent on day 3 post infection. A similar result was obtained in the respective control group (2/5 mice remained patency negative). This suggests that ID injection of  $1 \times 10^3$  sporozoites is below the 100 % infectious dose. Overall, the results demonstrated that *s23<sup>-</sup>* sporozoites are fully capable of infecting mice and that S23 is not critical for traversal of dermal tissue and for invasion of hepatocytes.

## Results

**Table 3.7** *s23<sup>-</sup>* sporozoites successfully establish liver infection and transition to blood-stage infection in mice.

<i>P. yoelii</i> genotype	No. of injected sporozoites <sup>a</sup>	No. of infected BALB/cJ mice	Day of patency <sup>b</sup>
<i>s23<sup>-</sup></i> clone 1	1 × 10 <sup>3</sup> IV	5/5	3
WT	1 × 10 <sup>3</sup> IV	3/3	3
<i>s23<sup>-</sup></i> clone 1	Mosquito bite (31,355 SPZ/mosquito)	5/5	3
WT	Mosquito bite (43,536 SPZ/mosquito)	5/5	3
<i>s23<sup>-</sup></i> clone 1	1 × 10 <sup>3</sup> ID	4/5	3
WT	1 × 10 <sup>3</sup> ID	3/5	3
<i>s23<sup>-</sup></i> clone 1	1 × 10 <sup>4</sup> ID	5/5	3
WT	1 × 10 <sup>4</sup> ID	5/5	3

a. Sporozoites (SPZ) were delivered intravenously (IV), intradermally (ID) and by mosquito bite, respectively. Mice were individually exposed to the bites of 12-15 mosquitoes for 7.5 min, rotating the mice between mosquito cages every 1.5 min. Salivary gland sporozoites of blood-fed mosquitoes were quantified; numbers are shown in parentheses.

b. The time to blood stage patency was monitored microscopically by Giemsa-stained thin blood smears.

Additionally, we analyzed the liver stage burden by quantitative reverse-transcription PCR. BALB/cJ mice were intravenously injected with 1 × 10<sup>5</sup> sporozoites and livers were harvested at 44 h post injection. Livers of mice infected with WT and *s23<sup>-</sup>* sporozoites displayed no significant differences in parasite burden (Figure 3.22).

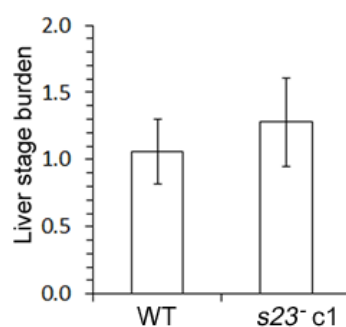


**Figure 3.22** The lack of S23 has no effect on the liver stage burden *in vivo*. BALB/cJ mice (n = 5) were injected intravenously with 1 × 10<sup>5</sup> salivary gland sporozoites. Liver stage burden was monitored 44 h post infection using quantitative reverse-transcription PCR. Parasite RNA was detected using primers specific to the *P. yoelii 18s rRNA* gene. Transcript expression levels were normalized to mouse *GAPDH* expression levels and are shown as mean ± SD.

In summary, this study demonstrated that S23 is a novel sporozoite surface protein that plays a role in gliding motility but is dispensable for the parasites' life cycle progression.

## 4 Discussion

### 4.1 The 6-Cys protein P38 is dispensable throughout the entire parasite life cycle

Proteins of the conserved 6-Cys family in *Plasmodium* have received attention as vaccine candidates because many of them were shown to locate on the parasite surface and have been implicated in cell-cell interactions (161,164,165). Sporozoites lacking the 6-Cys proteins P52 and P36 are arrested in their development soon after hepatocyte invasion, and are being pursued as a GAP vaccine for use in humans (49,50,144,174,175,209). Here, it was analyzed if P38 has a similar important function in liver infection as P52 and P36. P38 is shown to localize to secretory organelles in sporozoites, and so is appropriately positioned for involvement in tissue traversal and/or host cell invasion. However, there is no evidence for a crucial role of P38 in these processes.

Proteomic analyses of the human parasite *P. falciparum* and the rodent species *P. yoelii* and *P. berghei* demonstrated the presence of P38 in asexual blood stages, gametocytes and sporozoites (161,176,196). In the present study, using epitope-tagging and Western blot analysis it is shown that P38 is expressed in mixed blood stages and sporozoites in *P. yoelii* (Py). Expression in sporozoites was higher than in mixed blood stages, which is in agreement with microarray data showing a nearly twofold increase in *PyP38* transcript abundance in sporozoites compared to blood stages (210). *P. falciparum* P38 (PfP38) was demonstrated to localize to apical organelles and the surface of schizonts (161). Immunofluorescence assays suggest that PyP38 localizes to the schizont surface as well. However, while some schizonts clearly exhibited P38 on the surface, the majority showed a speckled localization for P38. It is possible that these different patterns resemble different stages of schizont development. Schizonts with a speckled P38 localization might not have yet accumulated P38 at the cell surface. Immunofluorescence assays of salivary gland sporozoites demonstrated for the first time that P38 localizes to micronemes, and it thus shares the same subcellular localization with the family member P52 (49). Micronemal proteins are involved in gliding motility, cell traversal, and host cell invasion. Indeed, P52 is believed to play a role in the formation and/or maintenance of the parasitophorous vacuole during

hepatocyte invasion (50). Sporozoites lacking P52 fail to develop as a liver stage and do not transition to blood stage (50). To study the importance of P38 in the parasite life cycle, we generated loss-of-function mutants in *P. yoelii*. P38-deficient parasites produced normal sporozoite numbers, demonstrating that P38 is not required for fertilization and development within the mosquito. This result is in agreement with studies in *P. berghei* where *P38* knockout parasites showed normal fertilization rates and produced similar numbers of oocysts as wild type (164). Here, we furthermore showed that sporozoites lacking P38 display normal gliding motility, cell traversal activity, and that they were capable of establishing infection in mice. Hence, P38-deficient sporozoites do not qualify as a GAP vaccine candidate as they are clearly not attenuated. The results demonstrate that the function of P38 is not important, or that it can be compensated for by another protein. Functional redundancy of *Plasmodium* proteins has been described for members of multi-gene families involved in invasion of erythrocytes (211,212). The subcellular localization of P52 and P38 suggest that the function of these proteins might be mutually redundant. However, the fact that P52-deficient sporozoites are strongly attenuated does not support this hypothesis. Two more 6-Cys family members are expressed in sporozoites, P36 and P12p (182). P36 is the paralog of P52 (49) and when disrupted yields a similar attenuated phenotype as disruption of P52 (49,174). P12p is a predicted GPI-anchored protein that has not been characterized yet. While unlikely for P36, it is possible that P12p and P38 have redundant roles in sporozoites. It will be interesting to see if targeted deletion of P12p or both, P12p and P38, affects sporozoite infectivity. As P38 and P12p are not adjacent to one another in the parasite genome, the generation of double knockout parasites requires sequential genetic modifications. Due to the limited number of selectable markers, it is necessary to recycle the selectable marker cassette. This could be accomplished by using the 'gene-insertion/marker-out' method that has been developed for use in *P. berghei* and *P. yoelii* (213).

Because P38 is also expressed in blood stages, the growth rate of P38-deficient parasites was analyzed *in vivo*. *p38*<sup>-</sup> parasites grew at a normal rate and had a similar peak parasitemia as WT, but their clearance was delayed by two days. Parasite clearance is dependent on humoral and cellular immunity (214,215). Given the localization on the merozoite surface, it is possible that mice mount antibody responses

to P38, like malaria-exposed humans (161). Although highly speculative, the delay in clearance of *p38* parasites might be attributed to the lack of anti-P38 antibodies opsonizing the parasite for phagocytosis.

Whether the results obtained in this study can be translated to the clinically relevant parasite *P. falciparum* remains to be addressed experimentally; a PfP38 knockout study has not been published to date. However, peptides derived from PfP38 were demonstrated to have erythrocyte binding activity and moderately inhibited erythrocyte invasion by merozoites (216). Furthermore, genomic analysis of *P. falciparum* field isolates revealed that P38 is under immune selective pressure (217,218). Interestingly, only the first 6-Cys domain was highly polymorphic while the second 6-Cys domain did not show evidence for balancing selection (218). The authors suggested that the second 6-Cys domain might be the functionally important one and is shielded from the host's immune response by the first 6-Cys domain. Together, these studies suggest that PfP38 is involved in erythrocyte attachment or invasion. It is important to consider that different *Plasmodium* species vary in their preferences for the type of erythrocytes they invade. *P. falciparum* invades erythrocytes of all ages while *P. yoelii* 17XNL, used in this study, predominantly invades immature erythrocytes (reticulocytes). It is possible that P38 is involved in attachment or invasion of mature red blood cells but not in that of reticulocytes. The lack of P38 might therefore not affect erythrocyte invasion by *P. yoelii* but might impair *P. falciparum*.

Overall, this study showed that P38 localizes to micronemes in salivary gland sporozoites and that it is dispensable throughout the entire life cycle of *P. yoelii*. Further research is required to unravel the function of P38.

#### **4.2 The sporozoite surface proteome**

Determining the sporozoite surface proteome is of fundamental importance in understanding host-parasite interactions in the initial phase of malaria infection. Although not exhaustive, we present the first description of the sporozoite surface proteome of *P. yoelii* and the human parasite *P. falciparum*. To identify surface proteins, we biotinylated surface-exposed proteins on purified live sporozoites, enriched them from whole sporozoite lysates, verified protein biotinylation by Western blot, and then subjected them to mass spectrometry (182).

We identified several proteins known to localize to the sporozoite surface and multiple novel surface-exposed proteins as well. Importantly, several proteins overlapped between the *P. falciparum* and *P. yoelii* datasets. Many of the identified proteins contain putative signal peptides or transmembrane domains, and additionally are predicted to have functions consistent with a surface localization, such as the transport of molecules across the sporozoite plasma membrane. Several other surface-exposed proteins have no known domains, and have not been previously characterized. However, we also observed multiple proteins that are associated with the inner membrane complex which lies just underneath the plasma membrane. These proteins were also detected by Wass and colleagues in their efforts to determine the ookinete surface proteome using a similar approach (219). The authors hypothesized that the parasite plasma membrane becomes partially permeable to the biotin reagent during the labeling procedure. This hypothesis was experimentally confirmed by the increasing accessibility of propidium iodide to the parasite under the progressive conditions used in the labeling process. It is likely that a similar phenomenon occurs with sporozoites as well. Because of this, we have placed stronger confidence in calling proteins as surface localized if they are predicted to be secreted or membrane-associated. The sporozoite samples were furthermore substantially contaminated with mosquito proteins, although the sporozoite purification method used in this study efficiently separates mosquito debris from sporozoites (183). As large-scale *in vitro* methods for sporozoite production are not available, sporozoites must be isolated from infected mosquito salivary glands by manual dissection. Contamination with mosquito proteins is thus unavoidable. The contaminating proteins can overwhelm the analysis capacity of the mass spectrometer and obscure the proteins of interest. Because we focused on a subset of sporozoite proteins, the contamination issue likely became more pronounced due to the lower abundance of parasite proteins in the sample.

However, overall, the sporozoite surface proteomes have allowed for the identification of several novel uncharacterized proteins which provide a good starting point for gene deletion studies to investigate their role in sporozoite biology.

### **4.3 Novel sporozoite surface proteins encoded by UIS genes are dispensable for infection of the mammalian host**

PY02432, PY06766 and PY05332 were identified in the putative surface proteomes of *P. falciparum* and *P. yoelii* sporozoites. These proteins are encoded by *UIS* genes, which are thought to be important for infection of the mammalian host (123,127). Several of them were shown to be essential, e.g. P52, UIS3, UIS4 (48,50,51). Parasites lacking these proteins are arrested in liver stage development and do not infect the blood. Because of the severe defects associated with the deletion of these *UIS* genes, the focus of the present study was to test if the lack of PY02432, PY06766 and PY05332 has a similar attenuating effect on sporozoites. However, targeted deletion of *PY02432*, *PY06766* or *PY05332* did not affect the sporozoites' ability to establish infection in mice. All mice inoculated with gene knockout sporozoites, either intravenously or by mosquito bite, became blood stage patent on the same day as the control group. It is important to mention that subtle differences in the infectivity between knockout and wild type sporozoites are not detected by monitoring the onset of blood stage infection due to the highly infectious nature of *P. yoelii* (220). Hence, while it cannot be ruled out that the here briefly analyzed proteins play a role in liver infection, it can be concluded that they are not essential.

PY02432 is a tyrosine-rich protein that is unique to *Plasmodium*. It is highly expressed in sporozoites (210), suggesting a sporozoite-specific role, yet its function is not required for progressing through the life cycle. PY02432 has no signal peptide or transmembrane domain, but it contains a putative palmitoylation site in the N-terminal region. Palmitoylation is catalyzed by membrane-bound palmitoyl transferases (PATs) (221). The *Plasmodium* genome encodes multiple PATs several of which are expressed in sporozoites (182,222). Furthermore, over 400 palmitoylated proteins were recently identified in *P. falciparum* blood stage schizonts, demonstrating the extensive use of this modification by the parasite (195). In order to undergo palmitoylation, the protein must first traffic to the proper membrane where the specific PAT localizes. This is often achieved by other lipid modifications such as N-myristoylation or prenylation during or after protein translation (223). PY02432 does not contain other predicted modifications, which however does not rule out their presence. PATs generally catalyze palmitoylation on the cytoplasmic face of the membrane, suggesting that PY02432 might be tethered either to the inner leaflet of the plasma membrane or to the

underlying IMC since we detected several IMC-associated proteins in the putative sporozoite surface proteome (182). Because attempts to epitope-tag PY02432 failed, the localization of PY02432 remains to be determined. It is unclear why tagging of PY02432 failed; a similar approach has been successfully used to tag S23 (section 3.4). Transgenic parasites which had integrated the tagging construct in the proper genomic locus were readily generated, demonstrating the accessibility of the locus to genetic modification. However, the DNA sequence of the epitope tag was repeatedly missing. It is possible that a gene conversion event led to the removal of the epitope DNA sequence.

PY06766 is conserved among *Plasmodium* but also has putative orthologs in the coccidian parasites *Toxoplasma*, *Eimeria* and *Neospora*. Unfortunately, no information about the function of these orthologous proteins is available. PY06766 and its orthologs contain four transmembrane domains with the N- and C-termini predicted to face the cytoplasm. They all have strong predictions for palmitoylation in the cytoplasmic N-terminal region. In several eukaryotic organisms it was shown that palmitoylation of transmembrane proteins affects protein conformation, transport function, adhesion, and signaling properties (224). However, it remains to be determined if this holds true for *Plasmodium* proteins. The cytoplasmic tail of PY06766 contains a stretch of conserved residues, including a VxKxGGxGxE motif which however was not found in other proteins when searched against a database. Epitope-tagging and immunofluorescence microscopy revealed that PY06766 is already expressed in oocyst sporozoites, which is in agreement with proteomic data (176). Oocyst and salivary gland sporozoites displayed a peripheral localization of PY06766 which in addition to the predicted transmembrane domains suggests that it indeed localizes to the sporozoite plasma membrane.

PY05332 is a putative sugar transporter that was not detected in oocyst sporozoites by IFA but was strongly expressed in salivary gland sporozoites, where it co-localized with CSP. In contrast to the other two sugar transporters that are encoded in the parasite genome, only PY05332 is upregulated in sporozoites. However, in addition to PY05332 sporozoites also express a hexose transporter (HT). Unlike PY05332, HT is expressed throughout the parasite life cycle and has been demonstrated to transport hexoses, which constitute a crucial energy source for the parasite during its intraerythrocytic development (198,199). Using a sugar analog that specifically inhibits *Plasmodium* HT,

it was demonstrated that not only asexual blood stages depend on glucose scavenging from the host but also ookinetes and liver stages (197). Whether PY05332 is a functional sugar transporter may be addressed by utilizing heterologous expression systems. *Leishmania mexicana* mutant parasites which lack glucose transport activity were previously used to demonstrate transport function of *Plasmodium* HT (197,225). PY05332 and HT share little sequence similarity which is not uncommon among proteins belonging to the MFS family (226). However, several residues that are conserved between *Plasmodium* HT and other eukaryotic sugar transporters are not conserved in PY05332. Some of these residues were previously shown to be important for substrate recognition and transport function (227). Furthermore, HT is more closely related to mammalian GluT1 than to PY05332 and no close orthologs of PY05332 are found outside the *Plasmodium* genus. Therefore, it is possible that PY05332 has evolved a different transport function. It may not transport hexose sugars but instead pentose sugars or other nutrients. Another possibility is that PY05332 lost its transport function but instead is involved in sensing specific nutrients, which has been described for transporter-like proteins in yeast (228,229).

In summary, this study described novel sporozoite surface proteins which are dispensable for sporozoite infectivity. Further in-depth analyses of the knockout sporozoites might reveal clues about the possible function of these proteins.

#### **4.4 S23 is a novel type I transmembrane protein with a role in gliding motility**

In this study, we characterized a novel sporozoite surface transmembrane protein S23 which we identified in the putative surface proteome of *P. yoelii* and *P. falciparum* salivary gland sporozoites. Expression and localization of S23 change as the sporozoites develop within the mosquito. S23 expression is initiated in oocyst sporozoites where it co-localized with the ER marker BiP. Hemolymph sporozoites exhibited heterogeneous intracellular staining patterns for S23 while most salivary gland sporozoites showed a peripheral staining that overlapped with the surface protein CSP. These data and the fact that S23 contains a predicted signal peptide suggest that S23 is transported to the sporozoite surface via the secretory pathway during sporozoite maturation, which culminates in its predominant peripheral localization in infectious sporozoites.

In an effort to determine the orientation of S23 in the sporozoite plasma membrane, we epitope-tagged both the N- and the C-termini and analyzed the accessibility of the tags

to antibodies. We were unable to reliably detect signal for either tag in fixed, non-permeabilized sporozoites, which was unexpected as IEM localized S23 on the sporozoite surface. One explanation is that the dense coat of CSP on the sporozoite surface might prevent antibodies from gaining access to S23. CSP has a predicted rod-like structure and is attached to the sporozoite plasma membrane by a putative GPI anchor (230). Based on apparent molecular mass, the putative ectodomain of S23 is not smaller than CSP but of similar size. However, S23 likely has a complex structure due to intramolecular disulfide bonds. It seems therefore reasonable to assume that S23 is masked by CSP and thus shielded from antibodies. Indeed, when we induced shedding of CSP in live sporozoites, we were able to detect the S23 N-terminal epitope tag more frequently but never the C-terminal tag. In terms of orientation, this suggests that the C-terminus faces the cytoplasm and that S23 is, as predicted, a type I transmembrane protein. However, since only some CSP-shed sporozoites stained HA-positive, other factors must play a role. Proteolytic processing might be one factor. Cleavage and shedding of surface proteins involved in motility and invasion is a key feature of apicomplexan parasites (231). It serves to either expose adhesive domains such as TSRs or to disengage adhesive interaction (84,231,232). S23 contains a TSR-like fold upstream of the predicted transmembrane domain. However, we did not detect S23 in sporozoite gliding trails by IFA or in the supernatant of sporozoites that have been incubated under motility-activating conditions. It seems therefore unlikely that the lack of tag detection in live sporozoites is due to a cleavage event. However, we cannot rule this out as cleaved fragments may be unstable and quickly degraded or too small to detect. It is also possible that the N-terminal tag is buried inside the ectodomain of S23 and may thus be difficult for antibodies to access even when CSP is shed.

To investigate the importance of S23 in sporozoites, we deleted the encoding gene from the parasite genome. *s23*<sup>-</sup> parasites showed no significant difference in their capacity to establish mosquito colonization when compared to WT parasites. However, *s23*<sup>-</sup> sporozoites displayed a gliding motility defect. WT sporozoites showed typical circular gliding trails whereas the vast majority of *s23*<sup>-</sup> sporozoites did not leave any trails behind. Video microscopy suggested that *s23*<sup>-</sup> sporozoites are able to attach to the substrate with one end but fail to establish subsequent adhesion sites and thus cannot initiate gliding motility. S23 might therefore act as an adhesin. However, it does not

contain motifs that suggest its linkage to the actomyosin motor, i.e. the stretches of negatively charged residues in the cytoplasmic tail and a subterminal tryptophan residue which are features of TRAP-family proteins (205). It is also possible that the lack of S23 on the sporozoite surface might alter the distribution or functionality of other proteins important for attachment and/or gliding *in vitro*. It has been shown that TRAP and S6, another TRAP family protein, are necessary for initial adhesion to glass slides (206). TRAP proteins are released from micronemes onto the sporozoite surface and are redistributed from the front to the end of the sporozoite. This or a similar process may be affected in *s23*<sup>-</sup> sporozoites leading to suboptimal attachment and/or gliding motility. Surprisingly, *s23*<sup>-</sup> sporozoites exhibited normal cell traversal activity and hepatocyte invasion rates that were similar to WT. Furthermore, transmission of *s23*<sup>-</sup> sporozoites via mosquito bite led to blood-stage infection in mice without a delay in patency, suggesting that the observed gliding motility defect does not translate into defects in cell traversal or invasion. The current model for host cell invasion suggests that the gliding motility is critical for cell traversal and that the same machinery drives the invasion process. Our results would argue that this model is in need of revision and are intriguing in the context of recent studies in *Toxoplasma* demonstrating that gliding motility is not essential for cell invasion (108). However, it is important to note that gliding on an artificial substrate likely poses different requirements on the sporozoite than gliding over cells or through tissues. Thus, another explanation for these results could be that the *in vitro* gliding defect is substrate-dependent and can be compensated by the presence of host cell ligands.

In summary, we showed that S23 is a novel sporozoite surface protein that plays a role in gliding motility but is dispensable for the parasites' life cycle progression.

In conclusion, this thesis revealed a previously unappreciated complexity of the sporozoite surface, which has implications for the development of antibody-based vaccines that target sporozoites to prevent malaria infection. Furthermore, the thesis highlights the versatility of sporozoites but also shows that the absence of observable phenotypic changes in gene knockout parasites is a major obstacle in unraveling gene function.

## References

1. World Health Organization. World Malaria Report 2013. Available from: [http://www.who.int/malaria/publications/world\\_malaria\\_report\\_2013/report/en/index.html](http://www.who.int/malaria/publications/world_malaria_report_2013/report/en/index.html)
2. Martinsen ES, Perkins SL, Schall JJ. A three-genome phylogeny of malaria parasites (Plasmodium and closely related genera): evolution of life-history traits and host switches. *Mol Phylogenet Evol.* 2008 Apr;47(1):261–73.
3. Singh B, Kim Sung L, Matusop A, Radhakrishnan A, Shamsul SSG, Cox-Singh J, et al. A large focus of naturally acquired Plasmodium knowlesi infections in human beings. *Lancet.* 2004 Mar 27;363(9414):1017–24.
4. Sidjanski S, Vanderberg JP. Delayed migration of Plasmodium sporozoites from the mosquito bite site to the blood. *Am J Trop Med Hyg.* 1997 Oct;57(4):426–9.
5. Jin Y, Kebaier C, Vanderberg J. Direct microscopic quantification of dynamics of Plasmodium berghei sporozoite transmission from mosquitoes to mice. *Infect Immun.* 2007 Nov;75(11):5532–9.
6. Vanderberg JP, Frevert U. Intravital microscopy demonstrating antibody-mediated immobilisation of Plasmodium berghei sporozoites injected into skin by mosquitoes. *Int J Parasitol.* 2004 Aug;34(9):991–6.
7. Amino R, Thiberge S, Martin B, Celli S, Shorte S, Frischknecht F, et al. Quantitative imaging of Plasmodium transmission from mosquito to mammal. *Nat Med.* 2006 Jan 22;12(2):220–4.
8. Meis JF, Verhave JP, Jap PH, Sinden RE, Meuwissen JH. Ultrastructural observations on the infection of rat liver by Plasmodium berghei sporozoites in vivo. *J Protozool.* 1983 May;30(2):361–6.
9. Sturm A, Amino R, van de Sand C, Regen T, Retzlaff S, Rennenberg A, et al. Manipulation of host hepatocytes by the malaria parasite for delivery into liver sinusoids. *Science.* 2006 Sep 1;313(5791):1287–90.
10. Tarun AS, Baer K, Dumpit RF, Gray S, Lejarcegui N, Frevert U, et al. Quantitative isolation and in vivo imaging of malaria parasite liver stages. *Int J Parasitol.* 2006 Oct;36(12):1283–93.
11. Krotoski WA, Krotoski DM, Garnham PC, Bray RS, Killick-Kendrick R, Draper CC, et al. Relapses in primate malaria: discovery of two populations of exoerythrocytic stages. Preliminary note. *Br Med J.* 1980 Jan 19;280(6208):153–4.
12. Krotoski WA, Collins WE, Bray RS, Garnham PC, Cogswell FB, Gwadz RW, et al. Demonstration of hypnozoites in sporozoite-transmitted Plasmodium vivax infection. *Am J Trop Med Hyg.* 1982 Nov;31(6):1291–3.
13. Talman AM, Domarle O, McKenzie FE, Ariey F, Robert V. Gametocytogenesis: the puberty of Plasmodium falciparum. *Malar J.* 2004 Jul 14;3:24.
14. Billker O, Shaw MK, Margos G, Sinden RE. The roles of temperature, pH and mosquito factors as triggers of male and female gametogenesis of Plasmodium berghei in vitro. *Parasitology.* 1997 Jul;115 ( Pt 1):1–7.

## References

---

15. Billker O, Lindo V, Panico M, Etienne AE, Paxton T, Dell A, et al. Identification of xanthurenic acid as the putative inducer of malaria development in the mosquito. *Nature*. 1998 Mar 19;392(6673):289–92.
16. Garcia GE, Wirtz RA, Barr JR, Woolfitt A, Rosenberg R. Xanthurenic acid induces gametogenesis in *Plasmodium*, the malaria parasite. *J Biol Chem*. 1998 May 15;273(20):12003–5.
17. Sinden RE, Canning EU, Spain B. Gametogenesis and Fertilization in *Plasmodium yoelii nigeriensis*: A Transmission Electron Microscope Study. *Proc R Soc B Biol Sci*. 1976 Mar 30;193(1110):55–76.
18. Vinetz JM. *Plasmodium* ookinete invasion of the mosquito midgut. *Curr Top Microbiol Immunol*. 2005;295:357–82.
19. Aly AS, Matuschewski K. A malarial cysteine protease is necessary for *Plasmodium* sporozoite egress from oocysts. *J Exp Med*. 2005 Jul 18;202(2):225–30.
20. Ménard R, Tavares J, Cockburn I, Markus M, Zavala F, Amino R. Looking under the skin: the first steps in malarial infection and immunity. *Nat Rev Microbiol*. 2013 Sep 16;11(10):701–12.
21. Schofield L, Grau GE. Immunological processes in malaria pathogenesis. *Nat Rev Immunol*. 2005 Sep;5(9):722–35.
22. Rowe JA, Claessens A, Corrigan RA, Arman M. Adhesion of *Plasmodium falciparum*-infected erythrocytes to human cells: molecular mechanisms and therapeutic implications. *Expert Rev Mol Med*. 2009;11:e16.
23. Handunnetti SM, David PH, Perera KL, Mendis KN. Uninfected erythrocytes form “rosettes” around *Plasmodium falciparum* infected erythrocytes. *Am J Trop Med Hyg*. 1989 Feb;40(2):115–8.
24. Pain A, Ferguson DJP, Kai O, Urban BC, Lowe B, Marsh K, et al. Platelet-mediated clumping of *Plasmodium falciparum*-infected erythrocytes is a common adhesive phenotype and is associated with severe malaria. *Proc Natl Acad Sci*. 2001 Feb 13;98(4):1805–10.
25. Miller LH, Ackerman HC, Su X, Wellems TE. Malaria biology and disease pathogenesis: insights for new treatments. *Nat Med*. 2013 Feb 6;19(2):156–67.
26. Moreno-Pérez DA, Ruíz JA, Patarroyo MA. Reticulocytes: *Plasmodium vivax* target cells. *Biol Cell Auspices Eur Cell Biol Organ*. 2013 Jun;105(6):251–60.
27. Rénia L, Howland SW, Claser C, Charlotte Gruner A, Suwanarusk R, Hui Teo T, et al. Cerebral malaria: mysteries at the blood-brain barrier. *Virulence*. 2012 Apr;3(2):193–201.
28. Doolan DL, Dobano C, Baird JK. Acquired immunity to malaria. *Clin Microbiol Rev*. 2009 Jan;22(1):13–36, Table of Contents.
29. Scherf A, Lopez-Rubio JJ, Riviere L. Antigenic variation in *Plasmodium falciparum*. *Annu Rev Microbiol*. 2008;62:445–70.
30. Stanisci DI, Barry AE, Good MF. Escaping the immune system: How the malaria parasite makes vaccine development a challenge. *Trends Parasitol*. 2013 Dec;29(12):612–22.

## References

---

31. Offeddu V, Thathy V, Marsh K, Matuschewski K. Naturally acquired immune responses against *Plasmodium falciparum* sporozoites and liver infection. *Int J Parasitol*. 2012 May 15;42(6):535–48.
32. Alonso PL, Brown G, Arevalo-Herrera M, Binka F, Chitnis C, Collins F, et al. A research agenda to underpin malaria eradication. *PLoS Med*. 2011;8(1):e1000406.
33. Thomé R, Lopes SCP, Costa FTM, Verinaud L. Chloroquine: modes of action of an undervalued drug. *Immunol Lett*. 2013 Jun;153(1-2):50–7.
34. Daily JP. Antimalarial drug therapy: the role of parasite biology and drug resistance. *J Clin Pharmacol*. 2006 Dec;46(12):1487–97.
35. Klonis N, Creek DJ, Tilley L. Iron and heme metabolism in *Plasmodium falciparum* and the mechanism of action of artemisinins. *Curr Opin Microbiol*. 2013 Dec;16(6):722–7.
36. Baird JK, Hoffman SL. Primaquine Therapy for Malaria. *Clin Infect Dis*. 2004 Nov 1;39(9):1336–45.
37. Patel SN, Kain KC. Atovaquone/proguanil for the prophylaxis and treatment of malaria. *Expert Rev Anti Infect Ther*. 2005 Dec;3(6):849–61.
38. Müller IB, Hyde JE. Antimalarial drugs: modes of action and mechanisms of parasite resistance. *Future Microbiol*. 2010 Dec;5(12):1857–73.
39. Mendis K, Rietveld A, Warsame M, Bosman A, Greenwood B, Wernsdorfer WH. From malaria control to eradication: The WHO perspective. *Trop Med Int Health TM IH*. 2009 Jul;14(7):802–9.
40. Richards JS, Beeson JG. The future for blood-stage vaccines against malaria. *Immunol Cell Biol*. 2009 Jul;87(5):377–90.
41. Arévalo-Herrera M, Solarte Y, Marin C, Santos M, Castellanos J, Beier JC, et al. Malaria transmission blocking immunity and sexual stage vaccines for interrupting malaria transmission in Latin America. *Mem Inst Oswaldo Cruz*. 2011 Aug;106:202–11.
42. Vanderberg J, Nussenzweig R, Most H. Protective immunity produced by the injection of x-irradiated sporozoites of *Plasmodium berghei*. V. In vitro effects of immune serum on sporozoites. *Mil Med*. 1969 Sep;134(10):1183–90.
43. Nussenzweig RS, Vanderberg J, Most H, Orton C. Protective immunity produced by the injection of x-irradiated sporozoites of *Plasmodium berghei*. *Nature*. 1967;216(111):160–2.
44. Clyde DF, Most H, McCarthy VC, Vanderberg JP. Immunization of man against sporozoite-induced *falciparum* malaria. *Am J Med Sci*. 1973 Sep;266(3):169–77.
45. Rieckmann KH, Carson PE, Beaudoin RL, Cassells JS, Sell KW. Letter: Sporozoite induced immunity in man against an Ethiopian strain of *Plasmodium falciparum*. *Trans R Soc Trop Med Hyg*. 1974;68(3):258–9.
46. Tsuji M, Zavala F. T cells as mediators of protective immunity against liver stages of *Plasmodium*. *Trends Parasitol*. 2003 Feb;19(2):88–93.
47. Hafalla JCR, Cockburn IA, Zavala F. Protective and pathogenic roles of CD8+ T cells during malaria infection. *Parasite Immunol*. 2006 Feb;28(1-2):15–24.

## References

---

48. Mueller AK, Camargo N, Kaiser K, Andorfer C, Frevert U, Matuschewski K, et al. Plasmodium liver stage developmental arrest by depletion of a protein at the parasite-host interface. *Proc Natl Acad Sci U A*. 2005 Feb 22;102(8):3022–7.
49. Ishino T, Chinzei Y, Yuda M. Two proteins with 6-cys motifs are required for malarial parasites to commit to infection of the hepatocyte. *Mol Microbiol*. 2005 Dec;58(5):1264–75.
50. Van Dijk MR, Douradinha B, Franke-Fayard B, Heussler V, van Dooren MW, van Schaijk B, et al. Genetically attenuated, P36p-deficient malarial sporozoites induce protective immunity and apoptosis of infected liver cells. *Proc Natl Acad Sci U A*. 2005 Aug 23;102(34):12194–9.
51. Mueller AK, Labaied M, Kappe SH, Matuschewski K. Genetically modified Plasmodium parasites as a protective experimental malaria vaccine. *Nature*. 2005 Jan 13;433(7022):164–7.
52. Vaughan AM, O'Neill MT, Tarun AS, Camargo N, Phuong TM, Aly AS, et al. Type II fatty acid synthesis is essential only for malaria parasite late liver stage development. *Cell Microbiol*. 2009 Mar;11(3):506–20.
53. Butler NS, Schmidt NW, Vaughan AM, Aly AS, Kappe SH, Harty JT. Superior antimalarial immunity after vaccination with late liver stage-arresting genetically attenuated parasites. *Cell Host Microbe*. 2011 Jun 16;9(6):451–62.
54. Belnoue E, Costa FTM, Frankenberg T, Vigário AM, Voza T, Leroy N, et al. Protective T cell immunity against malaria liver stage after vaccination with live sporozoites under chloroquine treatment. *J Immunol Baltim Md 1950*. 2004 Feb 15;172(4):2487–95.
55. Roestenberg M, McCall M, Hopman J, Wiersma J, Luty AJ, van Gemert GJ, et al. Protection against a malaria challenge by sporozoite inoculation. *N Engl J Med*. 2009 Jul 30;361(5):468–77.
56. Roestenberg M, Teirlinck AC, McCall MBB, Teelen K, Makamdop KN, Wiersma J, et al. Long-term protection against malaria after experimental sporozoite inoculation: an open-label follow-up study. *Lancet*. 2011 May 21;377(9779):1770–6.
57. Hoffman SL, Billingsley PF, James E, Richman A, Loyevsky M, Li T, et al. Development of a metabolically active, non-replicating sporozoite vaccine to prevent *Plasmodium falciparum* malaria. *Hum Vaccin*. 2010 Jan 1;6(1):97–106.
58. RTS,S Clinical Trials Partnership, Agnandji ST, Lell B, Fernandes JF, Abossolo BP, Methogo BGNO, et al. A phase 3 trial of RTS,S/AS01 malaria vaccine in African infants. *N Engl J Med*. 2012 Dec 13;367(24):2284–95.
59. White MT, Bejon P, Olotu A, Griffin JT, Riley EM, Kester KE, et al. The relationship between RTS,S vaccine-induced antibodies, CD4<sup>+</sup> T cell responses and protection against Plasmodium falciparum infection. *PLoS One*. 2013;8(4):e61395.
60. Agnandji ST, Lell B, Soulanoudjingar SS, Fernandes JF, Abossolo BP, Conzelmann C, et al. First results of phase 3 trial of RTS,S/AS01 malaria vaccine in African children. *N Engl J Med*. 2011 Nov 17;365(20):1863–75.
61. Olotu A, Fegan G, Wambua J, Nyangweso G, Awuondo KO, Leach A, et al. Four-Year Efficacy of RTS,S/AS01E and Its Interaction with Malaria Exposure. *N Engl J Med*. 2013 Mar 21;368(12):1111–20.

## References

---

62. Gardner MJ, Hall N, Fung E, White O, Berriman M, Hyman RW, et al. Genome sequence of the human malaria parasite *Plasmodium falciparum*. *Nature*. 2002;419(6906):498–511.
63. Carlton JM, Angiuoli SV, Suh BB, Kooij TW, Perteza M, Silva JC, et al. Genome sequence and comparative analysis of the model rodent malaria parasite *Plasmodium yoelii yoelii*. *Nature*. 2002;419(6906):512–9.
64. Carlton JM, Adams JH, Silva JC, Bidwell SL, Lorenzi H, Caler E, et al. Comparative genomics of the neglected human malaria parasite *Plasmodium vivax*. *Nature*. 2008 Oct 9;455(7214):757–63.
65. Pain A, Böhme U, Berry AE, Mungall K, Finn RD, Jackson AP, et al. The genome of the simian and human malaria parasite *Plasmodium knowlesi*. *Nature*. 2008 Oct 9;455(7214):799–803.
66. Dharia NV, Bright AT, Westenberger SJ, Barnes SW, Batalov S, Kuhlen K, et al. Whole-genome sequencing and microarray analysis of ex vivo *Plasmodium vivax* reveal selective pressure on putative drug resistance genes. *Proc Natl Acad Sci U S A*. 2010 Nov 16;107(46):20045–50.
67. Tachibana S-I, Sullivan SA, Kawai S, Nakamura S, Kim HR, Goto N, et al. *Plasmodium cynomolgi* genome sequences provide insight into *Plasmodium vivax* and the monkey malaria clade. *Nat Genet*. 2012 Sep;44(9):1051–5.
68. Van Dijk MR, Waters AP, Janse CJ. Stable transfection of malaria parasite blood stages. *Science*. 1995 Jun 2;268(5215):1358–62.
69. Wu Y, Sifri CD, Lei HH, Su XZ, Wellems TE. Transfection of *Plasmodium falciparum* within human red blood cells. *Proc Natl Acad Sci U S A*. 1995 Feb 14;92(4):973–7.
70. Wu Y, Kirkman LA, Wellems TE. Transformation of *Plasmodium falciparum* malaria parasites by homologous integration of plasmids that confer resistance to pyrimethamine. *Proc Natl Acad Sci U S A*. 1996 Feb 6;93(3):1130–4.
71. Crabb BS, Triglia T, Waterkeyn JG, Cowman AF. Stable transgene expression in *Plasmodium falciparum*. *Mol Biochem Parasitol*. 1997 Dec 1;90(1):131–44.
72. Menard R, Janse C. Gene targeting in malaria parasites. *Methods*. 1997 Oct;13(2):148–57.
73. Sattabongkot J, Yimamnuaychoke N, Leelaudomlipi S, Rasameesoraj M, Jenwithisuk R, Coleman RE, et al. Establishment of a human hepatocyte line that supports in vitro development of the exo-erythrocytic stages of the malaria parasites *Plasmodium falciparum* and *P. vivax*. *Am J Trop Med Hyg*. 2006 May;74(5):708–15.
74. Carter R, Diggs CL. *Parasitic Protozoa*. New York: Academic Press; 1977.
75. Vaughan AM, Mikolajczak SA, Wilson EM, Grompe M, Kaushansky A, Camargo N, et al. Complete *Plasmodium falciparum* liver-stage development in liver-chimeric mice. *J Clin Invest*. 2012 Oct 1;122(10):3618–28.
76. Van Dooren GG, Striepen B. The algal past and parasite present of the apicoplast. *Annu Rev Microbiol*. 2013;67:271–89.
77. Kappe SH, Buscaglia CA, Nussenzweig V. *Plasmodium* sporozoite molecular cell biology. *Annu Rev Cell Dev Biol*. 2004;20:29–59.

## References

---

78. Kudryashev M, Lepper S, Stanway R, Bohn S, Baumeister W, Cyrklaff M, et al. Positioning of large organelles by a membrane-associated cytoskeleton in *Plasmodium* sporozoites. *Cell Microbiol.* 2010 Mar;12(3):362–71.
79. Vanderberg JP. Studies on the motility of *Plasmodium* sporozoites. *J Protozool.* 1974 Oct;21(4):527–37.
80. Vanderberg JP. Development of infectivity by the *Plasmodium berghei* sporozoite. *J Parasitol.* 1975 Feb;61(1):43–50.
81. Keeley A, Soldati D. The glideosome: a molecular machine powering motility and host-cell invasion by Apicomplexa. *Trends Cell Biol.* 2004 Oct;14(10):528–32.
82. Sibley LD. The roles of intramembrane proteases in protozoan parasites. *Biochim Biophys Acta.* 2013 Dec;1828(12):2908–15.
83. Kappe S, Bruderer T, Gantt S, Fujioka H, Nussenzweig V, Menard R. Conservation of a gliding motility and cell invasion machinery in Apicomplexan parasites. *J Cell Biol.* 1999 Nov 29;147(5):937–44.
84. Ejigiri I, Ragheb DRT, Pino P, Coppi A, Bennett BL, Soldati-Favre D, et al. Shedding of TRAP by a rhomboid protease from the malaria sporozoite surface is essential for gliding motility and sporozoite infectivity. *PLoS Pathog.* 2012;8(7):e1002725.
85. Bosch J, Turley S, Daly TM, Bogh SM, Villasmil ML, Roach C, et al. Structure of the MTIP-MyoA complex, a key component of the malaria parasite invasion motor. *Proc Natl Acad Sci U S A.* 2006 Mar 28;103(13):4852–7.
86. Tucker RP. The thrombospondin type 1 repeat superfamily. *Int J Biochem Cell Biol.* 2004 Jun;36(6):969–74.
87. Whittaker CA, Hynes RO. Distribution and evolution of von Willebrand/integrin A domains: widely dispersed domains with roles in cell adhesion and elsewhere. *Mol Biol Cell.* 2002 Oct;13(10):3369–87.
88. Buscaglia CA, Coppens I, Hol WGJ, Nussenzweig V. Sites of interaction between aldolase and thrombospondin-related anonymous protein in plasmodium. *Mol Biol Cell.* 2003 Dec;14(12):4947–57.
89. Jewett TJ, Sibley LD. Aldolase Forms a Bridge between Cell Surface Adhesins and the Actin Cytoskeleton in Apicomplexan Parasites. *Mol Cell.* 2003 Apr;11(4):885–94.
90. Bosch J, Buscaglia CA, Krumm B, Ingason BP, Lucas R, Roach C, et al. Aldolase provides an unusual binding site for thrombospondin-related anonymous protein in the invasion machinery of the malaria parasite. *Proc Natl Acad Sci U S A.* 2007 Apr 24;104(17):7015–20.
91. Rogers WO, Malik A, Mellouk S, Nakamura K, Rogers MD, Szarfman A, et al. Characterization of *Plasmodium falciparum* sporozoite surface protein 2. *Proc Natl Acad Sci U S A.* 1992 Oct 1;89(19):9176–80.
92. Sultan AA, Thathy V, Frevert U, Robson KJ, Crisanti A, Nussenzweig V, et al. TRAP is necessary for gliding motility and infectivity of plasmodium sporozoites. *Cell.* 1997 Aug 8;90(3):511–22.

## References

---

93. Matuschewski K, Nunes AC, Nussenzweig V, Menard R. Plasmodium sporozoite invasion into insect and mammalian cells is directed by the same dual binding system. *EMBO J.* 2002 Apr 2;21(7):1597–606.
94. Stewart MJ, Vanderberg JP. Malaria Sporozoites Leave Behind Trails of Circumsporozoite Protein During Gliding Motility <sup>1</sup>. *J Protozool.* 1988 Aug;35(3):389–93.
95. Stewart MJ, Nawrot RJ, Schulman S, Vanderberg JP. Plasmodium berghei sporozoite invasion is blocked in vitro by sporozoite-immobilizing antibodies. *Infect Immun.* 1986 Mar;51(3):859–64.
96. Sinnis P, Coppi A. A long and winding road: the Plasmodium sporozoite's journey in the mammalian host. *Parasitol Int.* 2007 Sep;56(3):171–8.
97. Stewart MJ, Vanderberg JP. Malaria sporozoites release circumsporozoite protein from their apical end and translocate it along their surface. *J Protozool.* 1991 Aug;38(4):411–21.
98. Cochrane AH, Aikawa M, Jeng M, Nussenzweig RS. Antibody-induced ultrastructural changes of malarial sporozoites. *J Immunol Baltim Md 1950.* 1976 Mar;116(3):859–67.
99. Cowman AF, Crabb BS. Invasion of red blood cells by malaria parasites. *Cell.* 2006 Feb 24;124(4):755–66.
100. Sharma P, Chitnis CE. Key molecular events during host cell invasion by Apicomplexan pathogens. *Curr Opin Microbiol.* 2013 Aug;16(4):432–7.
101. Ono T, Cabrita-Santos L, Leitao R, Bettiol E, Purcell LA, Diaz-Pulido O, et al. Adenylyl Cyclase  $\alpha$  and cAMP Signaling Mediate Plasmodium Sporozoite Apical Regulated Exocytosis and Hepatocyte Infection. Kim K, editor. *PLoS Pathog.* 2008 Feb 29;4(2):e1000008.
102. Aikawa M, Miller LH, Johnson J, Rabbege J. Erythrocyte entry by malarial parasites. A moving junction between erythrocyte and parasite. *J Cell Biol.* 1978 Apr;77(1):72–82.
103. Amino R, Giovannini D, Thiberge S, Gueirard P, Boisson B, Dubremetz J-F, et al. Host cell traversal is important for progression of the malaria parasite through the dermis to the liver. *Cell Host Microbe.* 2008 Feb 14;3(2):88–96.
104. Baum J, Gilberger TW, Frischknecht F, Meissner M. Host-cell invasion by malaria parasites: insights from Plasmodium and Toxoplasma. *Trends Parasitol.* 2008 Dec;24(12):557–63.
105. Baum J, Richard D, Healer J, Rug M, Krnajski Z, Gilberger TW, et al. A conserved molecular motor drives cell invasion and gliding motility across malaria life cycle stages and other apicomplexan parasites. *J Biol Chem.* 2006 Feb 24;281(8):5197–208.
106. Andenmatten N, Egarter S, Jackson AJ, Jullien N, Herman J-P, Meissner M. Conditional genome engineering in Toxoplasma gondii uncovers alternative invasion mechanisms. *Nat Methods.* 2012 Dec 23;10(2):125–7.
107. Egarter S, Andenmatten N, Jackson AJ, Whitelaw JA, Pall G, Black JA, et al. The toxoplasma Acto-MyoA motor complex is important but not essential for gliding motility and host cell invasion. *PloS One.* 2014;9(3):e91819.
108. Meissner M, Ferguson DJP, Frischknecht F. Invasion factors of apicomplexan parasites: essential or redundant? *Curr Opin Microbiol.* 2013 Aug;16(4):438–44.

## References

---

109. Vanderberg JP, Chew S, Stewart MJ. Plasmodium sporozoite interactions with macrophages in vitro: a videomicroscopic analysis. *J Protozool.* 1990 Dec;37(6):528–36.
110. Mota MM, Pradel G, Vanderberg JP, Hafalla JC, Frevert U, Nussenzweig RS, et al. Migration of Plasmodium sporozoites through cells before infection. *Science.* 2001 Jan 5;291(5501):141–4.
111. Tavares J, Formaglio P, Thiberge S, Mordelet E, Van Rooijen N, Medvinsky A, et al. Role of host cell traversal by the malaria sporozoite during liver infection. *J Exp Med.* 2013 May 6;210(5):905–15.
112. Ishino T, Yano K, Chinzei Y, Yuda M. Cell-passage activity is required for the malarial parasite to cross the liver sinusoidal cell layer. *PLoS Biol.* 2004 Jan;2(1):E4.
113. Ishino T, Chinzei Y, Yuda M. A Plasmodium sporozoite protein with a membrane attack complex domain is required for breaching the liver sinusoidal cell layer prior to hepatocyte infection. *Cell Microbiol.* 2005 Feb;7(2):199–208.
114. Kariu T, Ishino T, Yano K, Chinzei Y, Yuda M. CeTOS, a novel malarial protein that mediates transmission to mosquito and vertebrate hosts. *Mol Microbiol.* 2006 Mar;59(5):1369–79.
115. Menard R, Sultan AA, Cortes C, Altszuler R, van Dijk MR, Janse CJ, et al. Circumsporozoite protein is required for development of malaria sporozoites in mosquitoes. *Nature.* 1997 Jan 23;385(6614):336–40.
116. Aly AS, Vaughan AM, Kappe SH. Malaria Parasite Development in the Mosquito and Infection of the Mammalian Host. *Annu Rev Microbiol* [Internet]. 2009 May 1; Available from: [http://www.ncbi.nlm.nih.gov/entrez/query.fcgi?cmd=Retrieve&db=PubMed&dopt=Citation&list\\_uids=19575563](http://www.ncbi.nlm.nih.gov/entrez/query.fcgi?cmd=Retrieve&db=PubMed&dopt=Citation&list_uids=19575563)
117. Ghosh AK, Devenport M, Jethwaney D, Kalume DE, Pandey A, Anderson VE, et al. Malaria parasite invasion of the mosquito salivary gland requires interaction between the Plasmodium TRAP and the Anopheles saglin proteins. *PLoS Pathog.* 2009 Jan;5(1):e1000265.
118. Sidjanski SP, Vanderberg JP, Sinnis P. Anopheles stephensi salivary glands bear receptors for region I of the circumsporozoite protein of Plasmodium falciparum. *Mol Biochem Parasitol.* 1997 Dec 1;90(1):33–41.
119. Myung JM, Marshall P, Sinnis P. The Plasmodium circumsporozoite protein is involved in mosquito salivary gland invasion by sporozoites. *Mol Biochem Parasitol.* 2004 Jan;133(1):53–9.
120. Kappe SH, Noe AR, Fraser TS, Blair PL, Adams JH. A family of chimeric erythrocyte binding proteins of malaria parasites. *Proc Natl Acad Sci U A.* 1998 Feb 3;95(3):1230–5.
121. Kariu T, Yuda M, Yano K, Chinzei Y. MAEBL is essential for malarial sporozoite infection of the mosquito salivary gland. *J Exp Med.* 2002 May 20;195(10):1317–23.
122. Steinbuechel M, Matuschewski K. Role for the Plasmodium sporozoite-specific transmembrane protein S6 in parasite motility and efficient malaria transmission. *Cell Microbiol.* 2009 Feb;11(2):279–88.

## References

---

123. Mikolajczak SA, Silva-Rivera H, Peng X, Tarun AS, Camargo N, Jacobs-Lorena V, et al. Distinct malaria parasite sporozoites reveal transcriptional changes that cause differential tissue infection competence in the mosquito vector and mammalian host. *Mol Cell Biol*. 2008 Oct;28(20):6196–207.
124. Combe A, Moreira C, Ackerman S, Thiberge S, Templeton TJ, Menard R. TREP, a novel protein necessary for gliding motility of the malaria sporozoite. *Int J Parasitol*. 2009 Mar;39(4):489–96.
125. Thompson J, Fernandez-Reyes D, Sharling L, Moore SG, Eling WM, Kyes SA, et al. Plasmodium cysteine repeat modular proteins 1-4: complex proteins with roles throughout the malaria parasite life cycle. *Cell Microbiol*. 2007 Jun;9(6):1466–80.
126. Touray MG, Warburg A, Laughinghouse A, Krettli AU, Miller LH. Developmentally regulated infectivity of malaria sporozoites for mosquito salivary glands and the vertebrate host. *J Exp Med*. 1992 Jun 1;175(6):1607–12.
127. Matuschewski K, Ross J, Brown SM, Kaiser K, Nussenzweig V, Kappe SHI. Infectivity-associated Changes in the Transcriptional Repertoire of the Malaria Parasite Sporozoite Stage. *J Biol Chem*. 2002 Nov 1;277(44):41948–53.
128. Perschmann N, Hellmann JK, Frischknecht F, Spatz JP. Induction of malaria parasite migration by synthetically tunable microenvironments. *Nano Lett*. 2011 Oct 12;11(10):4468–74.
129. Yamauchi LM, Coppi A, Snounou G, Sinnis P. Plasmodium sporozoites trickle out of the injection site. *Cell Microbiol*. 2007 May;9(5):1215–22.
130. Coppi A, Tewari R, Bishop JR, Bennett BL, Lawrence R, Esko JD, et al. Heparan Sulfate Proteoglycans Provide a Signal to Plasmodium Sporozoites to Stop Migrating and Productively Invade Host Cells. *Cell Host Microbe*. 2007 Nov 15;2(5):316–27.
131. Kaiser K, Camargo N, Coppens I, Morrissey JM, Vaidya AB, Kappe SHI. A member of a conserved Plasmodium protein family with membrane-attack complex/perforin (MACPF)-like domains localizes to the micronemes of sporozoites. *Mol Biochem Parasitol*. 2004 Jan;133(1):15–26.
132. Bhanot P, Schauer K, Coppens I, Nussenzweig V. A surface phospholipase is involved in the migration of plasmodium sporozoites through cells. *J Biol Chem*. 2005 Feb 25;280(8):6752–60.
133. Moreira CK, Templeton TJ, Lavazec C, Hayward RE, Hobbs CV, Kroeze H, et al. The Plasmodium TRAP/MIC2 family member, TRAP-Like Protein (TLP), is involved in tissue traversal by sporozoites. *Cell Microbiol*. 2008 Jul;10(7):1505–16.
134. Hellmann JK, Münter S, Kudryashev M, Schulz S, Heiss K, Müller A-K, et al. Environmental Constraints Guide Migration of Malaria Parasites during Transmission. Mota MM, editor. *PLoS Pathog*. 2011 Jun 16;7(6):e1002080.
135. Prudêncio M, Mota MM. To Migrate or to Invade: Those Are the Options. *Cell Host Microbe*. 2007 Nov;2(5):286–8.
136. Coppi A, Pinzon-Ortiz C, Hutter C, Sinnis P. The Plasmodium circumsporozoite protein is proteolytically processed during cell invasion. *J Exp Med*. 2005 Jan 3;201(1):27–33.

## References

---

137. Kaiser K, Matuschewski K, Camargo N, Ross J, Kappe SH. Differential transcriptome profiling identifies Plasmodium genes encoding pre-erythrocytic stage-specific proteins. *Mol Microbiol.* 2004 Mar;51(5):1221–32.
138. Labaied M, Camargo N, Kappe SH. Depletion of the Plasmodium berghei thrombospondin-related sporozoite protein reveals a role in host cell entry by sporozoites. *Mol Biochem Parasitol* [Internet]. 2007 Mar 6; Available from: [http://www.ncbi.nlm.nih.gov/entrez/query.fcgi?cmd=Retrieve&db=PubMed&dopt=Citation&list\\_uids=17418435](http://www.ncbi.nlm.nih.gov/entrez/query.fcgi?cmd=Retrieve&db=PubMed&dopt=Citation&list_uids=17418435)
139. Giovannini D, Spath S, Lacroix C, Perazzi A, Bargieri D, Lagal V, et al. Independent roles of apical membrane antigen 1 and rhoptry neck proteins during host cell invasion by apicomplexa. *Cell Host Microbe.* 2011 Dec 15;10(6):591–602.
140. Lebrun M, Michelin A, El Hajj H, Poncet J, Bradley PJ, Vial H, et al. The rhoptry neck protein RON4 re-localizes at the moving junction during Toxoplasma gondii invasion. *Cell Microbiol.* 2005 Dec;7(12):1823–33.
141. Besteiro S, Michelin A, Poncet J, Dubremetz J-F, Lebrun M. Export of a Toxoplasma gondii Rhoptry Neck Protein Complex at the Host Cell Membrane to Form the Moving Junction during Invasion. Carruthers VB, editor. *PLoS Pathog.* 2009 Feb 27;5(2):e1000309.
142. Straub KW, Cheng SJ, Sohn CS, Bradley PJ. Novel components of the Apicomplexan moving junction reveal conserved and coccidia-restricted elements. *Cell Microbiol.* 2009 Apr;11(4):590–603.
143. Collins CR, Blackman MJ. Apicomplexan AMA1 in Host Cell Invasion: A Model at the Junction? *Cell Host Microbe.* 2011 Dec;10(6):531–3.
144. Labaied M, Harupa A, Dumpit RF, Coppens I, Mikolajczak SA, Kappe SHI. Plasmodium yoelii sporozoites with simultaneous deletion of P52 and P36 are completely attenuated and confer sterile immunity against infection. *Infect Immun.* 2007 Aug;75(8):3758–68.
145. Mikolajczak SA, Jacobs-Lorena V, MacKellar DC, Camargo N, Kappe SH. L-FABP is a critical host factor for successful malaria liver stage development. *Int J Parasitol.* 2007 Apr;37(5):483–9.
146. Spielmann T, Ferguson DJ, Beck HP. etramps, a New Plasmodium falciparum Gene Family Coding for Developmentally Regulated and Highly Charged Membrane Proteins Located at the Parasite-Host Cell Interface. *Mol Biol Cell.* 2003 Apr;14(4):1529–44.
147. Spielmann T, Montagna GN, Hecht L, Matuschewski K. Molecular make-up of the Plasmodium parasitophorous vacuolar membrane. *Int J Med Microbiol.* 2012 Oct;302(4-5):179–86.
148. Kappe SH, Gardner MJ, Brown SM, Ross J, Matuschewski K, Ribeiro JM, et al. Exploring the transcriptome of the malaria sporozoite stage. *Proc Natl Acad Sci U S A.* 2001 Aug 14;98(17):9895–900.
149. Chattopadhyay R, Rathore D, Fujioka H, Kumar S, de la Vega P, Haynes D, et al. PfSPATR, a Plasmodium falciparum protein containing an altered thrombospondin type I repeat domain is expressed at several stages of the parasite life cycle and is the target of inhibitory antibodies. *J Biol Chem.* 2003 Jul 11;278(28):25977–81.

## References

---

150. Bottius E, BenMohamed L, Brahimi K, Gras H, Lepers JP, Raharimalala L, et al. A novel *Plasmodium falciparum* sporozoite and liver stage antigen (SALSA) defines major B, T helper, and CTL epitopes. *J Immunol Baltim Md 1950*. 1996 Apr 15;156(8):2874–84.
151. Fidock DA, Bottius E, Brahimi K, Moelans II, Aikawa M, Konings RN, et al. Cloning and characterization of a novel *Plasmodium falciparum* sporozoite surface antigen, STARP. *Mol Biochem Parasitol*. 1994 Apr;64(2):219–32.
152. Fidock DA, Pasquetto V, Gras H, Badell E, Eling W, Ballou WR, et al. *Plasmodium falciparum* sporozoite invasion is inhibited by naturally acquired or experimentally induced polyclonal antibodies to the STARP antigen. *Eur J Immunol*. 1997 Oct;27(10):2502–13.
153. Siau A, Silvie O, Franetich J-F, Yalaoui S, Marinach C, Hannoun L, et al. Temperature shift and host cell contact up-regulate sporozoite expression of *Plasmodium falciparum* genes involved in hepatocyte infection. *PLoS Pathog*. 2008;4(8):e1000121.
154. Templeton TJ, Kaslow DC. Identification of additional members define a *Plasmodium falciparum* gene superfamily which includes Pfs48/45 and Pfs230. *Mol Biochem Parasitol*. 1999;101:223–7.
155. Carter R, Coulson A, Bhatti S, Taylor BJ, Elliott JF. Predicted disulfide-bonded structures for three uniquely related proteins of *Plasmodium falciparum*, Pfs230, Pfs48/45 and Pf12. *Mol Biochem Parasitol*. 1995 May;71(2):203–10.
156. Williamson KC, Criscio MD, Kaslow DC. Cloning and expression of the gene for *Plasmodium falciparum* transmission-blocking target antigen, Pfs230. *Mol Biochem Parasitol*. 1993 Apr;58(2):355–8.
157. Gerloff DL, Creasey A, Maslau S, Carter R. Structural models for the protein family characterized by gamete surface protein Pfs230 of *Plasmodium falciparum*. *Proc Natl Acad Sci U S A*. 2005 Sep 20;102(38):13598–603.
158. Arredondo SA, Cai M, Takayama Y, MacDonald NJ, Anderson DE, Aravind L, et al. Structure of the *Plasmodium* 6-cysteine s48/45 domain. *Proc Natl Acad Sci U S A*. 2012 Apr 24;109(17):6692–7.
159. Jacquet A, Coulon L, De Nève J, Daminet V, Haumont M, Garcia L, et al. The surface antigen SAG3 mediates the attachment of *Toxoplasma gondii* to cell-surface proteoglycans. *Mol Biochem Parasitol*. 2001 Aug;116(1):35–44.
160. Boulanger MJ, Tonkin ML, Crawford J. Apicomplexan parasite adhesins: novel strategies for targeting host cell carbohydrates. *Curr Opin Struct Biol*. 2010 Oct;20(5):551–9.
161. Sanders PR, Gilson PR, Cantin GT, Greenbaum DC, Nebl T, Carucci DJ, et al. Distinct protein classes including novel merozoite surface antigens in Raft-like membranes of *Plasmodium falciparum*. *J Biol Chem*. 2005 Dec 2;280(48):40169–76.
162. Florens L, Washburn MP, Raine JD, Anthony RM, Grainger M, Haynes JD, et al. A proteomic view of the *Plasmodium falciparum* life cycle. *Nature*. 2002 Oct 3;419(6906):520–6.
163. Le Roch KG, Zhou Y, Blair PL, Grainger M, Moch JK, Haynes JD, et al. Discovery of gene function by expression profiling of the malaria parasite life cycle. *Science*. 2003 Sep 12;301(5639):1503–8.

## References

---

164. Van Dijk MR, van Schaijk BCL, Khan SM, van Dooren MW, Ramesar J, Kaczanowski S, et al. Three members of the 6-cys protein family of *Plasmodium* play a role in gamete fertility. *PLoS Pathog.* 2010 Apr;6(4):e1000853.
165. Van Dijk MR, Janse CJ, Thompson J, Waters AP, Braks JA, Dodemont HJ, et al. A central role for P48/45 in malaria parasite male gamete fertility. *Cell.* 2001 Jan 12;104(1):153–64.
166. Pradel G. Proteins of the malaria parasite sexual stages: expression, function and potential for transmission blocking strategies. *Parasitology.* 2007 Dec;134(Pt.14):1911–29.
167. Williamson KC, Keister DB, Muratova O, Kaslow DC. Recombinant Pfs230, a *Plasmodium falciparum* gametocyte protein, induces antisera that reduce the infectivity of *Plasmodium falciparum* to mosquitoes. *Mol Biochem Parasitol.* 1995 Dec;75(1):33–42.
168. Vermeulen AN, Ponnudurai T, Beckers PJ, Verhave JP, Smits MA, Meuwissen JH. Sequential expression of antigens on sexual stages of *Plasmodium falciparum* accessible to transmission-blocking antibodies in the mosquito. *J Exp Med.* 1985 Nov 1;162(5):1460–76.
169. Roeffen W, Geeraedts F, Eling W, Beckers P, Wizel B, Kumar N, et al. Transmission blockade of *Plasmodium falciparum* malaria by anti-Pfs230-specific antibodies is isotype dependent. *Infect Immun.* 1995 Feb;63(2):467–71.
170. Outchkourov N, Vermunt A, Jansen J, Kaan A, Roeffen W, Teelen K, et al. Epitope analysis of the malaria surface antigen pfs48/45 identifies a subdomain that elicits transmission blocking antibodies. *J Biol Chem.* 2007 Jun 8;282(23):17148–56.
171. Van Schaijk BCL, van Dijk MR, van de Vegte-Bolmer M, van Gemert G-J, van Dooren MW, Eksi S, et al. Pfs47, paralog of the male fertility factor Pfs48/45, is a female specific surface protein in *Plasmodium falciparum*. *Mol Biochem Parasitol.* 2006 Oct;149(2):216–22.
172. Taechalertpaisarn T, Crosnier C, Bartholdson SJ, Hodder AN, Thompson J, Bustamante LY, et al. Biochemical and Functional Analysis of Two *Plasmodium falciparum* Blood-Stage 6-Cys Proteins: P12 and P41. Spielmann T, editor. *PLoS ONE.* 2012 Jul 27;7(7):e41937.
173. Tonkin ML, Arredondo SA, Loveless BC, Serpa JJ, Makepeace KAT, Sundar N, et al. Structural and Biochemical Characterization of *Plasmodium falciparum* 12 (Pf12) Reveals a Unique Interdomain Organization and the Potential for an Antiparallel Arrangement with Pf41. *J Biol Chem.* 2013 Mar 19;288(18):12805–17.
174. VanBuskirk KM, O'Neill MT, De La Vega P, Maier AG, Krzych U, Williams J, et al. Preerythrocytic, live-attenuated *Plasmodium falciparum* vaccine candidates by design. *Proc Natl Acad Sci U S A.* 2009 Aug 4;106(31):13004–9.
175. Spring M, Murphy J, Nielsen R, Dowler M, Bennett JW, Zarling S, et al. First-in-human evaluation of genetically attenuated *Plasmodium falciparum* sporozoites administered by bite of *Anopheles* mosquitoes to adult volunteers. *Vaccine.* 2013 Oct 9;31(43):4975–83.
176. Lasonder E, Janse CJ, van Gemert GJ, Mair GR, Vermunt AM, Douradinha BG, et al. Proteomic profiling of *Plasmodium* sporozoite maturation identifies new proteins essential for parasite development and infectivity. *PLoS Pathog.* 2008 Oct;4(10):e1000195.
177. Khan SM, Franke-Fayard B, Mair GR, Lasonder E, Janse CJ, Mann M, et al. Proteome analysis of separated male and female gametocytes reveals novel sex-specific *Plasmodium* biology. *Cell.* 2005 Jun 3;121(5):675–87.

## References

---

178. Mikolajczak SA, Aly ASI, Dumpit RF, Vaughan AM, Kappe SHI. An efficient strategy for gene targeting and phenotypic assessment in the *Plasmodium yoelii* rodent malaria model. *Mol Biochem Parasitol*. 2008 Apr;158(2):213–6.
179. Thathy V, Ménard R. Gene targeting in *Plasmodium berghei*. *Methods Mol Med*. 2002;72:317–31.
180. Jongco AM, Ting LM, Thathy V, Mota MM, Kim K. Improved transfection and new selectable markers for the rodent malaria parasite *Plasmodium yoelii*. *Mol Biochem Parasitol*. 2006 Apr;146(2):242–50.
181. Witney AA, Doolan DL, Anthony RM, Weiss WR, Hoffman SL, Carucci DJ. Determining liver stage parasite burden by real time quantitative PCR as a method for evaluating pre-erythrocytic malaria vaccine efficacy. *Mol Biochem Parasitol*. 2001 Dec;118(2):233–45.
182. Lindner SE, Swearingen KE, Harupa A, Vaughan AM, Sinnis P, Moritz RL, et al. Total and putative surface proteomics of malaria parasite salivary gland sporozoites. *Mol Cell Proteomics MCP*. 2013 May;12(5):1127–43.
183. Kennedy M, Fishbaugher ME, Vaughan AM, Patrapuvich R, Boonhok R, Yimamnuaychok N, et al. A rapid and scalable density gradient purification method for *Plasmodium* sporozoites. *Malar J*. 2012;11:421.
184. Durocher Y, Perret S, Kamen A. High-level and high-throughput recombinant protein production by transient transfection of suspension-growing human 293-EBNA1 cells. *Nucleic Acids Res*. 2002 Jan 15;30(2):E9.
185. Sellhorn G, Caldwell Z, Mineart C, Stamatatos L. Improving the expression of recombinant soluble HIV Envelope glycoproteins using pseudo-stable transient transfection. *Vaccine*. 2009 Dec 11;28(2):430–6.
186. Carbonetti S, Oliver BG, Glenn J, Stamatatos L, Sather DN. Soluble HIV-1 Envelope Immunogens Derived from an Elite Neutralizer Elicit Cross-Reactive V1V2 Antibodies and Low Potency Neutralizing Antibodies. *PloS One*. 2014 Jan 23;9(1):e86905.
187. Thompson J, Janse CJ, Waters AP. Comparative genomics in *Plasmodium*: a tool for the identification of genes and functional analysis. *Mol Biochem Parasitol*. 2001 Dec;118(2):147–54.
188. Gilson PR. Identification and Stoichiometry of Glycosylphosphatidylinositol-anchored Membrane Proteins of the Human Malaria Parasite *Plasmodium falciparum*. *Mol Cell Proteomics*. 2006 Apr 7;5(7):1286–99.
189. Gantt SM, Myung JM, Briones MR, Li WD, Corey EJ, Omura S, et al. Proteasome inhibitors block development of *Plasmodium* spp. *Antimicrob Agents Chemother*. 1998 Oct;42(10):2731–8.
190. Hall N, Karras M, Raine JD, Carlton JM, Kooij TW, Berriman M, et al. A comprehensive survey of the *Plasmodium* life cycle by genomic, transcriptomic, and proteomic analyses. *Science*. 2005 Jan 7;307(5706):82–6.
191. Bendtsen JD, Jensen LJ, Blom N, Von Heijne G, Brunak S. Feature-based prediction of non-classical and leaderless protein secretion. *Protein Eng Des Sel PEDS*. 2004 Apr;17(4):349–56.

## References

---

192. Bendtsen JD, Kiemer L, Fausbøll A, Brunak S. Non-classical protein secretion in bacteria. *BMC Microbiol.* 2005;5:58.
193. Ren J, Wen L, Gao X, Jin C, Xue Y, Yao X. CSS-Palm 2.0: an updated software for palmitoylation sites prediction. *Protein Eng Des Sel PEDS.* 2008 Nov;21(11):639–44.
194. Bijlmakers M-J, Marsh M. The on-off story of protein palmitoylation. *Trends Cell Biol.* 2003 Jan;13(1):32–42.
195. Jones ML, Collins MO, Goulding D, Choudhary JS, Rayner JC. Analysis of Protein Palmitoylation Reveals a Pervasive Role in Plasmodium Development and Pathogenesis. *Cell Host Microbe.* 2012 Aug;12(2):246–58.
196. Silvestrini F, Lasonder E, Olivieri A, Camarda G, van Schaijk B, Sanchez M, et al. Protein export marks the early phase of gametocytogenesis of the human malaria parasite *Plasmodium falciparum*. *Mol Cell Proteomics.* 2010 Jul;9(7):1437–48.
197. Blume M, Hliscs M, Rodriguez-Contreras D, Sanchez M, Landfear S, Lucius R, et al. A constitutive pan-hexose permease for the Plasmodium life cycle and transgenic models for screening of antimalarial sugar analogs. *FASEB J Off Publ Fed Am Soc Exp Biol.* 2011 Apr;25(4):1218–29.
198. Woodrow CJ, Burchmore RJ, Krishna S. Hexose permeation pathways in Plasmodium falciparum-infected erythrocytes. *Proc Natl Acad Sci U S A.* 2000 Aug 29;97(18):9931–6.
199. Slavic K, Straschil U, Reininger L, Doerig C, Morin C, Tewari R, et al. Life cycle studies of the hexose transporter of Plasmodium species and genetic validation of their essentiality. *Mol Microbiol.* 2010 Mar;75(6):1402–13.
200. Kaiser K, Matuschewski K, Camargo N, Ross J, Kappe SHI. Differential transcriptome profiling identifies Plasmodium genes encoding pre-erythrocytic stage-specific proteins. *Mol Microbiol.* 2004 Mar;51(5):1221–32.
201. Adams JC, Tucker RP. The thrombospondin type 1 repeat (TSR) superfamily: diverse proteins with related roles in neuronal development. *Dev Dyn Off Publ Am Assoc Anat.* 2000 Jun;218(2):280–99.
202. Treeck M, Sanders JL, Elias JE, Boothroyd JC. The phosphoproteomes of Plasmodium falciparum and Toxoplasma gondii reveal unusual adaptations within and beyond the parasites' boundaries. *Cell Host Microbe.* 2011 Oct 20;10(4):410–9.
203. Pease BN, Huttlin EL, Jedrychowski MP, Talevich E, Harmon J, Dillman T, et al. Global analysis of protein expression and phosphorylation of three stages of Plasmodium falciparum intraerythrocytic development. *J Proteome Res.* 2013 Sep 6;12(9):4028–45.
204. Aly ASI, Vaughan AM, Kappe SHI. Malaria parasite development in the mosquito and infection of the mammalian host. *Annu Rev Microbiol.* 2009;63:195–221.
205. Morahan BJ, Wang L, Coppel RL. No TRAP, no invasion. *Trends Parasitol.* 2009 Feb;25(2):77–84.
206. Hegge S, Münter S, Steinbüchel M, Heiss K, Engel U, Matuschewski K, et al. Multistep adhesion of Plasmodium sporozoites. *FASEB J Off Publ Fed Am Soc Exp Biol.* 2010 Jul;24(7):2222–34.

## References

---

207. Kaushansky A, Rezakhani N, Mann H, Kappe SHI. Development of a quantitative flow cytometry-based assay to assess infection by *Plasmodium falciparum* sporozoites. *Mol Biochem Parasitol.* 2012 May;183(1):100–3.
208. Kaushansky A, Metzger PG, Douglass AN, Mikolajczak SA, Lakshmanan V, Kain HS, et al. Malaria parasite liver stages render host hepatocytes susceptible to mitochondria-initiated apoptosis. *Cell Death Dis.* 2013;4:e762.
209. Mikolajczak SA, Lakshmanan V, Fishbaugher M, Camargo N, Harupa A, Kaushansky A, et al. A Next-generation Genetically Attenuated *Plasmodium falciparum* Parasite Created by Triple Gene Deletion. *Mol Ther J Am Soc Gene Ther.* 2014 May 14;
210. Tarun AS, Peng X, Dumpit RF, Ogata Y, Silva-Rivera H, Camargo N, et al. A combined transcriptome and proteome survey of malaria parasite liver stages. *Proc Natl Acad Sci U A.* 2008 Jan 8;105(1):305–10.
211. Duraisingh MT, Triglia T, Ralph SA, Rayner JC, Barnwell JW, McFadden GI, et al. Phenotypic variation of *Plasmodium falciparum* merozoite proteins directs receptor targeting for invasion of human erythrocytes. *EMBO J.* 2003 Mar 3;22(5):1047–57.
212. Lopatnicki S, Maier AG, Thompson J, Wilson DW, Tham W-H, Triglia T, et al. Reticulocyte and erythrocyte binding-like proteins function cooperatively in invasion of human erythrocytes by malaria parasites. *Infect Immun.* 2011 Mar;79(3):1107–17.
213. Lin J, Annoura T, Sajid M, Chevalley-Maurel S, Ramesar J, Klop O, et al. A Novel “Gene Insertion/Marker Out” (GIMO) Method for Transgene Expression and Gene Complementation in Rodent Malaria Parasites. Kappe S, editor. *PLoS ONE.* 2011 Dec 27;6(12):e29289.
214. Langhorne J, Meding SJ, Eichmann K, Gillard SS. The response of CD4+ T cells to *Plasmodium chabaudi chabaudi*. *Immunol Rev.* 1989 Dec;112:71–94.
215. Meding SJ, Langhorne J. CD4+ T cells and B cells are necessary for the transfer of protective immunity to *Plasmodium chabaudi chabaudi*. *Eur J Immunol.* 1991 Jun;21(6):1433–8.
216. Garcia J, Curtidor H, Obando-Martinez AZ, Vizcaino C, Pinto M, Martinez NL, et al. Synthetic peptides from conserved regions of the *Plasmodium falciparum* early transcribed membrane and ring exported proteins bind specifically to red blood cell proteins. *Vaccine.* 2009 Nov;27(49):6877–86.
217. Tetteh KKA, Stewart LB, Ochola LI, Amambua-Ngwa A, Thomas AW, Marsh K, et al. Prospective identification of malaria parasite genes under balancing selection. *PloS One.* 2009;4(5):e5568.
218. Reeder JC, Wapling J, Mueller I, Siba PM, Barry AE. Population genetic analysis of the *Plasmodium falciparum* 6-cys protein Pf38 in Papua New Guinea reveals domain-specific balancing selection. *Malar J.* 2011;10:126.
219. Wass MN, Stanway R, Blagborough AM, Lal K, Prieto JH, Raine D, et al. Proteomic analysis of *Plasmodium* in the mosquito: progress and pitfalls. *Parasitology.* 2012 Feb 16;1–15.
220. Belmonte M, Jones TR, Lu M, Arcilla R, Smalls T, Belmonte A, et al. The infectivity of *Plasmodium yoelii* in different strains of mice. *J Parasitol.* 2003 Jun;89(3):602–3.

## References

---

221. Linder ME, Jennings BC. Mechanism and function of DHHC S-acyltransferases. *Biochem Soc Trans.* 2013 Feb 1;41(1):29–34.
222. Frénal K, Tay CL, Mueller C, Bushell ES, Jia Y, Graindorge A, et al. Global Analysis of Apicomplexan Protein S-Acyl Transferases Reveals an Enzyme Essential for Invasion: Repertoire of Essential PATs in Two Apicomplexans. *Traffic.* 2013 Aug;14(8):895–911.
223. Greaves J, Chamberlain LH. Palmitoylation-dependent protein sorting. *J Cell Biol.* 2007 Jan 22;176(3):249–54.
224. Blaskovic S, Blanc M, van der Goot FG. What does S-palmitoylation do to membrane proteins? *FEBS J.* 2013 Jun;280(12):2766–74.
225. Feistel T, Hodson CA, Peyton DH, Landfear SM. An expression system to screen for inhibitors of parasite glucose transporters. *Mol Biochem Parasitol.* 2008 Nov;162(1):71–6.
226. Law CJ, Maloney PC, Wang D-N. Ins and Outs of Major Facilitator Superfamily Antiporters. *Annu Rev Microbiol.* 2008 Oct;62(1):289–305.
227. Carruthers A, DeZutter J, Ganguly A, Devaskar SU. Will the original glucose transporter isoform please stand up! *AJP Endocrinol Metab.* 2009 Oct 1;297(4):E836–48.
228. Ozcan S, Dover J, Rosenwald AG, Wöfl S, Johnston M. Two glucose transporters in *Saccharomyces cerevisiae* are glucose sensors that generate a signal for induction of gene expression. *Proc Natl Acad Sci U S A.* 1996 Oct 29;93(22):12428–32.
229. Conrad M, Schothorst J, Kankipati HN, Van Zeebroeck G, Rubio-Texeira M, Thevelein JM. Nutrient sensing and signaling in the yeast *Saccharomyces cerevisiae*. *FEMS Microbiol Rev.* 2014 Mar;38(2):254–99.
230. Plassmeyer ML, Reiter K, Shimp RL Jr, Kotova S, Smith PD, Hurt DE, et al. Structure of the *Plasmodium falciparum* circumsporozoite protein, a leading malaria vaccine candidate. *J Biol Chem.* 2009 Sep 25;284(39):26951–63.
231. Carruthers VB, Blackman MJ. A new release on life: emerging concepts in proteolysis and parasite invasion. *Mol Microbiol.* 2005 Mar;55(6):1617–30.
232. Coppi A, Natarajan R, Pradel G, Bennett BL, James ER, Roggero MA, et al. The malaria circumsporozoite protein has two functional domains, each with distinct roles as sporozoites journey from mosquito to mammalian host. *J Exp Med.* 2011 Jan 24;208(2):341–56.
233. Sievers F, Wilm A, Dineen D, Gibson TJ, Karplus K, Li W, et al. Fast, scalable generation of high-quality protein multiple sequence alignments using Clustal Omega. *Mol Syst Biol.* 2014 Apr 16;7(1):539–539.
234. Gasteiger E, Gattiker A, Hoogland C, Ivanyi I, Appel RD, Bairoch A. ExpASY: The proteomics server for in-depth protein knowledge and analysis. *Nucleic Acids Res.* 2003 Jul 1;31(13):3784–8.
235. Pierleoni A, Martelli P, Casadio R. PredGPI: a GPI-anchor predictor. *BMC Bioinformatics.* 2008;9(1):392.

## List of publications

Parts of this thesis have been published:

Lindner SE, Swearingen KE, Harupa A, Vaughan AM, Sinnis P, Moritz RL, Kappe SH. Total and putative surface proteomics of malaria parasite salivary gland sporozoites. *Mol Cell Proteomics MCP*. 2013 May;12(5):1127–43.

<http://dx.doi.org/10.1074/mcp.M112.024505>

Harupa A, Sack BK, Lakshmanan V, Arang N, Douglass AN, Oliver BG, Stuart AB, Sather DN, Lindner SE, Hybiske K, Torii M, Kappe SH. SSP3 is a novel *Plasmodium yoelii* sporozoite surface protein with a role in gliding motility. *Infect Immun*. 2014 Nov;82(11):4643–53.

<http://dx.doi.org/10.1128/IAI.01800-14>



## Appendix B

Pf	M	STYSVEPLVYDRYEYVYLKPKKAGTSAVYYPLNISWKYVAKKRSVGCFGSRKKYTLTP	60	
Pk		-----MSPLVVDTYD CVYLRPQPA--RTYYYPLGMTWKYVSSKSTGCFGTTKKYTLTP	52	
Pcy		-----MSPLVVDTLDCVYLRPQPT--STYYYPLGMTWKYVSSKSTGCFGTTKKYTLTP	52	
Pv		-----MAPLVVDTLDCVYLRPQPT--STYYYPLGMTWKYVSSKSTGCFGTTKKYTLTP	52	
Pch		-----MTNQMLETYECSLLRPQPF--STLYYPANITWKYVLSKPSGCFGSTQKYVAVP	52	
Py		-----MSNQVLETYECSLLKPQLV--NTLYYPADITWKYVLSKPSGCFGSTKKYVAVP	52	
Pb		-----MTNQVLETYECSILKPHPV--NTIYYPADITWKYVLSKPSGCFGSTKKYVAVP	52	
	:	: : : : *:* : : ** : :*** ..: ****: :** .*		
Pf	EAY--	YPPYYYYYVYYP	PSAARLVRTTRKEK-----VLKENNNKESEDE-----NKE	105
Pk	ETY--	YPPYYYYYVYYP	TPVESSTVCSSNKKVIKDKKKKDEDKELKDESSKEGSEKEEE	110
Pcy	ETY--	YPPYYYYYVYYP	TPAESAIVCSSSKKVIKDKKKKDEDKALKDESSKEESEKEEG	110
Pv	ETY--	YPPYYYYYVYYP	TPAESPIVCLSSKKVIKDKKKKDEDKQELKDESSKEGSEKEEG	110
Pch	ETY--	SPPYYHYVYYP	RPYPLANITLSIKHEDKNKKVNLNNQEKKEELNDE-----DE	105
Py	ETY	YTSYPPYYVYYP	RPYVLGNTLSIKNADQSKKKVNLNNQEKKEEPSDE-----NG	107
Pb	ESY--	SPPYYHYVYYP	RPYTLGNITLSIKNADKSKKKVNESNDQEKKEESNDE-----NG	105
	*:*	*****:*** *	: : *	:: : : : :** .
Pf	DNVGTEKKECDCSEKEKIPTYVPLTESYFPPSALYVPHYSVLVP	151		
Pk	LKKSSGKKKNEYAEGERVVRTYLPVVEPFYTTSSY-YVPRA-ILFP	154		
Pcy	SKKSSGKKKYEYVEGERVVRTYLPVVEPFYTTSSY-YVPRA-ILFP	154		
Pv	SKKSSGKKKYEYVEREKVVRTYLPVVEPFYTTSSY-YVPRA-ILFP	154		
Pch	S--KTSKKNDECNDKENNTKKYVSVVSPYYIGSL-YYPTA-IFYP	147		
Py	S--KTSKKNDECNDRENNTKKYVSILTPPYIGSL-FYPTA-IVFP	149		
Pb	T--KTSKKNDECNDRENNTKKYVSVLTPPYIGSL-FYPTA-IFYP	147		
	: **:	: : *	.*: : * : * : * : *	

% aa identity	Pb	Pf	Pv
Py	88	36	47

**Figure B.1** Multiple sequence alignment of PY02432 with its *Plasmodium* orthologs (233). Palmitoylation sites are highlighted in green and were predicted with the CSS-Palm tool at high stringency except for *P. falciparum* where stringency was set to medium (193). Asterisks indicate identical residues in all sequences, colons and periods mark conserved and semi-conserved substitutions, respectively. Note the high abundance of tyrosine residues (13.4 % in PY02432) with a conserved stretch of tyrosines in the central region of the protein, boxed in red.



## Appendices

	<b>TM1</b> ▼	
PY05332	-----MMYLTKIVSNACLAIIINFGCLCLSLTSLSRRLI	33
PyHT	MNILRMDILSRGGTQIEHRDGF--FNT--SFQYVLSACLASFIFGYQVSVLNTIKSYIV	56
EcXy1E	-----MNTQYNSSYIFSIITLVATLGGLLFGYDTAVISGTVES--	37
AtHT1	-----MPAGGFVVDGQKAYPGKLT PFVLFTCVVAAMGGLIFGYDIGISGGVTSMP	52
MmG1uT1	-----MDP----SSKKVTGRMLLAVGGA VLGSLQFGYNTGVINAPQ---K	38
	* : : ** : :	
	<b>TM2</b> ▼▼▼	
PY05332	KGYDICPDGYRGCDKEK-----YFSTFYFTLYMSAFLGCFISLFF-----RNINRKK	81
PyHT	VEFE-----WCSTKTD-----TSCEDSILKSSFLLASVFIGAVLGSFGSGLY--VKFGRRF	105
EcXy1E	-LNTVFVAPQNLS--ESA-----ANSLLGFCVASALIGCIIGGALGGYCSNRFGRRD	86
AtHT1	FLKRFFPSVYRKQEDASTN-QYCQYDSPTLTMFTSSLYLAALISLAVSTVTRKFGRR	111
MmG1uT1	VIEEFYNQTNHRYGEPSTTLTWS----LSVAIFSVGGMIGSFSVGLFVNRFGRRN	94
	: : : : : : : : : : : :	
	▼ <b>TM3</b> ▼ <b>TM4</b>	
PY05332	FMQVIHYLYIIGSLFTI-----YYEPHVLFLFSQAFFGLAIGCTIVI	124
PyHT	SLMVIYIFFIFVSILTAIS---H-----HFHTILYARLLSGFGIGLITVS	147
EcXy1E	SLKIAAVLFFISGVGSAWPELGFTSINPDNTVPIYLAGYVPEFVIYRIIGGIGVGLASML	146
AtHT1	SMLFGGILFCAGALINGFA---K-----HWMLIVGRILLGFGIGFANQA	153
MmG1uT1	SMLMMNLLAFVAAVLMGFSKLGK-----SFEMLILGRFIIGVYCGLTTF	139
	: . : : : : : : : : : * . *	
	▼ <b>TM5</b>	
PY05332	VGFYVFEYSPKEHQNYGFTIQTFFSIGLLISYLFVGIYEHMK-----FNKITSSYW	176
PyHT	VPMYI SEMTHKDKKGA YGVLHQLFITFGIFVAVLLGLFLGDGPKINGKSIELSNFEMFW	207
EcXy1E	SPMYIAELAPAHIRGKLVSNQFAIFGQLLVYCVNYFIARSG-----DASWLNTDGW	199
AtHT1	VPLYL SEMAPYKYRGALNIGFQLSITIGILVAEVLNYFFAKIK-----GGWGW	201
MmG1uT1	VPMYVGEVSPALRGALGTLHQLGIVVGILIAQVFGGLDS-IMG-----NADLW	186
	: * : * : : * : : * : : *	
	<b>TM6</b> ▼ ▼	
PY05332	ILMILQKLHMLMPLIFSIISILLNLFVFTMDTPLH-LYKSQKYDKFEEIKKKISKVGIDE	235
PyHT	RFMF-----FLPTIISLLGIILLIAFYKEETPYF-LYENGNIEGSKNILKKIYGPSDVD	260
EcXy1E	RYMF-----ASECIPALLFLML-L-YTVPESPRW-LMSRGKQEQAESILRKIMGNTLAT	250
AtHT1	RLSL-----GGAVVPALIITIG-S-LVLPDTPNS-MIERGQHEEAKTKLRRIRGVDDVS	252
MmG1uT1	PLLL-----SVIFIPALLQCIL-L-PFCPEsprllINRNEENRAKSVLKKLRGTADVT	238
	: : : : : : : : : : : : :	
	<b>TM7</b> ▼▼ ▼▼	
PY05332	K-HEYHSNEKNNEINIILNDLTIIDFFRNKRLRNCIIGSILCYLFCFSGCIIIFNNLFL	294
PyHT	DALRAIKDAIDQNKAKESSL SLLSALKIPAYRNVII LGCILSGFQQFTGINVLVANSNE	320
EcXy1E	QAVQEIKHSLDHGRKTG-----GRLL--MFGVGVIVIGVMLSIFQQFVGINVVLYAPE	302
AtHT1	QEFDDLVAASKESQSIE----HPWRNLLRRKYRPHLTMVMIPFFQQLTGINVIMFYAPV	308
MmG1uT1	RDLQEMKEEGRQMMREK--KVTILELFRSPAYRQPI LIAVVLQLSQQLSGINAVFYYSTS	296
	. : : : : : : : : : : * : :	
	▼ <b>TM8</b> ▼▼ <b>TM9</b>	
PY05332	FYNIFETKRESSIISMI-FIFIYFLFTIITTKLANYYNNKNKLIILGFVLQLISSFIMMI	353
PyHT	LYKEFLDKNLITILS-VIMTAVNFLMTFPAIYII EKIG-RKTL LGGCIGV-ICAF LPTV	377
EcXy1E	VFKTLGASTDIAL LQTIIIVGVINL TFTVLAIMTVDFKG-RKPLQIIGALGMAIGMFSLGT	361
AtHT1	LFNTIGFTTDASLMSAVVTGSVNVAATLVSIYGVDRWG-RRFLFLEGGTQMLICQAVVAA	367
MmG1uT1	IFEKAGVQQP--VYATIGSGIVNTAFTVVSLFVVERAG-RRTLHLIIGLAGMAGCAVLMTI	353
	: : : : * : : : * : *	
	<b>TM10</b> ▼	
PY05332	CSLC-----NLPQVLNKIIISIDIILYIIGFSFGFGHIIWTHIFHFSEYKVVGA	404
PyHT	IARQVWGP-----TKI-VNGLSIAGTFLMIISFAVSYGPVLWIIY LHEMYPSEIKDSAA	429
EcXy1E	AFY-----TQA-SGIVALLSMLFYAAAFAMSWGVCWVLLSEIFPNAIRGKAL	408
AtHT1	CIGAKFGVDGTPGELPKW-YAIVVVTFCIYVAGFAWSGPGLGWLPSEIFPLEIRSAAQ	426
MmG1uT1	ALA-----LLERLPW-MSYLSIVAI FGFVAFVEVGPPIPWFIVAE LFSQGPRPAAI	404
	: : * . * : * : : : :	

## Appendices

---

	TM11	TM12	
PY05332	FCSYYAIFIGTFIMSIFLEFSNIN-----KHSYLFIIIFIIFLIVSILFFKSIYINNTE		457
PyHT	SLASLINWVCAIIVVFPDIIKK-----SPSILFMFFSVMCIIFLFI-MFFIKETK		481
EcXy1E	AIAVAAQWLANYFVSWTFPMMDKNSWLVAHFHNGFSYWYIGCMGVLAALFM-WKFVPETK		467
AtHT1	SITVSVNMIFTFIIAQIF--LTMLCHL-----KFGLFLVFAFFVVMSIFV-YIFLPETK		478
MmGluT1	AVAGFSNWTSNFIVGMCQYVEQLCG-----PYVFIIFTVLLVLFIFT-YFKVPETK		456
	:           ::	: .: : :: :*       : :*:	
	▼		
PY05332	DPPKQEQ--ITESHNSI----D---ISE--AIDDASKVQEAEI-	489	
PyHT	GGEIGTSPYISLEERQKH-----IGKSKV-----	505	
EcXy1E	GKTLEELEALWEPETKKTQQTATL-----	491	
AtHT1	GIPIEEMQVWRSHWYWSRFVEDGEYGNALMGKNSNQAQTKHV	522	
MmGluT1	GRTFDEIASGFRQGGASQSDKTPEELF--HPLGADSQV-----	492	

**Figure B.3** Multiple sequence alignment of sugar transporters. PY05332 is aligned with *P. yoelii* hexose transporter (PyHT; PY00899) and homologs of glucose transporters from phylogenetically distant organisms. Transmembrane domains (TM) are shaded gray and were predicted with the TMHMM Server v. 2.0 (<http://www.cbs.dtu.dk/services/TMHMM/>). Identical residues in all sequences are marked by asterisks, conserved and semiconserved substitutions by colons and periods, respectively. Triangles mark residues that are identical in all sequences but PY05332. Green triangles denote residues that were found to be important for transport function and substrate discrimination in mammalian GluTs (227).

Appendix C

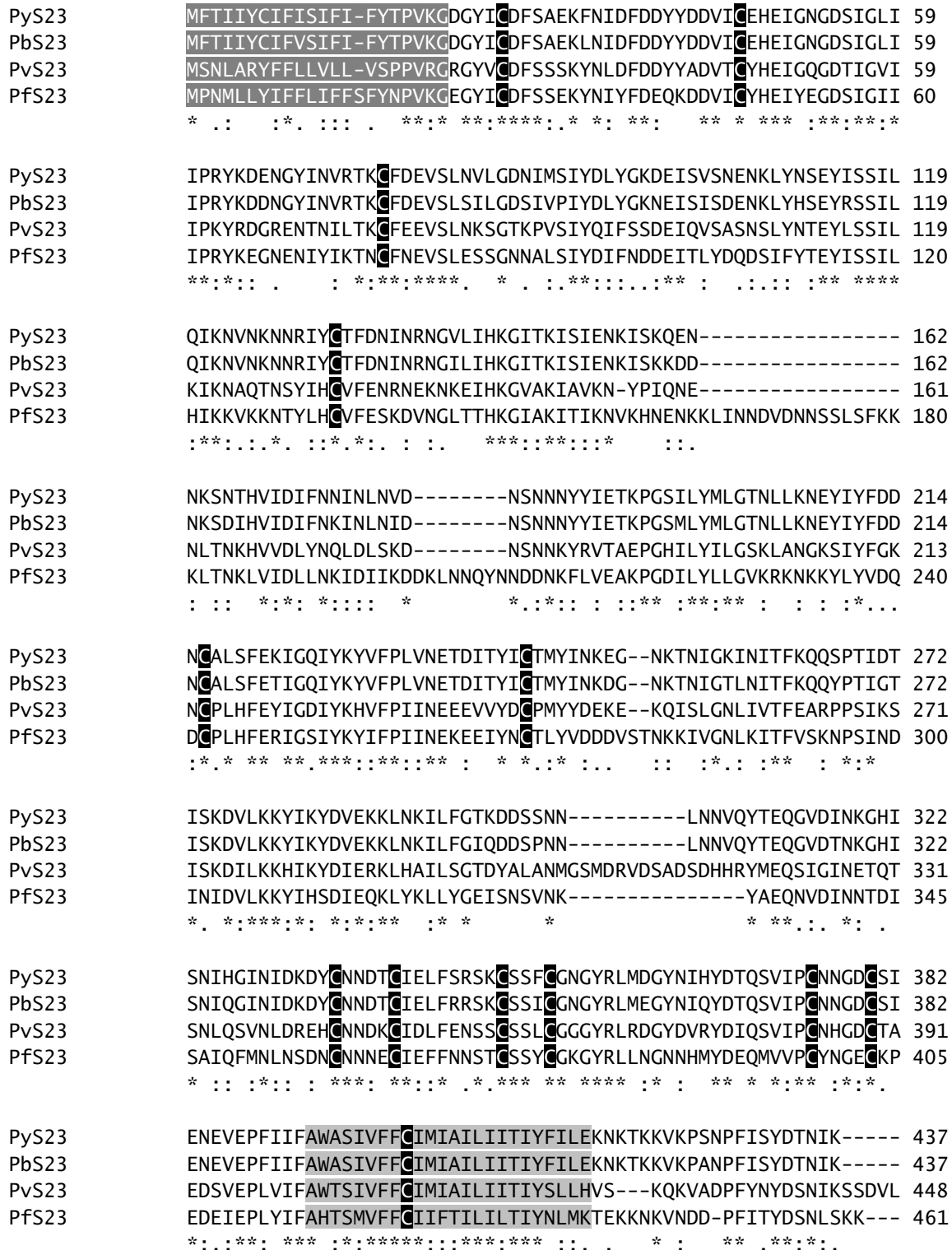


**Figure C.1** Multiple sequence alignment of *P. yoelii* S23 with its orthologs in *P. berghei* (PBANKA\_142520), *P. vivax* (PVX\_123155) and *P. falciparum* (PF3D7\_0812300) (233). The signal peptide is highlighted in dark grey with white font, the transmembrane domain in light grey. Black boxes indicate conserved cysteine residues. An asterisk indicates identical residues, a colon indicates conserved substitutions and a period indicates semi-conserved substitutions.

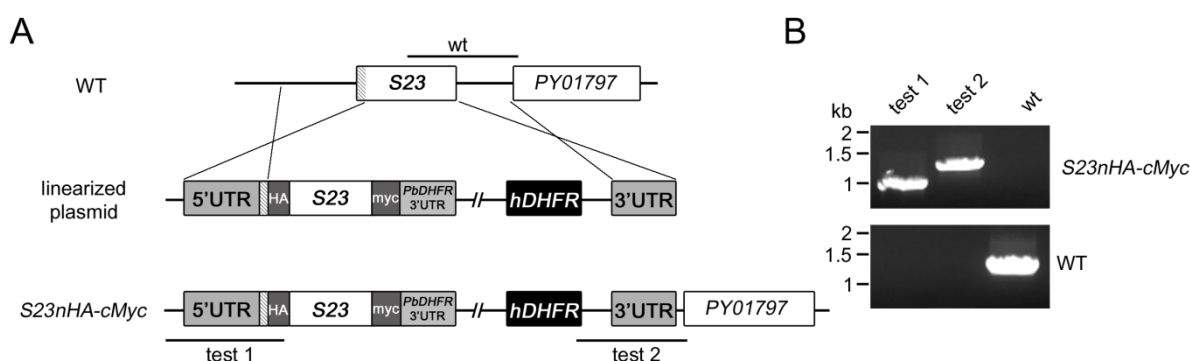


**Figure C.2** Generation of *Py S23nHA-cMyc* parasites. (A) Schematic of replacement strategy. The HA tag was introduced downstream of the predicted signal sequence (striped box) and the Myc tag was fused to the C-terminus of *S23*. Expression of tagged *S23* is under the control of its endogenous promoter and the 3' regulatory elements of the *P. berghei DHFR/TS* gene. The 5' and 3' UTRs of *S23* were used as regions for homologous recombination. (B) PCR genotyping with primers (bars in A) specific to the wild-type locus (wt) and the transgenic locus (test 1 and test 2) shows proper integration of the construct.

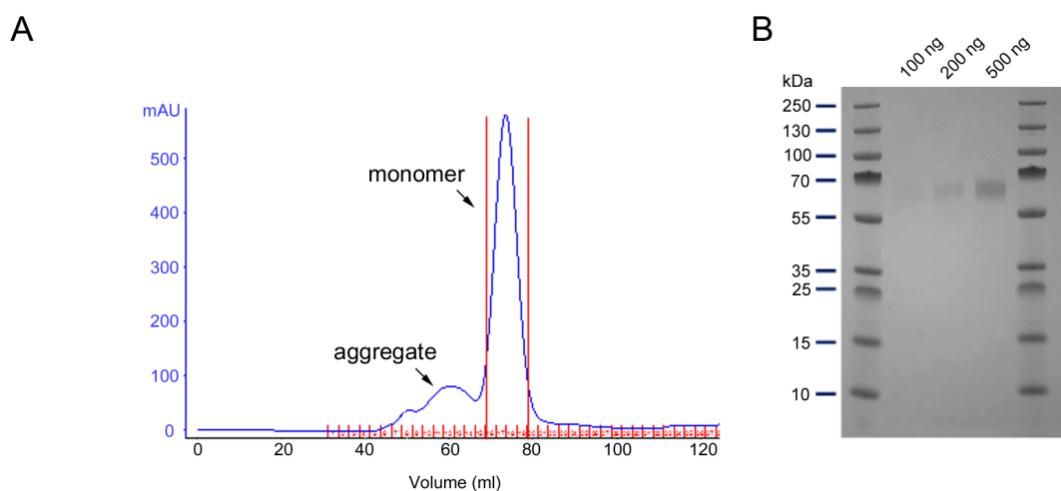


**Figure C.3** Production of recombinant *S23*. (A) Soluble recombinant *S23* was produced in HEK293F cells and purified by a two-step chromatography protocol. Shown is the UV trace from the size exclusion chromatography (SEC) step, illustrating the separation of different protein species by size. The red bars denote the monomeric fractions from the SEC step that were collected for the final protein preparation. mAU, milli-absorbance units. (B) Denaturing SDS PAGE of the final pooled *S23* protein. 100 ng, 200 ng, and 500 ng of purified protein were run on a 4-12 % gradient gel and stained with Simply Blue stain.

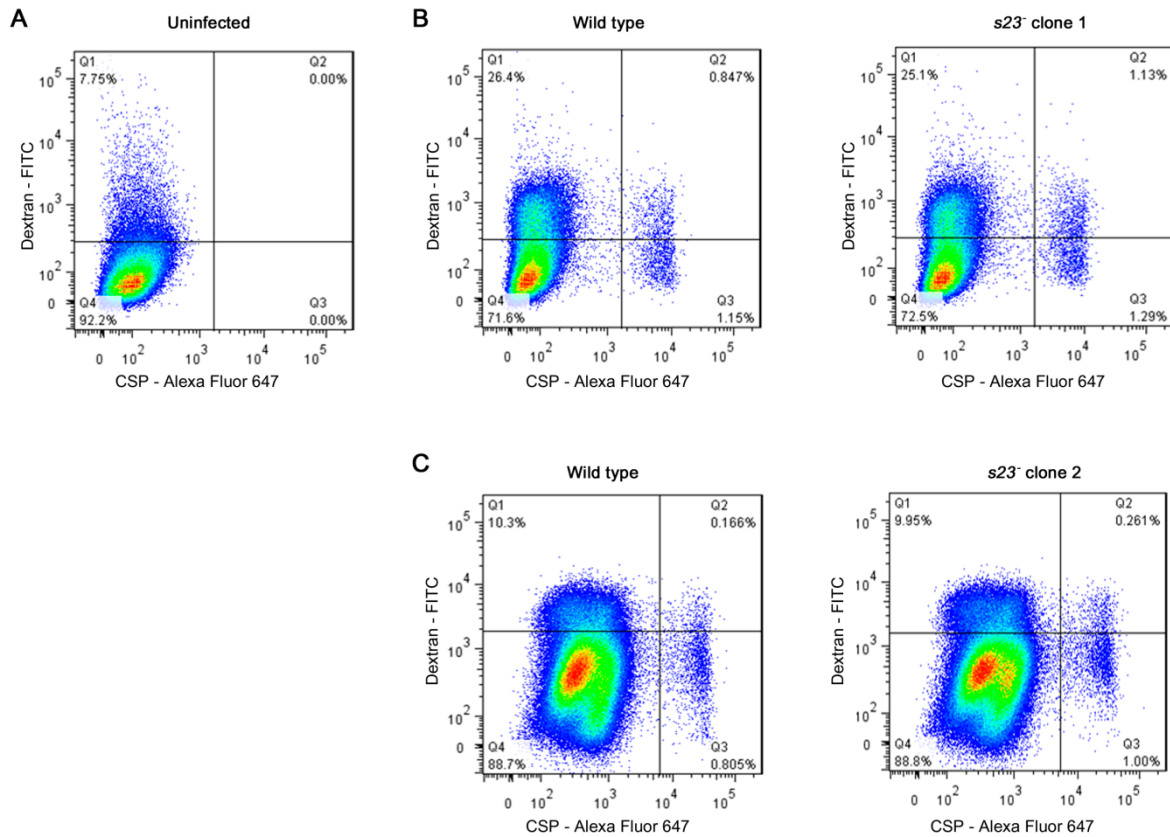


**Figure C.4** Flow cytometry analyses of sporozoite cell traversal and invasion rates *in vitro*. Following infection of Hepa 1-6 cells with either wild type or *s23<sup>-</sup>* sporozoites in the presence of FITC-dextran, cells were fixed, permeabilized and stained for parasites, using a monoclonal antibody to CSP conjugated to Alexa Fluor 674. Panel A shows a representative plot of uninfected cells whereas B and C are example plots from separate experiments comparing wild type to two unique *s23<sup>-</sup>* clones.

### Acknowledgements

I would like to express my gratitude to my supervisor Stefan H.I. Kappe for giving me the opportunity to work in his research group and for his support throughout my thesis studies.

I would like to thank Rupert Mutzel for kindly agreeing to review this thesis.

I would like to acknowledge our collaborators who contributed to this thesis: Kristian E. Swearingen (Institute for Systems Biology, USA) for mass spectrometry, Motomi Torii (Ehime University, Japan) for immunoelectron microscopy, Kevin Hybiske (University of Washington, USA) for live microscopy, and Noah Sather and colleagues (Seattle BioMed, USA) for producing recombinant S23.

Many thanks go to all past and present members of the Kappe group for their help and support, for always having an open door and altogether for a great work environment. Special thanks go to Scott E. Lindner for the good teamwork on the sporozoite proteome project. Thanks to Viswanathan Lakshmanan for cloning the S23 knockout construct. I would like to thank Brandon Sack for generating antibodies to S23 and for helping with the manuscript. I am thankful to Alyse N. Douglass for technical assistance with flow cytometry.

Finally, I would like to thank my family and friends for their endless support.